FINAL REPORT

NASA GRANT NSG-1168

ANALYSIS OF UF_6 ~~BREEDER~~ REACTOR POWER PLANTS

J. D. Clement and J. H. Rust

NASA Program Manager, F. Hohl

Prepared for the

National Aeronautics and Space Administration

by the

School of Nuclear Engineering
Georgia Institute of Technology
Atlanta, Georgia 30332

February 6, 1976

FINAL REPORT

NASA GRANT NSG-1168

ANALYSIS OF UF_6 BREEDER REACTOR POWER PLANTS

J. D. Clement and J. H. Rust

NASA Program Manager, F. Hohl

Prepared for the

National Aeronautics and Space Administration

by the

School of Nuclear Engineering
Georgia Institute of Technology
Atlanta, Georgia 30332

February 6, 1976

ACKNOWLEDGMENTS

This work was originally supported by NASA Grant NSG-7068 and continued under NASA Grant NSG-1168. The authors express their appreciation to the respective program managers--Dr. Karlheinz Thom and Dr. Frank Hohl--for helpful suggestions during the performance of this research.

The following graduate students, supported by the grant, made significant contributions to the research project: Bruce Byrne, Yen-Wan Y. Hsueh, Lyu Kim, and Clyde Lightfoot, Jr.

In addition, the NASA research program was also used as a design project for the Nuclear Engineering design course in the academic curriculum. The following students were of great assistance in the research work:

Alan Bruce	Tom McTeer
John Delle Site	Larry J. Petcu
Scott Faulkner	S. N. Radcliffe
R. B. Holland	Frank Rives
Martin Kehoe	Frank R. Savage
John V. Massey	Paul E. Turner

Jeffery L. Tuttle

TABLE OF CONTENTS

TABLE OF CONTENTS (Concluded)

LIST OF TABLES

LIST OF ILLUSTRATIONS

LIST OF ILLUSTRATIONS (Continued)

LIST OF ILLUSTRATIONS (Concluded)

ABSTRACT

As part of its policy of supporting research and development programs which reside on the frontier of power technology, the National Aeronautics and Space Administration has sponsored work in gaseous fueled reactors and plasma research. The original thrust of the NASA sponsored research, aimed toward development of a space propulsion engine, led to two gas-core reactor concepts -- the light bulb and the coaxial flow nuclear reactor concepts. Although budgetary and policy factors terminated the development of nuclear powered propulsion engines, the concept of a UF_6 fueled gas core reactor was shown to be very attractive for several other applications. Studies have shown that UF_6 fueled reactors can be quite versatile with respect to power, pressure, operating temperature, and the modes of power extraction. Possible cycles include Brayton cycles, Rankine cycles, MHD generators, and thermionic diodes. Recent results of research on the pumping of lasers by fission fragment interactions with a laser gas mixture indicate the possibility of power extraction in the form of coherent light. Another potential application of the gas core reactor is its use for nuclear waste disposal by nuclear transmutation.

Circulating-fuel breeder reactors with continuous fission-product removal and simplified on-site reprocessing have a potential for generating cheaper power and greatly reducing the safety and safeguards problems associated with fuel transportation. In addition, uranium hexafluoride gas fueled breeder reactors may "burn up" most, or possibly all, of their long-lived radioactive waste products. Because of the highly favorable economics, greatly simplified on-site fuel processing, enhanced safety (no fuel melt-

down possible), and considerably reduced safeguards and radwaste problems, the uranium-hexafluoride breeder reactor may well be the solution to the problems facing the nuclear industry.

The reactor concept analyzed was a $^{233}UF_6$ core surrounded by a molten salt (Li^7F, BeF_2, ThF_6) blanket. Nuclear survey calculations were carried out for both spherical and cylindrical geometries. The nuclear analysis techniques were assessed by comparison with a previous check-point calculation. The core diameter was approximately one meter. The blanket thickness ranged from 60 to 130 cm. A breeding ratio of approximately 1.16 and a critical mass about 379 kg were found. Further neutronic calculations were made to assess the effect on the critical mass, breeding ratio, and spectrum of substituting moderator, Be or C, for the molten salt in the blanket.

The major problem of the materials selection was to find materials compatible with the UF_6 in the core region and the molten salt in the blanket region. The materials selected for use in the reactor system were Monel and modified Hastelloy-N. Modified Hastelloy-N is an alloy developed specifically for use with molten fluoride systems. Its major constituent is nickel. The ductility of modified Hastelloy-N enables its use together as a liner between the core and blanket and also the containment structure for the blanket. Another problem is the selection of turbine blade materials. The high temperature of the UF_6 gas poses severe problems as far as corrosion and strength are concerned.

Thermodynamic cycle calculations were performed for the Rankine cycle. Calculations were also done for a cycle with no reheater to determine how the cycle efficiency is affected by the reheater. Because material limitations of the duct walls limited UF_6 temperature to less than 1660°R (921.89°K),

the average temperature at the outlet of the reactor was chosen to be 1560°R (866.33°K). The reactor outlet pressure was set at 1450 psia (99.97 bars) which is approximately the pressure required from the core physics calculations to obtain a critical reactor.

The minimum temperature difference in the regenerative heat exchanger, ΔT_{6-7}, was specified as 50°R (28°K). The boiler feed pump and turbine efficiencies were taken to be 0.88 and the condenser pressure was maintained at 21.76 psia (1.5 bars)$_b$. The pressure loss across the reactor was assumed to be 14.89 psi (1.03 bars) and the pressure loss across each side of the regenerator and reheater was taken to be 7.445 psi (.51 bar). In these calculations, the pressure loss through the pipes was neglected because the plant design was not complete and therefore the length of the pipes between components was unknown.

Initially, cycle parameters were calculated without reheating. This gave a plant efficiency of 39.03 percent. Then reheat was added between stages of the turbine using the heat generated in the blanket. It was apparent that an optimum pressure existed for removing the UF_6 from the high pressure turbine and, consequently, p_2 was varied. Overall plant efficiencies as a function of the high pressure turbine outlet pressure were calculated. The maximum efficiency was 41.44% at a pressure of 435.12 psia (30 bars). The efficiency begins to increase for pressures greater than 720 psia (50 bars). However, higher pressures cannot be used because calculations indicate that for these higher pressures the reheat temperatures exceed 1560°R (866°K) which was not allowed because of material limitations.

A conceptual mechanical design is presented along with a system layout for a 1000 MW stationary power plant. Further work is required before a final design can be completed.

In summary, the advantages of the GCBR include:

(1) high efficiency,

(2) simplified on-line reprocessing,

(3) inherent safety considerations,

(4) high breeding ratio,

(5) possibility of burning all or most of the long-lived nuclear waste actinides, and

(6) possibility of extrapolating the technology to higher temperatures and MHD direct conversion.

I. INTRODUCTION

As part of its policy of supporting research and development programs which reside on the frontier of power technology, the National Aeronautics and Space Administration has sponsored work in gaseous fueled reactors and plasma research. The original thrust of the NASA sponsored research, aimed toward development of a space propulsion engine, led to two gas-core reactor concepts - the light bulb and the coaxial flow nuclear reactor concepts.[1-10]

Although budgetary and policy factors terminated the development of nuclear powered propulsion engines, the concept of a UF_6 fueled gas core reactor was shown to be very attractive for several other applications.

NASA has continued supporting an ongoing fissioning plasma research program consisting of cavity reactor criticality tests, fluid mechanics tests, investigations of uranium optical emission spectra, radiant heat transfer power plant studies, and related theoretical work.[10-13] These studies have shown that UF_6 fueled reactors can be quite versatile with respect to power, pressure, operating temperature, and the modes of power extraction. Possible power conversion systems include Brayton cycles, Rankine cycles, MHD generators, and thermionic diodes.[12,13,14] Recent results of research on the pumping of lasers by fission fragment interactions with a laser gas mixture indicate the possibility of the power extraction in the form of coherent light.[10,12] Another potential application of the gas core reactor is its use for nuclear waste disposal by nuclear transmutation (Gas Core Actinide Transmutation Reactor, GCATR).[10,12,15,17]

One of the major advantages of UF_6 reactors for power generation is the simplified fuel reprocessing scheme which the gaseous fuel makes possible. Part of the UF_6 from the reactor can be passed through a fractional distillation process to remove fission products with higher or lower boiling points than the pure UF_6. Also, because of the large mass difference, fission products can be separated from the UF_6 in a centrifuge. The long-lived radioactive fission products are appropriately returned to the reactor where they undergo intense neutron irradiation in the reactor core, or in a region in the blanket near the core interface. In the latter case the irradiated fission product mixture gradually diffuses into the core to mix with the gaseous fuel. During irradiation, a large fraction of the long-lived fission products are transmuted into short-lived radioactive isotopes. In this manner, the long-lived radioactive isotopes are recycled until they are burned up. Thus, the UF_6 reactor produces considerably less radioactive waste than other fission reactors for disposal, and possibly none of the long-lived isotopes.

The UF_6 breeder reactor is inherently safe because the conventional loss-of-coolant accident cannot occur, radioactive fission products are continuously removed from the fuel stream resulting in steady-state operation with a core that contains only a minimum steady-state concentration of fission products, and the temperature coefficient or reactivity is negative which prevents accidental power excursions. Another important safety aspect of the UF_6 breeder is the use of U-233 instead of Pu-239 as the fissile isotope; U-233 is considerably less toxic. Work at Georgia Tech has demonstrated the potential of UF_6 fueled reactors for breeding and investigated several energy conversion schemes.[14,16] The nuclear analysis method used multigroup diffusion theory. A benchmark experiment carried out at Idaho Falls was analyzed to show that the nuclear analytical

technique was sufficiently accurate. The UF_6 fueled breeder reactor was considered spherical with U-233-F_6 as fuel and beryllium and thorium in the blanket. A breeding ratio of 1.25-1.26 was calculated for core diameters varying from 1 to 5m. Fuel doubling times were a few years or less. Conventional Rankine cycle and Brayton cycle efficiencies ranged from 35% to 50%.

A further analysis of the gas core breeder reactor has been sponsored at Georgia Tech under NASA Research Grant 1168 (April 6, 1975 to February 6, 1976). This final report describes the results to date.

REFERENCES FOR CHAPTER I

1. Ragsdale, R. G., "To Mars in 30 Days by Gas Core Nuclear Rocket," Astronautics and Aeronautics, 10 (1) (1971).

2. Kuhrt, W. A., "Space Propulsion in the Fiscal Year 2001," Fourth Goddard Memorial Symposoim, Space Age in the Fiscal Year 2001, American Astronautical Society, Washington, D. C., 1966.

3. "Research on Uranium Plasmas and Their Technological Applications," Thom, K., and Schneider, R. T., editors, Proceedings of a Symposium, NASA SP-236 (1971); U.S. Government Printing Office.

4. "2nd Symposium on Uranium Plasmas: Research and Applications, Ragsdale, R. G., editor, AIAA (1971).

5. Clement, J. D., and Williams, J. R., "Gas Core Reactor Technology," Reactor Technology, 13 (3) (1970).

6. Thom, K., "Review of Fission Engine Concepts," J. Spacecraft and Rockets, 9 (1972).

7. Thom, K., and Schneider, R. T., "Fissioning Uranium Plasmas," Nuclear Data in Science and Technology, 1, 15-38 (1973); International Atomic Energy Agency, Vienna, Austria.

8. Rom, F. E., and Ragsdale, R. G., "Advanced Concepts for Nuclear Rocket Propulsion," NASA SP-20 (1969); U.S. Government Printing Office.

9. Schwenk, F. C., and Franklin, C. E., "Comparison of Closed-and Open-Cycle Systems," Research on Uranium Plasmas and Their Technological Applications, NASA SP-236, 3-13 (1971); U.S. Government Printing Office.

10. Thom, K., Schneider, R. T., and Schwenk, F. C., "Physics and Potentials of Fissioning Plasmas for Space Power and Propulsion," International Astronautical Federation 25th Congress, Paper No. 74087, Amsterdam (October 1974).

11. Williams, J. R., Clement, J. D., and Rust, J. H., "Analysis of UF_6 Breeder Reactor Power Plants," Progress Rept. No. 1, NASA Grant NSG-7067, Georgia Institute of Technology, Atlanta, Ga. (November 1974).

12. Schwenk, F. C., and Thom, K. T., "Gaseous Fuel Nuclear Reactor Research," Paper presented at the Oklahoma State University Conference on Frontiers of Power Technology (October 1974).

13. Williams, J. R., and Clement, J. D., "Exploratory Study of Several Advanced Nuclear-MHD Power Plant Systems," Final Status Report, NASA Grant NGR-11-002-145, Georgia Tech, Atlanta, Georgia (March 1973).

14. Clement, J. D., Rust, J. H., and Williams, J. R., "Analysis of UF_6 Breeder Reactor Power Plants," Semi-annual Report NASA Grant NSG-1168 (October 1975).

15. Paternoster, R., Ohanian, M. J., Schneider, R. T., and Thom, K., "Nuclear Waste Disposal Utilizing a Gaseous Core Reactor," Transactions of the American Nuclear Society, 19, 203 (October 1974).

16. Williams, J. R., Clement, J. D., and Rust, J. H., "The UF_6 Breeder: A Solution to the Problems of Nuclear Powers." Presented at the Inter Society Energy Conversion Conference, August 11-15, 1975.

17. Clement, J. D., and Rust, J. H., "Analysis of the Gas Core Actinide Transmutation Reactor, GCATR," Research Proposal, December 1975.

II. BACKGROUND

Critical Experiments

The first uranium hexafluoride gas fueled reactor built and operated in the Soviet Union in the 1950's,[1] is shown in Fig. II-1. The uranium hexafluoride gas flowed through a 148 channel beryllium moderator which was surrounded by a 50 cm thick graphite reflector. This reactor was critical with 3.34 Kg (7.36 lb) of 90% enriched uranium hexafluoride gas and operated at a power level of 1.5 Kwt. Two boron carbide control rods were inserted into the core to control the reactivity. Table II-1 described the characteristics of the reactor.

Table II-1 Characteristics of the Soviet UF_6 Gas Fueled Reactor Operated in the 1950's[1]

Core diameter, m (ft)	1.16	(3.81)
Core height, m (ft)	1.08	(3.51)
Core gas volume, l (ft^3)	213	(7.52)
Weight of Be in core, Kg (lb)	1370	(3020)
Weight of Al in core, Kg (lb)	62.8	(138)
Graphite reflector thickness, cm (in)	50	(20)
Pitch of square lattice, cm (in)	8	(2.15)
Number of channels	148	
Critical mass of UF_6, Kg (lb)	3.34	(7.36)
Critical mass of U-235, Kg (lb)	2.024	(4.46)

This reactor demonstrated several positive aspects of uranium hexafluoride fueled reactors. Since refueling is done continuously, the reactor is always operating with a "clean core," and there is no need for fuel fabrication. The absence of poisons in the core significantly improves the neutron economy and breeding ratio, and reduces the fuel doubling time. Besides, the reactor shows large negative temperature reactivity due to the large expansion coefficient of gaseous UF_6 in the core.

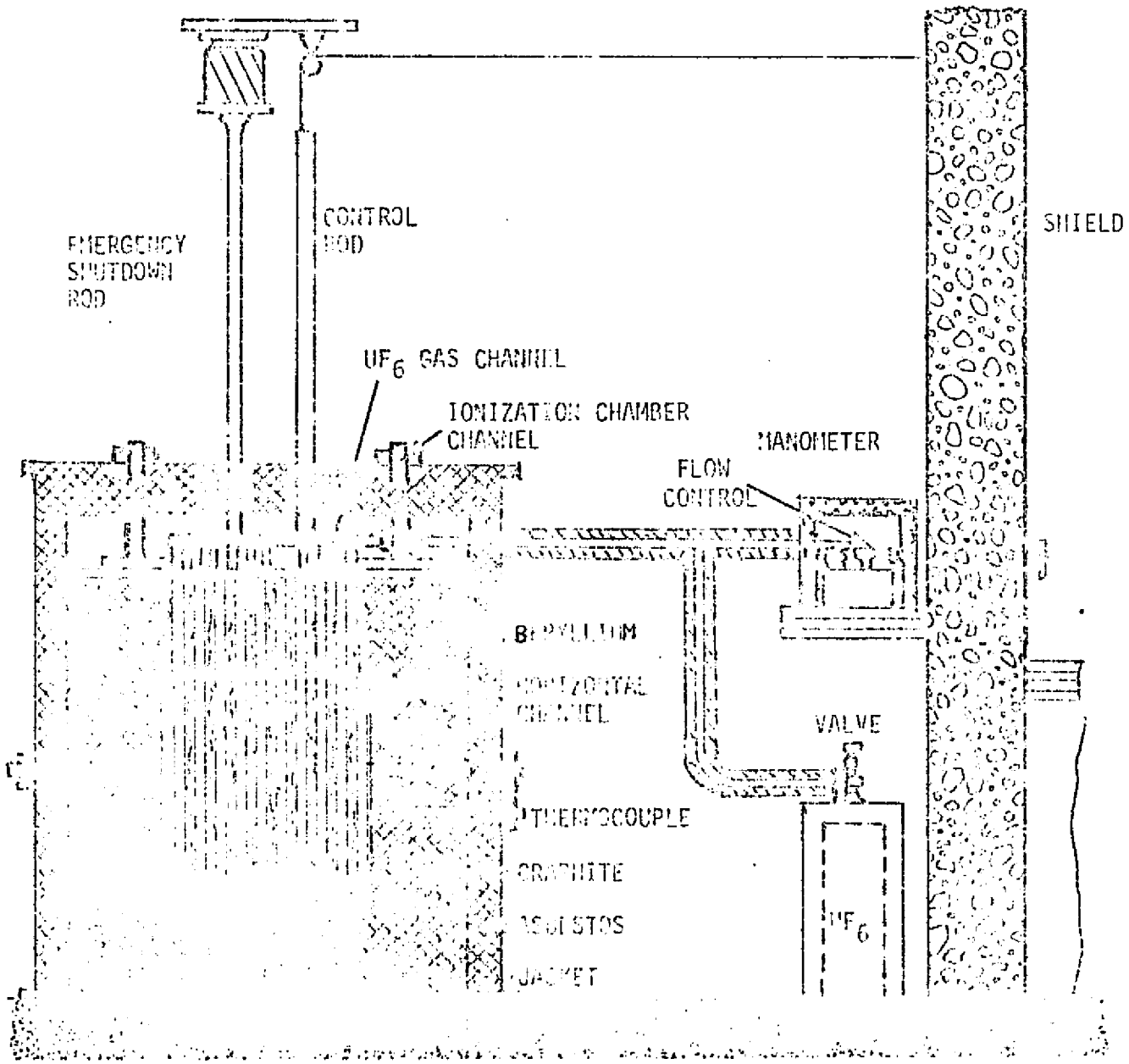

Figure II-1 UF_6 Fueled Reactor Operated in the U.S.S.R. in the 1950's

In recent years, interest in uranium hexafluoride reactors has turned toward the cavity reactor concept in which the uranium hexafluoride gas is contained within a large cavity surrounded by a neutron moderator. The reason for pursuing the cavity reactor approach is the higher temperatures which may be possible with such reactor system. However, the earlier approach of using channels in a solid moderator such as graphite should not be ruled out, since in the near future the UF_6 reactor with somewhat lower temperature may be possible.

On May 17, 1967, a cylindrical uranium hexafluoride gaseous core cavity reactor was made critical at Idaho Falls, Idaho.[2] The gaseous uranium hexafluoride was contained inside a cylindrical aluminum tank with a diameter of 1.22 meters (4 feet) and a length of 1.09 meters (3.58 feet) as illustrated in Fig. II-2. The surrounding moderator-reflector tank was a cylinder with an inside diameter of 1.83 meters (6 feet) and a length of 1.22 meters (4 feet). The outside diameter was 3.66 meters (12 feet) and its length was 3.05 meters (10 feet). The annular reflector region was filled with heavy water to a nominal thickness of 0.89 meter (3 feet) and contained a 10.2 centimeter (4 inch) thick beryllium slab placed 6.7 cm (2.64 inches) from the cavity wall. The UF_6 fuel was 93% enriched in the U-235 isotope, and the experiment had a critical mass of 21.3 Kg (47 lb) of U-235.

This UF_6 cavity reactor critical facility used a split table arrangement with one of the tanks consisting of an end reflector which could be pulled back for easy access to the cavity region. The cavity was contained within the larger fixed tank and was 1.22 meters (4 feet) long and 1.83 meters (6 feet) in diameter. The surrounding tanks contained heavy water which served as the reflector-moderator. The reflector region was nominally 88.9 cm (35 in)

thick. The reactor was controlled with stainless steel clad boron carbide rods which were inserted into the end of the fixed tank.

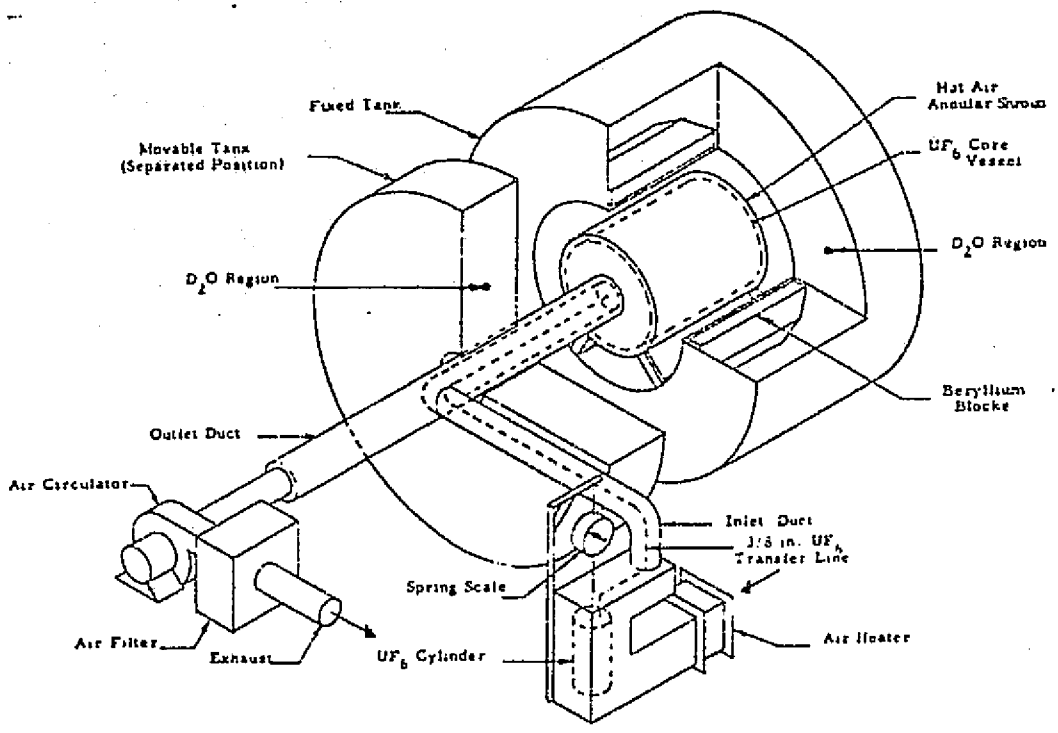

Fig. II-2 First U.S. UF_6 Reactor Critical Experiment[6]

During the latter half of 1969 a spherical cavity reactor experiment was constructed and operated with enriched uranium hexafluoride gas at the National Reactor Test Site in Idaho.[3] The uranium hexafluoride gas was contained within a tank of aluminum surrounded by a heavy water moderator blanket. The tank was spherical, consisting of two spun hemispheres welded together, with dimensions of 1.27 meters (4.18 feet) outside diameter and 0.635 centimeter (0.25 inch) wall thickness. The 90.72 Kg (200 lb) tank was designed for a maximum internal pressure of 4.46 bars (64.7 psi) and a maximum temperature of 400°K (260°F). In order to keep the uranium hexafluoride gas from condensing, heated air flowed around the core between the outside of the spherical core tank (No. 1 in the figure) and the air

flow guide baffles (No. 2). The reactor was designed to simulate a two region gaseous core reactor in which the central fissioning core is surrounded by a working fluid gas, so the core tank was surrounded by a void of 27.14 cm (10.69 in) thickness. The outer tank was also constructed of aluminum and had an outside diameter of 183.1 cm (72 in), a weight of 170 Kg (375 lb) and a wall thickness of 0.635 cm (0.25 in). This outer tank is shown as item 3 in Fig. II-3. The outer spherical tank was immersed in a much larger tank of D_2O (heavy water) to provide a minimum D_2O thickness of 91.4 cm (3 feet). Control rod guide tubes (No. 11) extended from the side of the tank to permit the insertion of control rods by means of control rod actuators (No. 9). The reactor was started up by turning on the electric heaters (No. 28) causing uranium hexafluoride vapor to flow through the fuel line (No. 14) into the inner tank, so the reactor went critical when enough vaporized uranium hexafluoride fuel had entered the cavity. Prior to start-up, a 19-group transport calculation had been performed to determine the critical mass. The calculated critical mass was 8.4 kilograms (18.52 lb) of uranium; the actual critical mass turned out to be 8.434 kilograms (18.59 lb).

Three configurations were studied in this series of experiments. The difference was in the region between the core tank and the cavity tank. In the first experiment this void was filled with air, in the second it contained hydrogen in the form of polystyrene with polyethylene sheets dispersed uniformly between the slabs of polystyrene. The third experiment contained a stainless steel liner 0.076 cm (0.03 in) thick on the inside of the outer tank forming the cavity. The critical mass increased from 8.43 kilograms (18.59 lb) with only aluminum baffles in the void region to 29.38 Kg (64.8 lb) with both hydrogen and the stainless steel liner added to the void region.

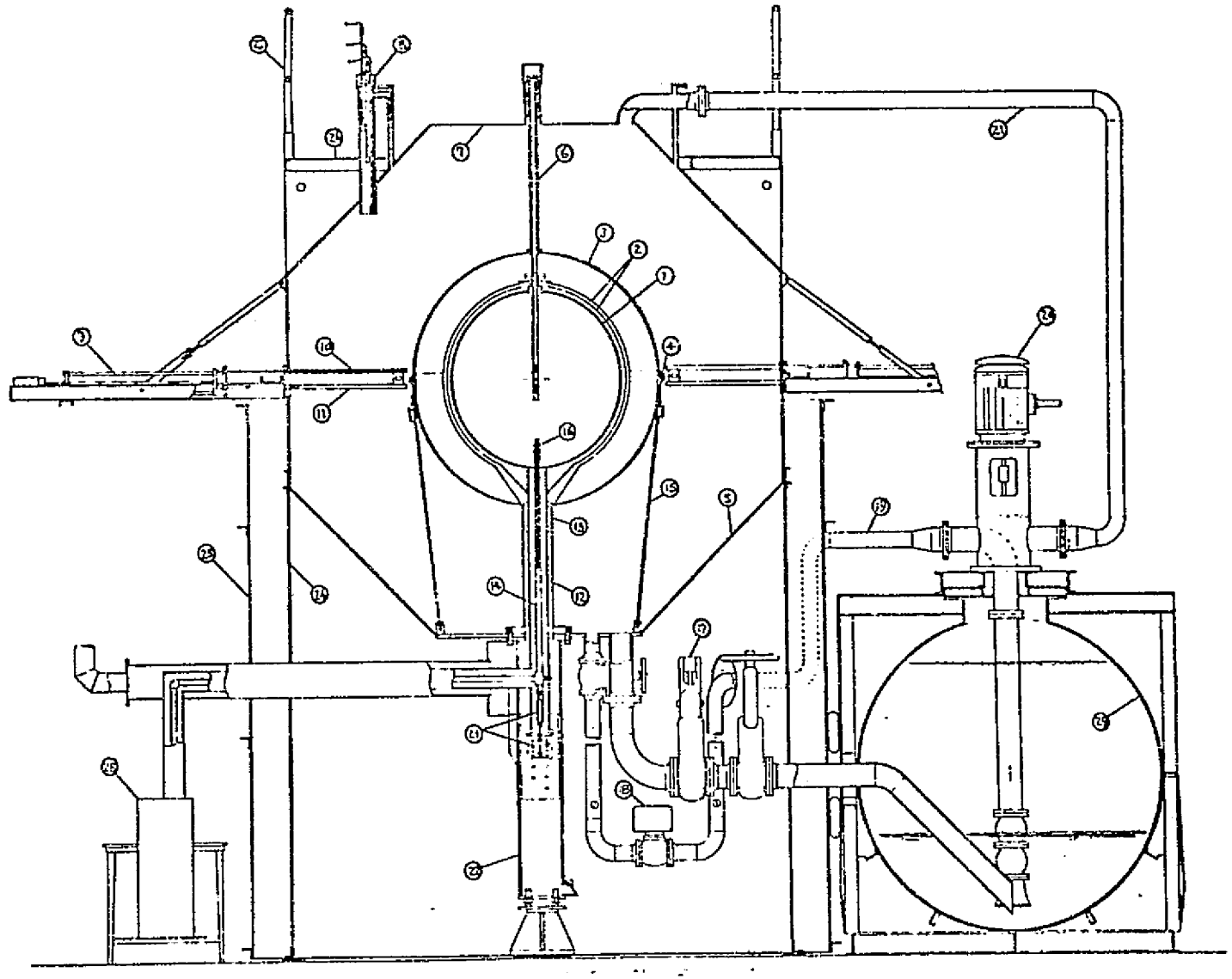

Figure II-3 Overall Diagram of the Spherical Cavity Reactor Configuration[3]
(See Table II-2 for Component Code)

Table II-2provides a comparison of the Soviet and U.S. uranium hexafluoride reactor experiments.

Table II-2 Comparison of UF_6 Critical Experiments

Location	USSR	Idaho Falls	Idaho Falls
Year Operated	1964-57	1967	1969
Enrichment	90%	93%	93%
Moderator in core	Beryllium	none	none
Reflector	Graphite	D_2O	D_2O
Core Geometry	Cylinder	Cylinder	Sphere
Core Diameter	1.16 m (3.81 ft)	1.22 m (4 ft)	1.26 m (4.13 ft)
Core Height	1.08 m (3.51 ft)	1.09 m (3.58 ft)	1.26 m (4.13 ft)
Volume of UF_6 in core	213 l (7.52 ft^3)	1274 l (45 ft^3)	1047 l (37 ft^3)
Reflector thickness	50 cm (20 in)	91 cm (36 in)	91 cm (36 in)
Critical Mass of U-235	2.024 Kg (4.46 lb)	21.3 Kg (47 lb)	8.4 Kg (18.5 lb)

Thermodynamic Cycle Analysis

The thermodynamic cycle analysis in the previous report (Progress Report No. 1)[4] showed that high efficiencies can be achieved using UF_6 as the working fluid for Rankine or Brayton cycles without requiring excessive temperatures. In both cycles gaseous phase UF_6 was employed in the reactor core, and a regenerative heat exchanger was recommended between the turbine and condenser to improve the cycle efficiencies.

The plant schematic and T-S diagram for the regenerative Rankine cycle are shown in Fig. II-4. The cycle calculations were performed for reactor outlet temperatures ranging from 900°K to 1500°K (1160°F to 2240°F) and for reactor outlet pressures ranging from 10 to 160 bars (145.04 to 2320.64 psia). The turbine outlet pressure was taken to be 14.6 bars (211.76 psia), which corresponds to the condensation temperature at 338°K (148°F). The boiler feed pump and turbine effeciencies were taken to be 0.88, the condenser pressure 1.5 bars (21.76 psi), and the minimum temperature difference in the regenerative heat exchanger ΔT_{3-5}, was taken to be 28°K (50°F). As expected the higher pressure and temperatures give the best overall efficiences. For a turbine inlet temperature of 1500°K (2700°R) and pressure of 160 bars (2320.6 psia), the overall efficiency is 58%. Table II-3 summarizes the results of Rankine cycle calculations.

Table II-3 Rankine Cycle Parameters for P_4 = 21.76 psi and T_4 = 606.9°R

	T_1 °R	η(%)	W_T (Btu/lb$_m$)	W_{net}	T_2 °R	T_6 °R	T_3 °R
P_1 = 145.04 psi							
	1620	29.58	16.54	16.42	1458	1088	658
	1980	33.45	19.88	19.76	1788	1525	658
	2340	37.57	23.64	23.53	2110	1746	658
	2700	41.76	28.16	28.04	2437	2072	658
P_1 = 580.16 psi							
	1620	38.02	24.68	24.17	1362	1027	660
	1980	43.66	31.05	30.54	1668	1323	660
	2340	47.55	36.23	35.69	1985	1634	660
	2700	51.98	43.16	42.64	2291	1937	660
P_1 = 1450.04 psi							
	1620	41.87	29.84	28.52	1291	998	667
	1980	48.01	38.07	36.75	1591	1283	667
	2340	52.03	44.49	43.18	1898	1577	667
	2700	55.74	51.18	49.87	2199	1809	667
P_1 = 2320.64 psi							
	1620	43.40	32.64	30.52	1246	963	671
	1980	50.07	42.03	39.92	1546	1281	671
	2340	54.23	49.27	47.16	1824	1549	671
	2700	58.25	57.64	55.53	2147	1829	671

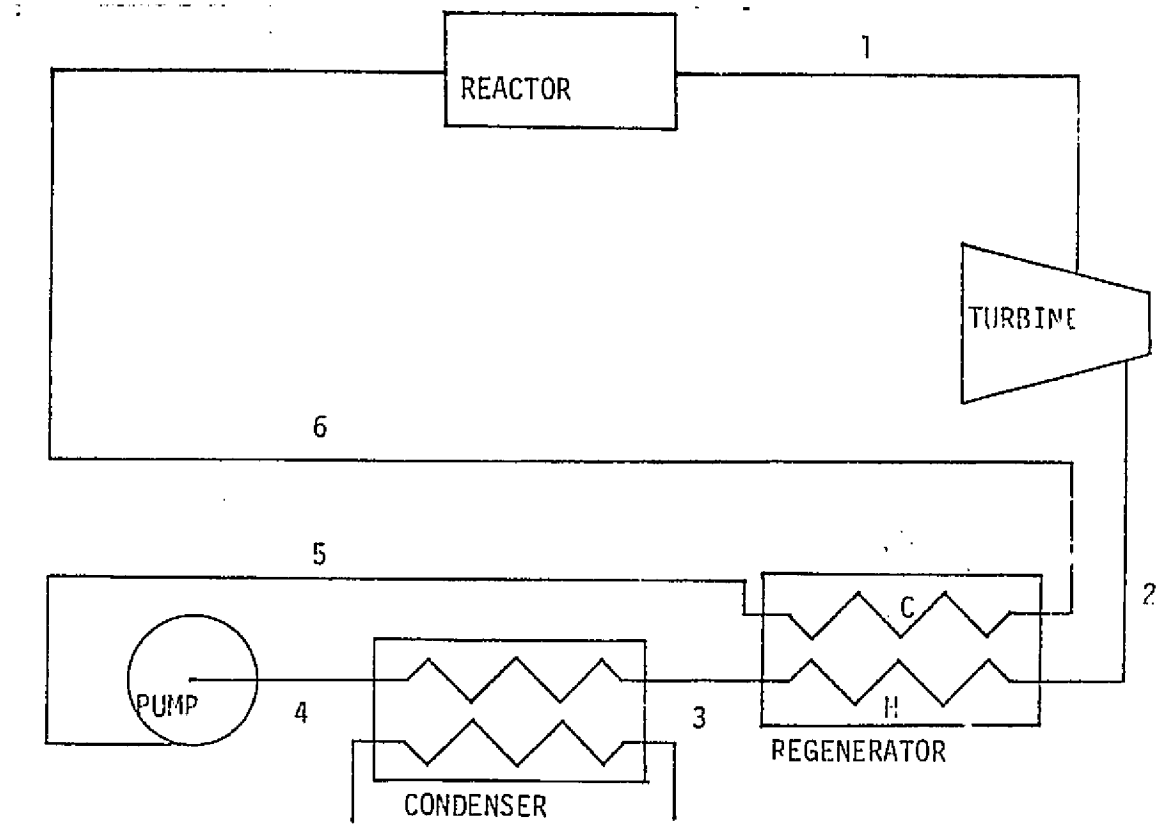

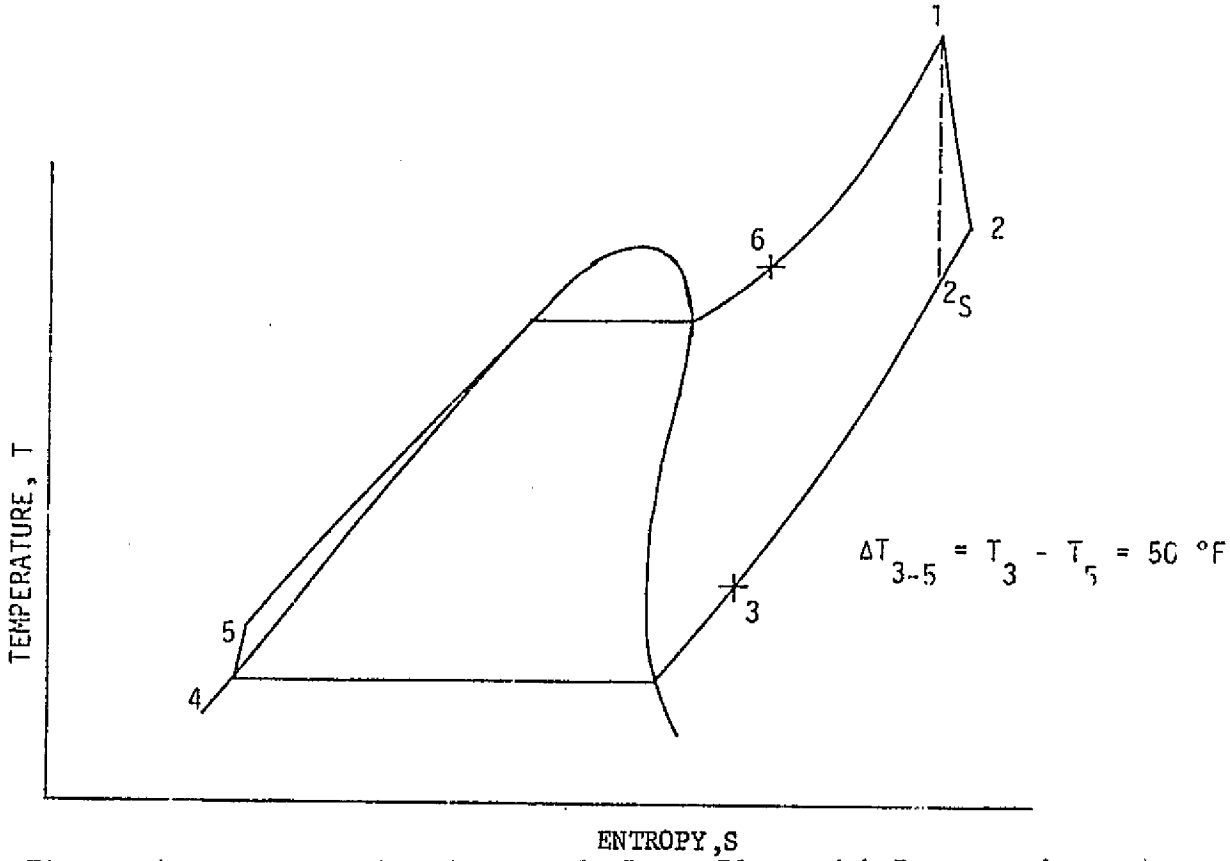

Fig. II-4 Schematic of Rankine Cycle Power Plant with Regenerative and its Temperature-Entropy Diagram

A plant schematic and temperature entropy diagram for the regenerative gas turbine cycle using UF_6 as the working fluid is illustrated by Fig. II-5. Calculations were done for reactor outlet temperatures ranging from 1100°K to 1500°K. Since there is an optimum compressor pressure ratio for the maximum efficiency of the Brayton cycle, the turbine inlet pressure was varied from 10 bars to 160 bars (145.04 psia to 2320.6 psia) for fixed compressor inlet pressure of 1 bar (14.50 psia) and 4.5 bar (65.63 psia). Also a pressure loss of 0.25 bar (3.63 psia) was assumed for each pass of heat exchangers and reactors, because the Brayton cycle efficiency is significantly depended on the pressure losses in the system. The minimum temperature difference between the two fluid streams in the regenerator was set at 28°K (50°R). Turbine and compressor efficiencies were 0.88. Figures II-6 and II-7 show that Brayton cycle efficiencies as a function of the ratio of turbine inlet pressure to compressor inlet pressure. As shown in the figure, the maximum efficiency occurred around the pressure ratio of 20. For the same inlet temperature the efficiencies for plants with the lower compressor inlet pressure of 1 bar (14.50 psia) are higher than the plant with a compressor inlet pressure of 4.5 bar. This is due to compressor inlet temperatures being lower for the lower compressor inlet pressure.

Comparison of Rankine and Brayton cycles shows that for the same reactor exit temperature, Rankine cycle can achieve higher thermodynamic efficiency. This due to the fact that Rankine cycle reject most of the heat at a low temperature than the Brayton cycle. However, this does not mean that Brayton cycles are undesirable because their higher temperature for heat rejection may make them more suitable for space applications.

UF_6 Breeder Reactor Studies

If the UF_6-fueled reactor is to serve as a large-scale energy resource,

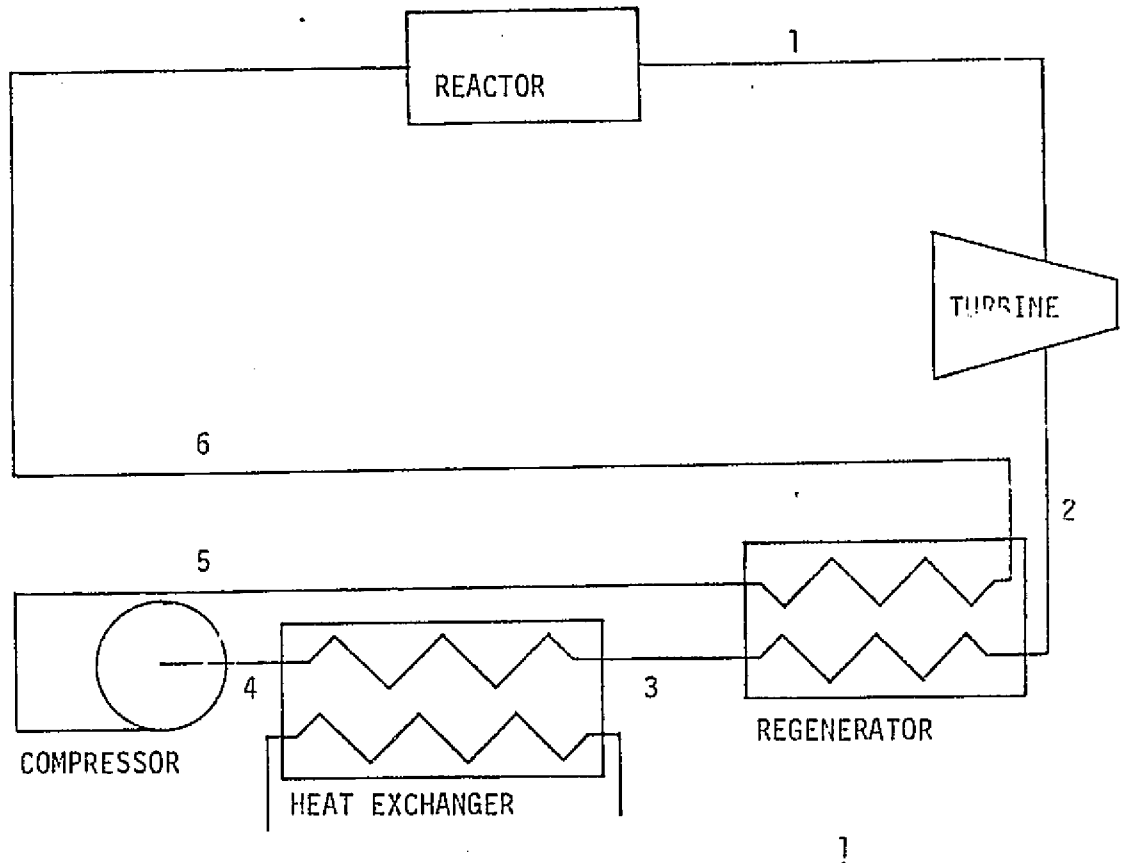

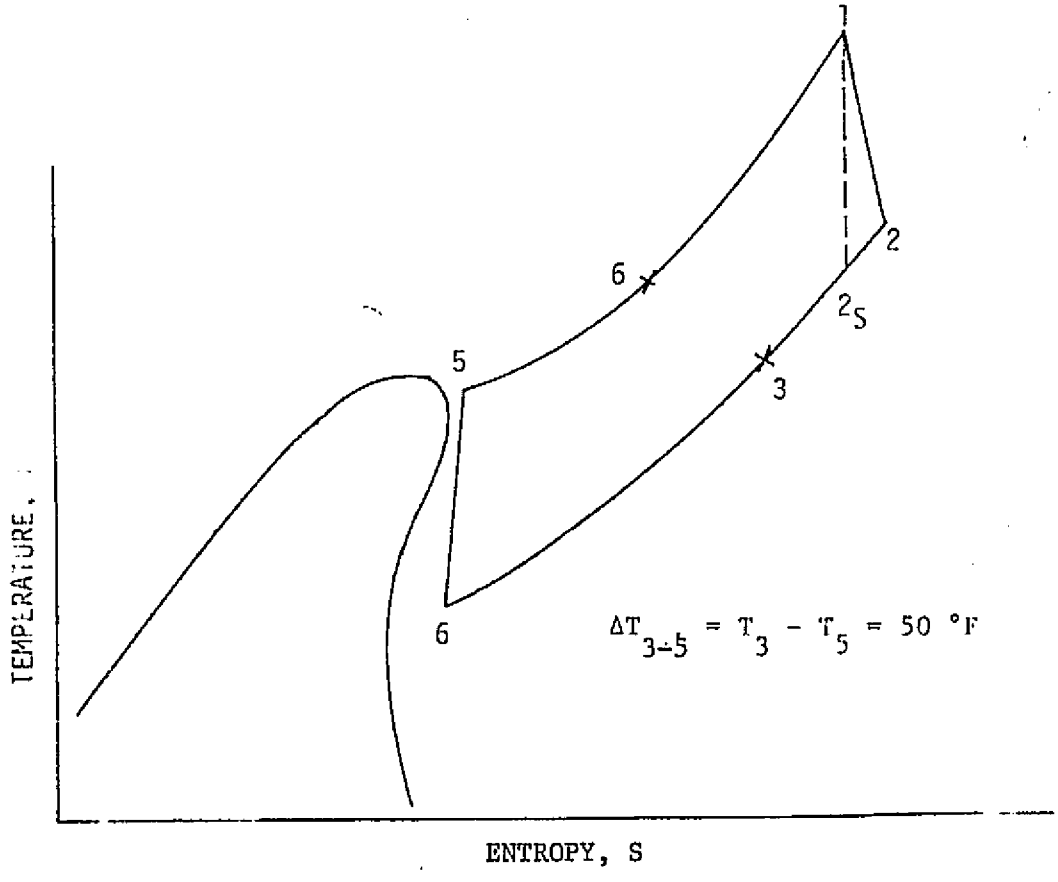

Figure II-5 Regenerative Brayton Cycle Schematic and T-S Diagram

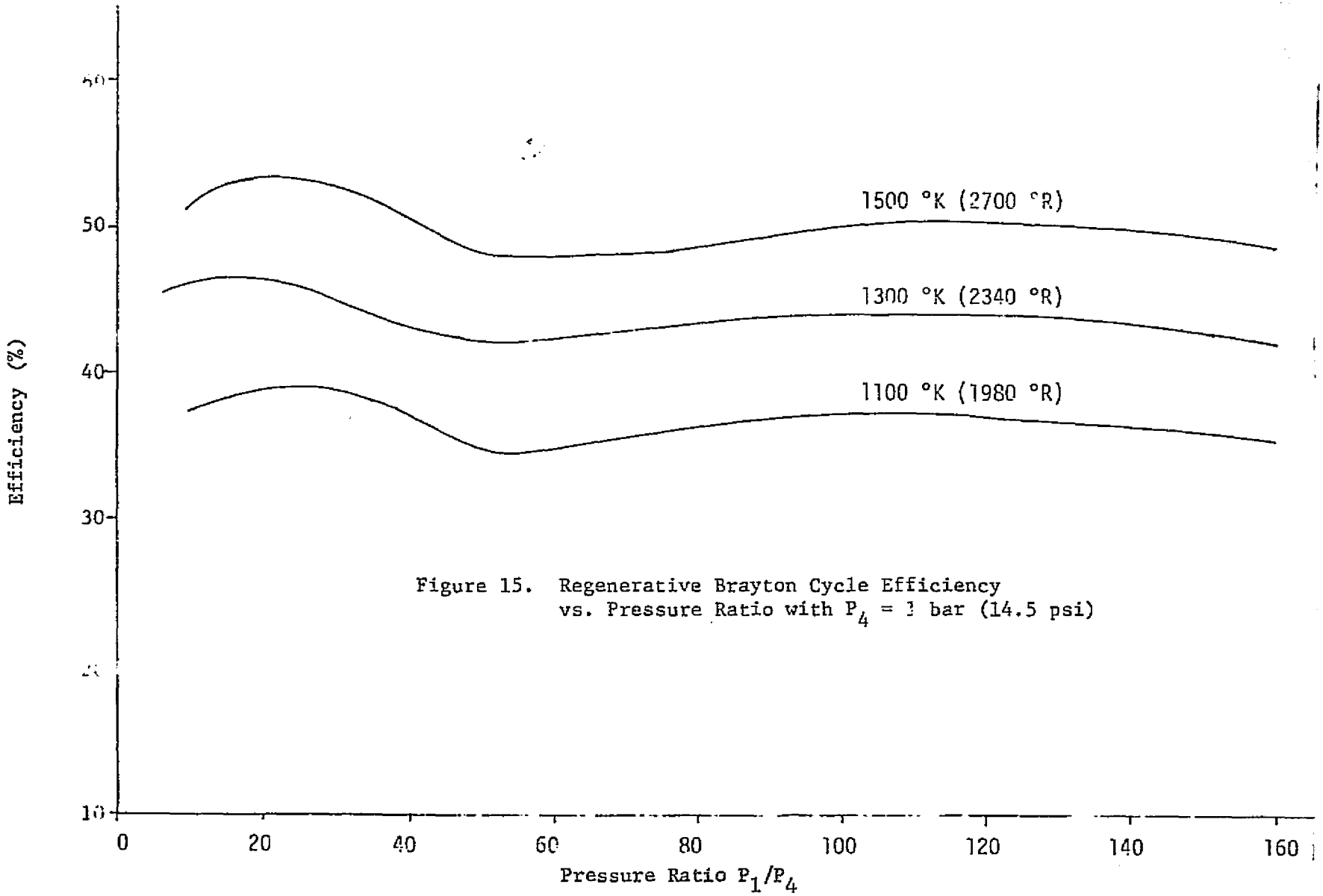

Figure 15. Regenerative Brayton Cycle Efficiency vs. Pressure Ratio with P_4 = 1 bar (14.5 psi)

Fig. II-6 Regenerative Brayton Cycle Efficiency vs. Pressure Ratio with P_4 = 1 bar (14.5 psi)

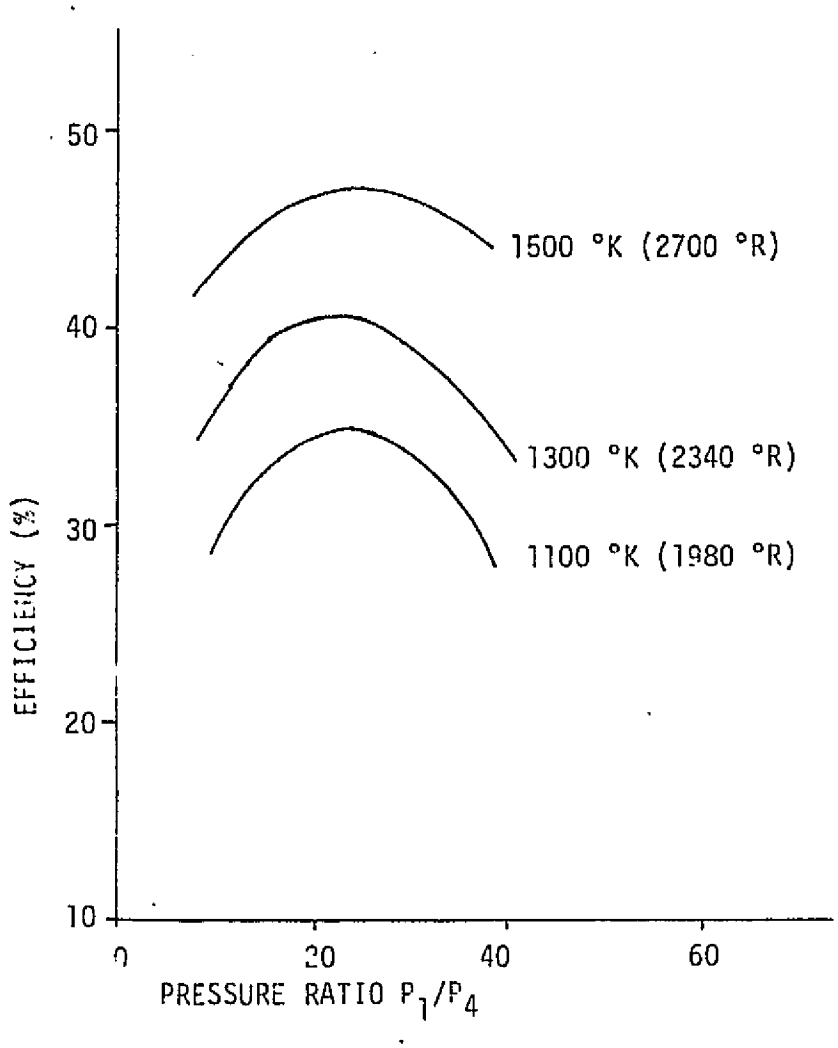

Figure II-7 Regenerative Brayton Cycle Efficiency vs. Pressure Ratio with P_4 = 4.5 bar (65.63 psi)

either on the ground or in synchronous orbit, it must breed its own fissionable fuel. A UF_6-fueled fast breeder reactor study was carried out in the Soviet Union and reported in 1970.[5] The UF_6 flowed through a large number of small tubes joined by manifolds above and below the reactor core, as shown in Fig. II-8. Sodium coolant flowing between the tubes removes heat from the core. The reactor is brought to criticality at a pressure of 400 atmospheres. Inconel-X could be used as the tube material since it is corrosion resistant to UF_6 and sodium at temperature of around 800°K (1000°F). The problem of the radioactive decomposition of the UF_6 can be eliminated by

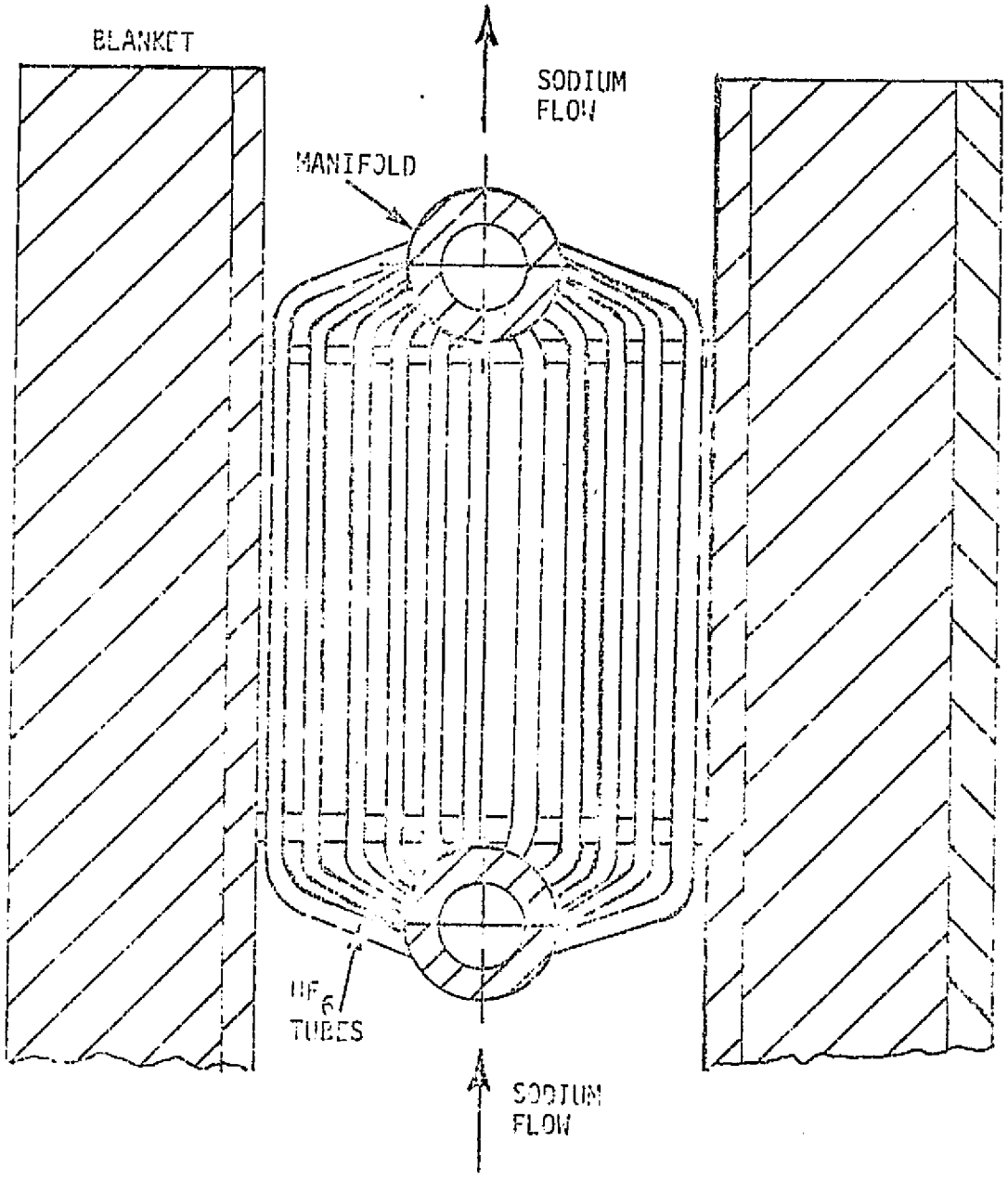

Figure II-8 Diagram of a UF_6-Fueled Fast Breeder Reactor[8]

the addition of a strong fluorinating agent such as BF_3. Table II-4 provides a comparison between this UF_6 gas fueled fast breeder and the Fermi reactor[5].

Table II-4 Comparison of UF_6 Fast Breeder with the Fermi Fast Reactor[8]

	Fermi Reactor	UF_6 Breeder
Thermal Power	300 MWt	300 MWt
U-235 Critical Mass	485 Kg (1069 lbs)	250 Kg (551 lbs)
Core Diameter	0.77 m (2.53 ft)	1.01 m (3.31 ft)
Core Height	0.77 m (2.53 ft)	1.01 m (3.31 ft)
Sodium Inlet Temperature	561 °K (550 °F)	561 °K (550 °F)
Sodium Outlet	700 °K (800 °F)	700 °K (800 °F)
Velocity of Na in Core	9.9 m/sec (32.5 ft/sec)	7.4 m/sec (24.3 ft/sec)

In the U.S.A. until recently the nuclear analytical and system studies had dealt only with non-breeder UF_6 reactors. Research was undertaken at Georgia Tech to determine the potential for breeding of UF_6 fueled reactors. The 26 energy group, Mach computer code with thermal group cross section, prepared by THERMOS, was used to calculate critical masses and breeding ratios of spherical, UF_6 gas-core reactors with 70 centimeters (27.6 inches) of blankets. The blankets were composed of thorium and beryllium. The atom-percent of thorium in the blanket was varied from 0.5 to 2.5 and the core diameter varied from 1 to 5 meters. The average core temperature was taken to be 1000°K. The results of survey calculations showing the dependence of breeding ratio, critical mass, and core pressure upon the atom % of thorium in the blanket and core diameter are listed in Table II-5.

Table II-5 Breeding Ratio at 1000°K

Atom % Thorium in Blanket

Core Dia	0.5	1.0	1.5	2.0	2.5
1M	1.1229	1.2161	1.2581	1.2913	1.3093
2M	1.1569	1.2157	1.2574	1.2840	1.3020
3M	1.1662	1.2160	1.2549	1.2821	1.2992
4M	1.1755	1.2166	1.2536	1.2795	1.2977
5M	1.1525	1.2073	1.2502	1.2775	1.2962

Kg. Uranium 233 Required at 1000 °K

Atom % Thorium in Blanket

Core Dia	0.5	1.0	1.5	2.0	2.5
1m	30.432	119.58	185.15	223.58	252.32
2m	65.612	368.68	613.8	781.31	898.74
3m	122.60	751.96	1304.0	1674.2	1934.8
4m	192.20	1268.9	2234.4	2903.3	3375.4
5m	428.95	2332.9	3745.8	4705.9	5382.2

Core Pressure at 1000 °K (bar)

Atom % Thorium in Blanket

Core Dia	0.5	1.0	1.5	2.0	2.5
1m	20.41	79.15	120.0	150.6	170.1
2m	5.90	30.77	51.19	67.9	75.91
3m	4.46	19.24	32.55	41.28	47.78
4m	3.51	14.90	24.19	30.15	35.70
5m	3.82	13.96	19.99	26.04	29.01

These results are encouraging since they indicate that a UF_6 breeder reactor with a 1 meter (3.28 ft) diameter and a 120 Kg (265 lbs.) critical mass could operate at a core pressure of about 80 bar (1160 psi) with a breeding ratio of 1.22, with only 1% thorium in the beryllium blanket. Also a reactor with a 2 meter (6.56 feet) diameter and 614 Kg (1354 lbs.) critical mass could operate at 50 bar (725 psia) with a breeding ratio of 1.26.

An analysis of the effect of structural materials on the performance of the gaseous core breeder estimated only a few percent loss in breeding ratio and less than one percent increase in critical mass and pressure.[6]

Recent studies on structural materials of the UF_6 breeder reactors pursued at Georgia Tech indicate that careful selection of coolant in the blanket is vitally important in the design of breeder reactor.

Nuclear Analysis

Analytical investigations of the nuclear characteristics of gaseous core reactors were begun in the mid 1950's as interest began to develop in the possibility of using reactors of this type for rocket propulsion. These calculations were one dimensional in nature and did not take into account complicating factors such as temperature distributions within the cavity and the effect of up-scattering of neutrons. Figure II-9 illustrates the critical mass as a function of reactor diameter and cavity void fraction for a cavity with length equal to its diameter, as calculated at the Jet Propulsion Laboratory using one-dimensional diffusion theory and the Fermi age approximation.[7] This figure illustrates some of the basic neutronics characteristics of cavity reactors. For example, there is a minimum cavity size at which the moderator can support a self-sustaining reaction in a thermal reactor.

At the Douglas Aircraft Corporation calculations were performed for a cavity reactor containing a central region of uranium surrounded by an annular

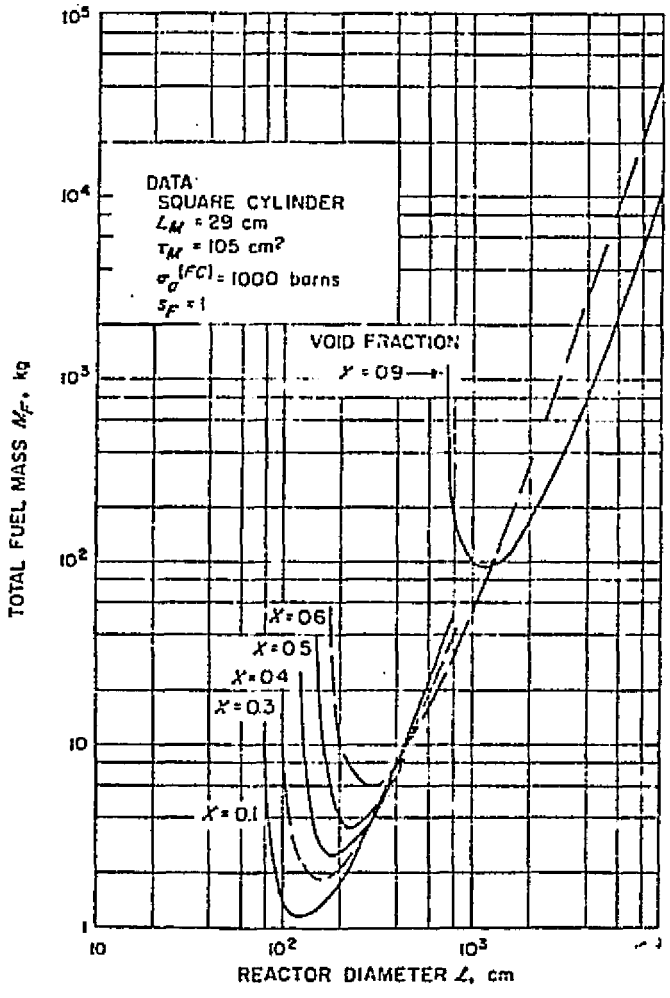

Figure II-9 Pu-239 Critical Mass in a Cylindrical BeO Moderated Cavity Reactor[4]

hydrogen zone contained within the reflector-moderator with a nozzle at the end of the chamber. One and two dimensional transport calculations were performed using 14 energy groups.[8] The difference in reactivity determinations between diffusion and S_8 transport theory was only 0.0005. These techniques were used to survey a variety of fuel materials, reflector materials, core geometries, and reflector thicknesses. Figure II-10 shows the critical mass in kilograms of U-235 versus core size for graphite and beryllium oxide reflectors with data given for various reflector thicknesses. For the graphite moderated reactor the minimum critical mass occurred for a cavity diameter of about 1.6 m. (5.25 ft.) and for beryllium oxide the minimum critical mass occurred for a 0.8 m. (2.62 ft) diameter. Beryllium oxide is a superior moderator because it slows down the neutrons closer to the core so that they have a greater probability of returning to the core to cause further fission, rather than leaking out of the system. Beryllium moderators typically have more neutron absorption than graphite, whereas graphite has a greater loss through leakage.

The nozzel of the reactor can have a significant effect on critical mass, causing it to increase as much as 50%. Both Figs. II-9 and II-10 fail to account for the presence of a nozzle.

One important neutronics aspect of cavity reactors is that the fuel temperature does not reflect very greatly on the neutron temperature. The neutron temperature is dominated by the temperature of the reflector. The fuel Doppler effect does have a minor influence, but the only important effect of the fuel temperature on the system results from the high pressure necessary to contain a critical mass of extremely hot fissioning plasma.

Researchers at the United Aircraft Corporation calculated the critical mass requirements for a vortex stabilized gaseous core reactor using one and two dimensional diffusion theory.[9] The length and diameter of the cylindri-

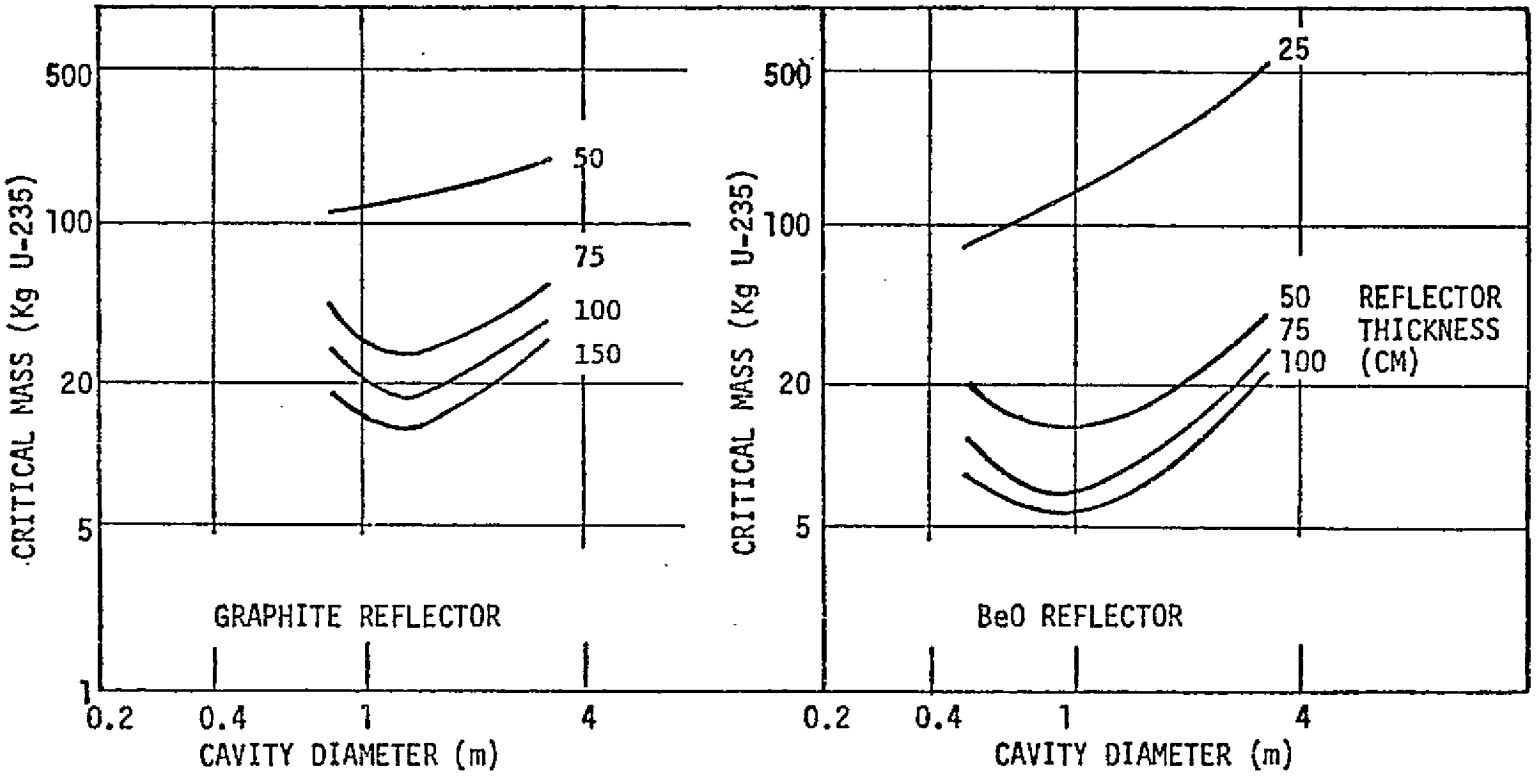

Figure II-10 U-235 Critical Mass of BeO and Graphite Moderated Spherical Cavity Reactors (Reflector Temperature 2800°K)[5]

cal cavity was taken to be equal to 1.83 m. (6 ft.), the cavity liner was composed of the tungsten-184 isotope (which has a lower cross section than natural tungsten), and the surrounding moderator region consisted of successive layers of beryllium, beryllium oxide, graphite, and heavy water. The calculations made allowances for an annular duct leading from the cavity to the exhaust nozzle, a fuel-injection port, voids in the moderator, the radial distribution of hydrogen temperature in the propellant region, and the radial fuel density distribution. In addition the moderator was considered to be surrounded by layers of natural tungsten and iron to simulate the external piping in the pressure vessel.

The critical mass of U-233 fuel in the cavity was calculated to be 22.7 kg. (50.1 lbs.). One dimensional calculations indicated that this critical mass could be reduced about 40% by using a cavity liner of beryllium tubes covered with niobium carbide coated graphite sleeves, instead of the tungsten-184. This result again indicates the importance of neutron absorbing materials at the moderator-core interface.

Researchers at the Kurchatov Institute for Atomic Energy in Moscow investigated acoustical instabilities in boty cylindrical and spherical gaseous fueled reactors.[14-16] The problem was formulated in the age diffusion approximation by applying the appropriate boundary conditions to develop an analytical solution which describes the development and amplification of fuel density oscillations as a function of reactor parameters. Acoustical oscillations and also total fuel mass oscillations, in which the fuel density varied simultaneously throughout the core volume, were considered for a variety of reactor parameters and system geometries. The acoustical oscillations were symmetric about the reactor center in the spherical reactor and were asymmetric in the cylindrical reactor, that is the oscillations propagated from the center to the wall and back again. It

was shown that the dynamic effects which occur in a gaseous core reactor during fuel density oscillations can be completely described by two terms: the dynamic reactivity and the variable component of the neutron flux. The dynamic reactivity is the net reactivity introduced by an oscillation over a complete cycle and the variable component of the neutron flux is the amplitude of the oscillation. The dynamic reactivity was shown to always be negative for beryllium and graphite moderated gaseous core reactors, but it could be positive for heavy water moderated reactors. Thus fuel density oscillations in beryllium and graphite moderated cavity reactors would tend to cause the reactor to shut down. Another result was that acoustical oscillations introduce a negative reactivity effect, except in the case of very slow oscillations along the channel axis of a cylindrical reactor, in which case the reactivity arises as a first order effect with respect to the oscillation amplitude.

Previous Studies in Georgia Tech (Nuclear analysis)

Exploratory calculations were performed at Georgia Tech for several very high temperature gas core breeder reactor configurations.[6] The computation method involved the use of the MACH-1 one-dimensional diffusion theory code[10] and the THERMOS integral transport theory code[11] for thermal cross sections. Results of the parametric survey showed that breeding ratios in the range of 1.06 - 1.12 could be obtained with critical masses of 300 to 850 kg. of U-233 for various material compositions in a 5 meter diameter cavity with a 0.5 meter thick blanket. The effects of changes in fissile material in the blanket were examined. The addition of structural material in the blanket decreased the breeding ratio by approximately 2% for 0.2 atom percent natural molybdenum or 4% for fully enriched molybdenum. The effect of changes in cavity temperature were also examined. MACH-1 was

used as the primary computational tool in these studies, and THERMOS was used to supply thermal neutron parameters to MACH-1. MACH-1 is a one-dimensional diffusion theory code with one thermal group (no upscatter) and Thermos is a one-dimensional integral transport theory code in the thermal range with complete upscattering. All the reactor configurations were spherical and hence amenable to one-dimensional analysis. For the MACH-1 code the 26 group ABBN cross section set of Bondarenko, et al. was used. The thermal group of the ABBN set is for 2200 m/sec. (0.0253 eV) neutrons and hence is not realistic for the high temperatures which can be produced in a gaseous core reactor. The THERMOS code was thus used to determine thermal cross sections to be inserted into the MACH-1 computation along with the ABBN set. For a given configuration the computational method was as follows:

1. Run MACH-1 with 26 group ABBN to estimate critical concentrations preliminary results.
2. Run THERMOS with 50 groups (up to 2.15 eV) using above concentrations and calculate spatial and spectral averaged cross sections.
3. Run MACH-1 with 22 fast groups from ABBN (2.15 eV) and thermal cross sections from THERMOS run.

Thus the final results of a computation may be thought of as a 23 group calculation with one thermal group using a thermal cutoff of 2.15 eV. Steps 2 and 3 were repeated if the final concentrations varied markedly from the estimates; steps 1 and 2 were omitted for very similar configurations. The high thermal cutoff value is required because of the possibility of a large increase in neutron energy due to upscatter in the hot gaseous core.

Explicit in all calculations were the assumptions associated with the two computer codes. Diffusion theory does not seem to be very restrictive based on previous comparisons to transport theory for gaseous fueled cavity

reactors. For example, Hall[8] found a difference of only 0.0005 in k_{eff} between diffusion and S_8 transport theory. THERMOS contains the assumption of isotropic scattering but this is felt to be reasonable at the energies involved (< 2.15 eV). More restrictive assumptions for the THERMOS runs were the slowing-down source and the U-233 resonances below 2.15 eV. The slowing-down source was assumed to be spatially independent; MACH estimates showed that the epithermal flux is rather flat in the cavity but decreases rapidly in the blanket region. This would imply then that the flat source assumption is rather good for the cavity and not good in the blanket. Since the temperature is not as high in the blanket and resonance capture is important in thorium, the results are not as sensitive to thermal cross sections for blanket materials as in the cavity. No Doppler broadening capabilities exist with THERMOS so these resonances were included at room temperature only. The assumption of no Doppler broadening should not be too severe since the resonances are very broad even at room temperature. Since only eight of the fifty THERMOS groups are used to span these resonances, the results were probably less sensitive to Doppler broadening than to the low number of groups in that interval.

A general assessment of the computational method and its assumptions was provided by analyzing a configuration previously analyzed by Whitmarsh[11] with a 3.05 m (10 foot) cavity diameter and 0.61 m (2 foot) thick reflector. An essentially equivalent configuration was obtained by reducing the number of regions and by homogenizing similar regions, then the computational method outlined previously was used to analyze this configuration. The THERMOS computational was performed for the cavity regions only. Final results gave a value of k of 0.986 as compared with 1.000 for Whitmarsh, a difference of only 1.4%. In light of the homogenization used to obtain a nearly equivalent configuration, the agreement indicates that the computational techniques

are valid for survey calculations. The largest source of discrepancy was attributed to the sensitivity to U-235 thermal cross sections. The agreement does show that his computational method should be sufficient to identify trends and perform parametric studies for various gaseous core nuclear reactors. All the configurations examined were spherical in geometry. The cavity region contained hydrogen as moderator/coolant and U-233 as fuel. The blanket consisted of graphite and thorium. The relative concentrations of the materials as well as the size of the regions were varied parametrically to examine a matrix of cases in an attempt to obtain the most feasible gaseous core thermal breeder concept. Some of the results are illustrated in Table II-6. Heat transfer and system analysis studies had estimated the bulk average cavity temperature in the reactor core to be in the range of 3000°K to 4000°K; thermal cross sections and pressures were calculated for the case of 4000°K. For the doubling time calculations a power level of 1000 MWt(th) was assumed. A higher power level shortens the doubling time proportionally.

Table II-6 Parametric Study of Relative Material Concentrations in a Gaseous Core Breeder Reactor[7]

Cavity H/U Ratio	Blanket C/Th Ratio	U-233 Mass (Kg)	Breeding Ratio	H Press (atm) (a)	H Press (atm) (b)	Doubling Time (yr) (c)
140/1	2/1	452	1.1026	710	514	9.6
	4/1	390	1.0962	612	443	8.9
	10/1	301	1.0636	472	342	10.3
100/1	2/1	576	1.1056	646	468	11.9
	4/1	494	1.0997	553	401	10.8
	10/1	375	1.0662	420	304	12.4
60/1	2/1	847	1.1029	569	413	17.8
	4/1	721	1.0966	485	351	16.2
	10/1	537	1.0635	361	261	18.4

(Cavity radius 250 cm, Blanket thickness 50 cm)

(a) Hydrogen partial pressure at 4000 °K, H_2 mole fraction 0.92.

(b) Hydrogen partial pressure at 3000 °K, H_2 mole fraction 0.99.

(c) For 1000 Mw (t), proportionally lower per higher average power.

REFERENCES FOR CHAPTER II

1. Kikoin, I. K., Dmitrievskii, V. A., et al., "Experimental Reactor with Gaseous Fissionable Substance (UF_6)", Proceedings of the 2nd International Conference on the Peaceful Uses of Atomic Energy, Vol. 2, p. 232, published in Moscow, 1959.

2. Masson, L. S., et al., "Cavity Reactor Gas-Core Critical Experiment", ANS Transactions, Vol. 10, No. 2, pp. 419-420, November, 1967.

3. Lofthouse, J. H. and Kunze, J. F., "Spherical Gas Core Reactor Critical Experiment", NASA CR-72781, February, 1971.

4. Williams, J. R., Clement, J. D. and Rust, J. H., "Analysis of UF_6 Breeder Reactor Power Plants". Progress Report No. 1, NASA Grant NSG-7067, November, 1974.

5. Dmitrievskii, V.A., Voinov, E. M. and Telelbaum, S. D., "Use of Uranium Hexafluoride in Nuclear Power Plants", Atomnaya Energiya, Vol. 29, No. 4, pp. 251-255, October, 1970 (in Russian).

6. Williams, J. R. and Clement, J. D., "Exploratory Study of Several Advanced Nuclear-MHD Power Plant Systems", Final Status Report, NASA Grant NGR-11-002-145, Georgia Institute of Technology, Atlanta, Ga., March, 1973.

7. Meghreblian, R. V. and Stumpf, H. J., "Gaseous Core Reactors", Proceedings of the 3rd Symposium on Advanced Propulsion Concepts, Vol. 1, pp. 293-342, October, 1962.

8. Holl, R. J., "Criticality of Gas Core Reactors", Proceedings of an Advanced Nuclear Propulsion Symposium, Los Alamos Scientific Laboratory Report LA-3229-MS, pp. 315-343, 1965.

9. Latham, T. S., "Nuclear Criticality Study of a Specific Vortex-Stabilized Gaseous Nuclear Rocket Engine", United Aircraft Corp. Research Laboratories, Report E-910375-1, October, 1966.

10. Meneley, D. A., et al., "MACH-1, A One-Dimensional Diffusion Theory Package", ANL-7223, 1866.

11. Toppel, B. J. and Baksys, I., "The Argonne-Revised THERMOS Code", ANL-7023, 1965.

12. Bondarenko, I.I., et al., Group Constants for Nuclear Reactor Calculations, Consultants Bureau, New York, 1964.

13. Whitmarsh, C. L., Jr., "Neutronics Analysis of an Open-Cycle High-Impulse Gas-Core Reactor Concept", NASA TM X-2534, April, 1972.

14. Blinkin, V. L. and Novikov, V. M., "On the Theory of Cavity Reactors with Compressible Fuel: II. Dynamic Reactivity Dependence on System Parameters", Kurchatov Atomic Energy Institute, Moscow, USSR, Report IAE-2140, 1971 (in Russian)

15. Novikov, V. M. and Blinkin, V. L., "On the Theory of Cavity Reactors with Compressible Fuel: I. Dynamic Characteristics in the Case of Fuel Density Oscillations", Kurchatov Atomic Energy Institute, USSR, Report IAE-2139, 1971 (in Russian).

16. Blinkin, V. L. and Novikov, V. M., "On the Theory of Cavity Reactors with Compressible Fuel: III. Dynamical Characteristics in the Case of the Periodical Configuration Changes", Institute of Atomic Energy, Report-2315, Moscow, 1973. (in Russian).

CHAPTER III

MATERIALS CONSIDERATIONS FOR THE GAS CORE BREEDER REACTOR

The design of the gas core breeder reactor required selection of materials for the reactor fuel, reactor blanket, core liner, reactor pressure vessel, system piping, and turbine blades. This chapter discusses the selection of these materials and summarizes some of the properties needed for the system design.

3.1 Reactor Fuel

The reactor design criteria specified a gaseous fuel. Since uranium hexafluoride is the only chemical compound of uranium that exists in a gaseous state at reasonable temperatures, UF_6 is the selected reactor fuel. Appendices A and B list thermodynamic and thermo-physical property data for UF_6.

3.2 Reactor Blanket

Several concepts were considered for the reactor blanket as discussed in Chapter VII. The final selection was to use a molten salt for the reactor blanket which is similar to the fuel used in the Molten Salt Breeder Reactor (MSBR).

The fuel salt used in the MSBR is $LiF\text{-}BeF_2\text{-}ThF_4\text{-}UF_4$ (71.7-16-12-0.3 mole %). In order to reduce parasitic neutron capture in the lithium, the lithium is enriched to 99.995% in Li^7. For use as a blanket for a gas core breeder reactor, the MSBR fuel has the UF_4 replaced with ThF_4 and the blanket composition becomes $LiF\text{-}BeF_2\text{-}ThF_4$ (71.7-16-12.3 mole %). This salt melts at

about 930°F, has a low vapor pressure at the operating temperature, and is stable in the proposed range of application (1000-1600°F). The blanket salt, with a vsicosity twice that of kerosene, a volumetric heat capacity close to that of water, and a thermal conductivity about twice that of water has adequate heat transfer characteristics and acceptable pressure losses due to flow. Some of the properties of the molten salt are given in Appendix C.

The $LiF-BeF_2-ThF_4$ salt has been found to be compatible with the materials in the system, modified Hastelloy-N, UF_6, etc. In reaching the final selection for an adequate blanket salt for the gas core breeder reactor, a blanket salt consisting of elements having the following qualities had to be picked:

a) low neutron capture cross section

b) thermally stable mixture

c) low operating pressure

d) non-aggressive toward other materials

e) able to survive fissioning of U and Pu

f) Tolerant of fission product accumulation without serious deterioration of its essential properties

g) low fuel cycle cost dependent on (1) ability to be reprocessed for turn around of unburned fissile material, (2) ability to recover bred fissile material, and (3) ability to remove fission product poisons.

Grimes[1] discusses why the fluorides form the only salts with acceptable absorption cross sections, stability, and melting temperature. This is due primarily to the stability of the ThF_4 in the salt since the ThF_4 is the weak link. Fortunately its high melting temperature is reduced with the addition of diluent fluorides (BeF_2 and LiF).

For successful operation of the reactor, the oxide contamination of the blanket must be kept at low levels. In addition, the ratio of LiF to BeF_2 should be high in order to keep the viscosity at the desirable low level. The BeF_2 concentration is advised to be kept in the range of 16 to 25% (for a ThF_4 concentration of 12%) in order to maintain the liquidus temperature below 932°F.

3.3 Structural Materials

3.3.1 Modified Hastelloy-N for Pressure Vessel and Piping

A material that has been developed for containing the molten salt blanket is an alloy which is a slight modification of the present commercial Hastelloy-N. The modified Hastelloy-N is very similar in composition and other related physical properties to standard Hastelloy-N. However, the modified version is superior because of its ability to resist helium embrittlement due to neutron irradiation. Helium embrittlement is the result of helium production in alloys due to the (n,α) reaction of boron under neutron irradiation. Boron is found in minute quantities in most alloys as a result of the manufacturing process. However, the amount of boron present is sufficient to result in serious damage to the alloy when it undergoes neutron irradiation.

The problem of irradiation embrittlement of Hastelloy-N has been solved by the addition of 2% titanium to the alloy.[2] Experiments have been performed on the modified Hastelloy-N in which it has been irradiated with a neutron fluence of 10^{22} nvt at 650°C and then stressed at 650°C. It appears that for stresses below 10,000 psi, irradiation has no effect on the stress-rupture properties, i.e. for stresses below 10,000 psi the material will have an "infinite" life.[2] Figure III-1 illustrates stress-rupture characteristics of modified Hastelloy-N for various neutron fluences.[2]

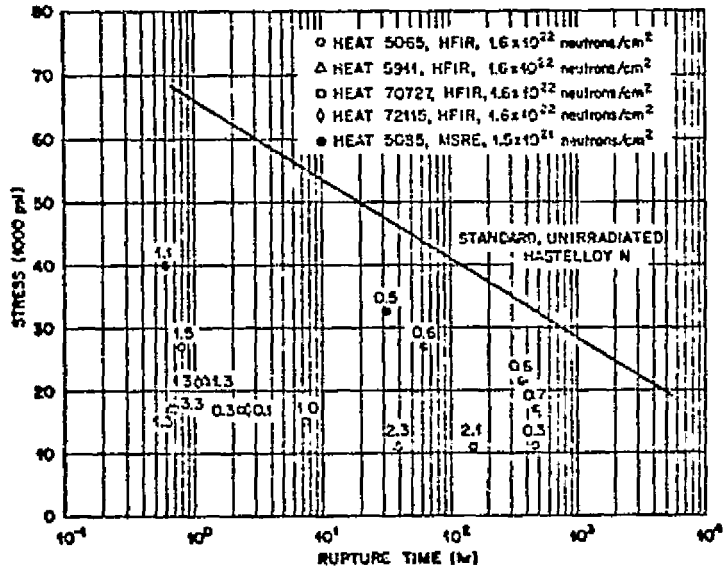

Fig. III-1 Stress-Rupture Properties of Several Heats of Hastelloy-N Irradiated at 650°C to the Indicated Thermal Neutron Fluence and Tested at 650°C. (The number by each point indicates the strain.)

Hastelloy-N is an alloy developed specifically for use with molten fluoride systems. Among the constituents, Cr is the least resistant to attack by fluorides. Fortunately, the Cr content of Hastelloy-N is low enough for the alloy to have excellent corrosion resistance toward the salts. Also, the Cr content is high enough for high oxidizing resistance.

Corrosion by fluoride salts is by selective chromium removal, thus alloys such as stainless steels with a high Cr content are more susceptible to corrosion.[2] For the molten salt used for the gas core breeder reactor blanket, the environment is moderately oxidizing and the corrosion process is dependent on the diffusion of chromium to the surface of the alloy and its subsequent removal. Under these conditions the Hastelloy-N exposed to the blanket salt should suffer no greater depth of chromium removal than 8 to 10 mils over a 30 year life.[3] If UF_6 is also only moderately oxidizing, then the rate of corrosion will also be dependent on the diffusion of chromium and hence the depth of chromium removal will also be 8 to 10 mils over a 30 year life.

From the standpoint of the MSBR project, all of the major questions with regard to the use of modified Hastelloy-N had been solved with the exception of the intergranular cracking of Hastelloy-N by tellurium.[2] The problem of intergranular cracking was not "discovered" until late in the MSBR project when the MSRE (Molten Salt Reactor Experiment) was shut down after three years of operation and its components examined. Intergranular cracking is the result of the diffusion of the fission product tellurium along the grain boundaries of the alloy where it combines with nickel to form a weak structural compound. Consequently, when the alloy is then stressed, cracks form along the grain boundaries.[2]

Tellurium forms a weak fluorine compound which is easily broken down resulting in tellurium being deposited on the alloy's surface thus beginning the intergranular cracking process. The cracking process increases with increasing tellurium concentration and the rate of deposition of tellurium. There is a slight increase in cracking with an increase in temperature from 650°C to 700°C. It has been found that intergranular cracking was significantly reduced and in some cases almost non-existent in alloys with a high chromium content, i.e., 15 to 16% and above. For example, type 304L stainless steel shows a high resistance to tellurium cracking. It is also theorized that the diffusion rate influences the depth of cracking. This tends to explain the effect of chromium, since the chromium concentration is directly related to the diffusion rate.[2] Based on conclusions drawn from the MSRE analysis, irradiation does not seem to be a major factor in intergranular cracking.[3]

In experiments with Hastelloy-N and other alloys, the chromium content was seen to have the greatest effect in reducing intergranular cracking, although the titanium content also may be beneficial in resisting tellurium cracking. This conclusion was drawn mainly from the fact that modified Hastelloy-N (2% Ti) showed better resistance to cracking than did standard Hastelloy-N. With regard to standard Hastelloy-N, minor changes in the composition yielded no significant results. Experiments also indicated that Al, Nb, and Ce might also help resist cracking.[2] There seems to be some confusion in the references as to the effects of stress on intergranular cracking.[2,4] A good summary of the results of the study of MSRE components (effects of Te) can be found in Ref. 4.

Since chromium reacts readily with tellurium to form a relatively stable compound which doesn't diffuse readily, it may be desirable to increase the

chromium content of the modified Hastelloy-N in order to reduce the effects of intergranular cracking. However, the question does arise as to whether the increased chromium content may cause increased corrosion problems with the molten blanket salt.

In case the intergranular cracking problem of Hastelloy-N cannot be solved, type 304L stainless steel is a possible alternative material. This is based on the operating experience of a fluoride salt loop built of this material. As of August, 1972, this loop had operated satisfactorily for 9 years at 1250°F and suffered only a 1.5 mil per year corrosion rate (estimated). However, a close control of the oxidation state is required. The problem of the irradiation embrittlement of the stainless steel has been solved by the addition of 0.2% titanium. The remaining question is whether or not the corrosion rate can be reduced to an acceptable level by either lowering the temperature or by alloy changes.[3] The question then arises with regard to alloy changes as to whether or not type 304L stainless steel can be made corrosion resistant without reducing its resistance to Te intergranular cracking.

Another possible alternative is the use of modified Hastelloy-N in combination with a Monel 404 liner on the core side. In a telephone conversation with Jack Davant of Oak Ridge National Laboratory, it was determined that Monel 404 could be welded to Hastelloy-N, and both would be corrosion resistant. However, at the operating temperatures there could be an expansion deviation between the two of about 0.25 inch. This number came from an extrapolation of the known data at room temperature, since there are no published data about Monel 404 at the desired temperatures.

Theoretically then, modified Hastelloy-N and Monel 404 can be used together as reactor materials. However, if the expansion deviation is much

greater than 0.25 inch, this option is removed.

Properties of Monel 404 (Ni-55%; Cu-44%; Mn-0.01%; Fe-0.05%; C-0.06%) at 77°F are given in Table III-1.

Table III-1

Properties of Monel 404 at 77°F[5]

Form and Condition	Rod, Hot Rolled
Yield S. (0.2% offset)	3.1×10^4 psi
Tensile S.	6.9×10^4 psi
Elongation in 2 inches	45%
Hardness	R_b 67
Specific Gravity	8.88
Melting Point	2460°F
Thermal Expansion Coefficient	7.4×10^{-6} in./in./°F
Tensile Mod. of Elasticity	25×10^6 psi

3.3.2 Turbine Blades

From ANL-7241, it was noted that Inconel alloys had reasonable corrosion resistance to UF_6 as well as good structural properties at 1200°F. Therefore, nickel based, high temperature, high strength alloys were checked. Such alloys as TD-Nickel, Alloy 713 C, Alloy 701, Mar M246, M-252, etc. were eliminated because they either contained boron or cobalt. Boron is undesirable because it is a poison which would have to be removed in a reprocessing loop before reentering the reactor. Cobalt is easily activated, making turbine maintenance difficult.

Pratt and Whitney Aircraft has developed a process for casting high strength gas turbine blades from standard nickel based alloys. Therefore, regular Inconel alloys could be investigated for use in the UF_6 turbine. By eliminating grain boundaries that lie perpendicular to the principal stress axis (this axis lies parallel to the length of the blade), the earlier processes imparted ductility and thermal shock resistance to creep-resistant nickel-base super-alloys. The newer process, by eliminating all grain boundaries, produces a superior material when it is applied to Mar-M1200 and similar alloys. This is the first of a new family of gas-turbine materials that are called "monocrystaloys." It has, for example, exceptional thermal shock resistance since it has not cracked during 2400 shock cycles between room temperature and 2200°F.[6]

The two best Inconel candidates, Inconel 718 and Inconel X-750, were examined because of their superior strength properties with respect to all other Inconel alloys. Based upon a telephone conversation with Luke Yrkovich of International Nickel, Inconel X-750 was ultimately chosen because of its excellent corrosion resistance to UF_6, as well as for its superior strength properties.

Inconel X-750 is an age-hardenable, nickel-chromium alloy used for its corrosion and oxidation resistance, and high creep rupture strength at temperatures up to 1500°F. The alloy, also containing aluminum and titanium, is made age hardenable by the combination of Al and Ti with Ni to form gamma prime--the intermetallic compound $Ni_3(Al,Ti)$. Although much of the effect of age hardening is lost with increasing temperatures over 1300°F, the fully heat-treated or directly aged alloy will still have useful strength up to 1800°F.[7] Therefore, it is reasonable to assume that the turbine blades should be constructed entirely of Inconel X-750.

3.4 Conclusions and Recommendations

3.4.1 Blanket Salts

The blanket salt composition was chosen on the basis of neutron cross section, viscosity, chemical stability, and liquidus temperature. There is little uncertainty with regard to its phase behavior, its physical properties, and its interaction with the container and moderator materials.

More uncertain, however, are the effects of oxidation-reduction state[8] of the salt on its surface tension, and on the behavior of the noble metal fission products. Significant limitations on the blanket salt are imposed by the rather high liquidus temperature (932°F), and the restricted choice of containment material.

The problem that should be looked into is the production of relatively large amounts of tritium by neutron interaction with the lithium.

Variations of the blanket composition are possible and may prove desirable, to mitigate some of the aforementioned limitations. The ThF_4 concentration may be varied as required, even for such things as optimization of the breeding ratio. The processing is expected to keep the oxide concentration in the fuel low.

The constraints of high LiF temperature and high tritium levels cannot be circumvented. Since the reactor is to breed with thermal neutrons, the cross sections limit the choice of diluent salt constituents to the fluorides of Be and Li. The tritium production could be cut to not much more than fission yield, if a $NaF-ZrF_4-ThF_4$ blanket salt were used. But, neutron absorption in the Na and Zr would eliminate breeding. If the reactor is to breed, there is no alternative.

3.4.2 Component Materials

Hastelloy-N, modified with 2% Ti, is the main choice for the core and

blanket construction. Although additional work is required to solve the problem of tellurium intergranular cracking, preliminary results indicate this problem can be resolved satisfactorily.

With regard to the design stresses of modified Hastelloy-N, if extrapolation of values from the test results does not prove to be satisfactory, then the operating temperature and total neutron fluence that the components are subject to must be reduced. Theoretically, the irradiation should be limited to the extent that the creep ductility will not be less than 5%. Based on the available data, a maximum design stress of 10,000 psi is recommended when the material is subject to 650°C and a neutron fluence of 10^{20} nvt over a 30 year period.

Inconel X-750 is recommended for use as the turbine blade material in the power conversion unit.

REFERENCES FOR CHAPTER III

1. Grimes, W. R., "Molten Salt Reactor Chemistry," Nuclear Applied Technology 8(2), 137-145 (February 1970)

2. "Molten-Salt Reactor Program Semi-Annual Progress Report for Period Ending August 31, 1972," ORNL-4832, pp. 63-86 and 117-127 (1972)

3. "The Development Status of Molten-Salt Breeder Reactors," ORNL-4812, pp. 196-216 (August 1972)

4. McCoy, H. E. and B. McNabb, "Intergranular Cracking of INOR-8 in the MSRE," ORNL-4829, pp. 159-169 (November 1972)

5. "Properties of Some Metals and Alloys," International Nickel Co., Inc., New York, 1968.

6. Pearcey, B. J. and F. L. Ver Snyder, "Monocrystaloys: A New Concept in Gas Turbine Materials," Advanced Research and Development Laboratory, Pratt and Whitney Aircraft Report No. 66-007 (February 1966)

7. "Engineering Properties of Inconel X-750," Technical Bulletin T-38, International Nickel Co., Inc., New York, 1963

8. "Conceptual Design Study of a Single-Fluid Molten-Salt Breeder Reactor," ORNL-4541 (June 1971)

IV. NUCLEAR ANALYSIS

One and Two Dimensional Diffusion Theory Calculations

Several analyses[1,2,3] of the gas core nuclear reactor have been performed. For examining a broad range of designs, one may utilize multigroup diffusion theory to observe trends and perform parametric studies in order to identify concepts for further study.

The first phase in performing exploratory nuclear analysis for the gaseous core nuclear reactor involved implememting the necessary computational tools and formalizing a computational method. The major portion of the effort early in the study was devoted to this area. In order to expedite this phase, the MACH-I code[4] was used as the primary computational tool in the nuclear analysis. To allow a more realistic model of thermal neutron processes in the high temperature gaseous core reactor concept, the THERMOS code[5] was implemented to supply thermal neutron parameters to MACH-I.

One dimensional survey calculations were carried out for a UF fueled core surrounded by a molten salt blanket as shown in Fig. IV-1. Table IV-1 lists the composition of the coolant in the blanket. Later, two-dimensional calculations were made with r-z geometry using the EXTERMINATOR program.

The spherical reactor configurations were amenable to one-dimensional analysis. For the MACH-I code the 26 group ABBN cross section set of Bondarenko, et al.[6] was used. The thermal group of the ABBN set is for 2200 m/sec (0.0253 eV) neutrons and hence is not realistic for the high temperatures which can be produced in a gaseous core reactor. In some cases the thermal cross sections were taken as Maxwellian. In other cases the THERMOS code was used. The THERMOS code was thus used to determine thermal cross sections to be inserted into the MACH-I computation along with the

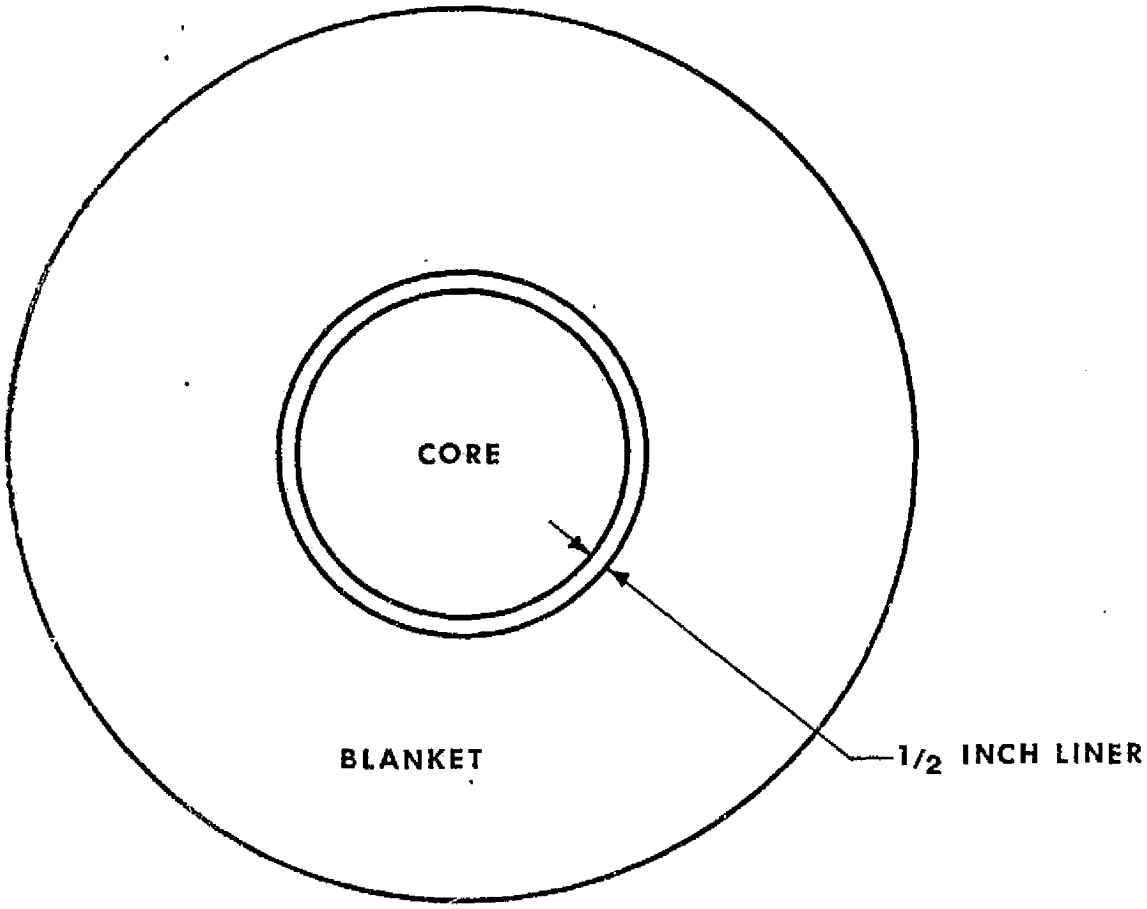

CORE -- $U^{233}F_6$

BLANKET -- BeF_2, ThF_4, Li^7F

LINER -- ONE-HALF INCH MONEL LINER - Cu AND Ni

FIG. IV-1. Spherical UF_6 Reactor

TABLE IV-1

COMPOSITION OF COOLANT IN BLANKET

	MOLE %	VOLUME %	DENSITY (Gr/cm^3)
LiF*	71.7	42.28	2.635
BeF_2	16.0	22.08	1.986
ThF_4	12.3	35.00	6.32

*The Li is 99.99% Li^7 because Li^6 has a large thermal absorption cross section.

ABBN set. For a given configuration the computational method was as follows:

1. Run MACH-I with 26 group ANNB to estimate critical concentrations preliminary results.
2. Run THERMOS with 50 groups (up to 2.15 eV) using above concentrations and calculate spatial and spectral averaged cross sections.
3. Run MACH-I with 22 fast groups from ANNB (2.15 eV) and thermal cross sections from THERMOS run.

Thus the final results of a computation may be thought of as a 23 group calculation with one thermal group using a thermal cutoff of 2.15 eV. Table IV-2 lists the energy groups for the MACH Calculations. Steps 2 and 3 were repeated if the final concentrations varied markedly from the estimates; steps 1 and 2 were omitted for very similar configurations. The high thermal cutoff value is required because of the possibility of a large increase in neutron energy due to upscatter in the hot gaseous core.

Implicit in all calculations were the assumptions associated with the two computer codes. Diffusion theory does not seem to be very restrictive based on previous comparisons to transport theory for gaseous fueled cavity reactors. For example, Hall found a difference of only 0.0005 in k_{eff} between diffusion and S_8 transport theory. THERMOS contains the assumption of isotropic scattering but this is felt to be reasonable at the energies involved (<2.15 eV). More restrictive assumptions for the THERMOS runs were the slowing-down source and the U-233 resonances below 2.15 eV. The slowing-down source was assumed to be spatially independent; MACH estimates showed that the epithermal flux is rather flat in the cavity but decreases rapidly in the blanket region. This would imply then that the flat source assumption is rather good for the cavity and not good in the blanket. Since the temperature is not as high in the blanket and resonance

TABLE IV-2

MACH-I ENERGY GROUP SCHEME

GROUP NO.	ENERGY	RANGE
1	6.5-10.5	MeV
2	4.0-6.5	MeV
3	2.5-4.0	MeV
4	1.4-2.5	MeV
5	0.8-14	MeV
6	0.4-0.8	MeV
7	0.2-0.4	MeV
8	0.1-0.2	MeV
9	46.5-100	keV
10	21.5-46.5	keV
11	10.0-21.5	keV
12	4.65-10.0	keV
13	2.15-4.65	keV
14	1.0-2.15	keV
15	465-1000	eV
16	215-465	eV
17	100-215	eV
18	46.5-100	eV
19	21.5-46.5	eV
20	10.0-21.5	eV
21	4.65-10.0	eV
22	2.15-4.65	eV
23	1.0-2.15	eV
24	0.465-1.0	eV
25	0.215-0.465	eV
26	0.0252	eV

capture is important in thorium, the results are not as sensitive to thermal cross sections for blanket materials as in the cavity. No Doppler broadening capabilities exist with THERMOS so these resonances were included at room temperature only. The assumption of no Doppler broadening should not be too severe since the resonances are very broad even at room temperature. Since only eight of the fifty THERMOS groups are used to span these resonances, the results were probably less sensitive to Doppler broadening than to the low number of groups in that interval.

A general assessment of the computational method and its assumptions was provided by analyzing a configuration previously analyzed by Whitmarsh with a 3.05 m (10 foot) cavity diameter and 0.61 m (2 foot) thick reflector. An essentially equivalent configuration was obtained by reducing the number of regions and by homogenizing similar regions, then the computational method outlined previously was used to analyze this configuration. The THERMOS computational was performed for the cavity regions only. Final results gave a value of k_{eff} of 0.986 as compared with 1.000 for Whitmarsh, a difference of only 1.4%. In light of the homogenization used to obtain a nearly equivalent configuration, the agreement indicates that the computational techniques are valid for survey calculations.

The major goal after completing the one-dimensional calculations was to do two-dimensional calculations. Instead of using a spherical core as was done previously using MACH-I, a cylindrical core was analyzed utilizing EXTERMINATOR II,[7] a two-dimensional diffusion theory code. This code enabled us to get fluxes in the (r-z) direction and, from these point-wise fluxes, the reactor breeding ratio could be calculated.

The first problem encountered when using EXTERMINATOR II is how to calculate the region and energy dependent microscopic cross-sections which are input for EXTERMINATOR. This was achieved by using MACH-I for 26

groups and collapsing these to 4 groups (thermal) for use in EXTERMINATOR. The MACH-I cross-section library, however, did not contain any cross sections for fluorine and these cross sections (σ_a, σ_s) had to be found from another source and then input into the MACH-I library before being collapsed into 4 groups. The cross-sections obtained for fluorine were from a 123 group set and had to be collapsed into a 26 group set for use in the MACH library. The 26 group flux spectrum from a previous MACH-I run was used as the weighting parameter when collapsing the 123 group set into 26 groups. The collapsed fluorine cross sections were then input into the MACH-I cross-section library where 4 group cross-sections were obtained for the desired dimensions and compositions. Dashed lines on Table IV-1 indicate the four energy groups for EXTERMINATOR. These region and energy dependent cross-sections were then used in EXTERMINATOR. Various EXTERMINATOR runs were made to get k_{eff} equal to 1.0, with the dimensions of the core being the varied parameter to get k_{eff} equal to 1.0. The height of the core was taken to be twice the radius. The core was surrounded by a half-inch Hastelloy-N liner and this was in turn surrounded by the molten salt blanket. This was the same arrangement as in the previous one-dimensional case.

Figure IV-2 is a diagram of the geometry used for the two-dimensional EXTERMINATOR calculations. Three axial regions were used in the core to match the axial temperature distribution more accurately. Table IV-3 summarizes assumptions made in the calculations.

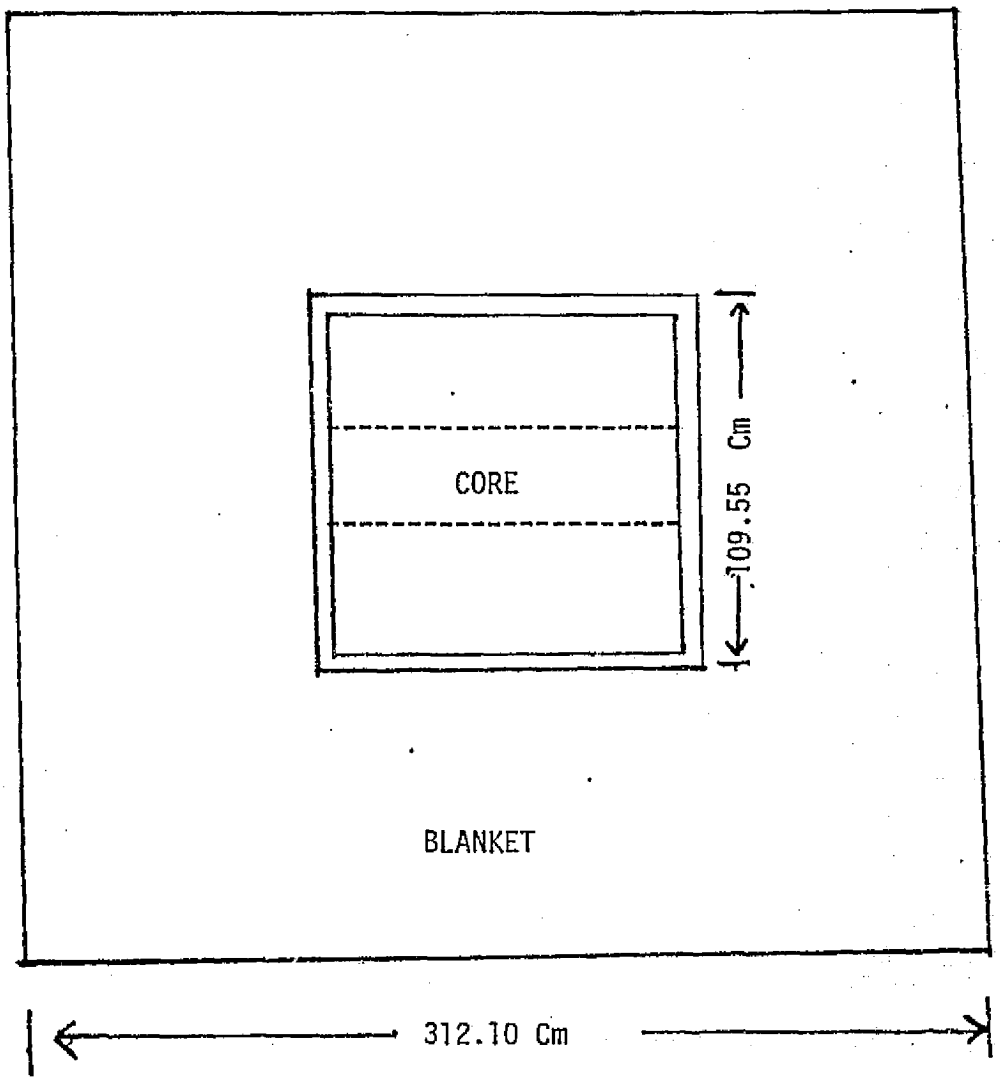

FIG. IV-2. Cylindrical UF_6 Reactor

(critical configuration using 4 group cross section)

TABLE IV-3

TWO DIMENSIONAL CALCULATIONS

-- CYLINDRICAL CORE WITH REFLECTOR WAS DIVIDED INTO 3 REGIONS AXIALLY.

-- TEMPERATURE DISTRIBUTION IN THE CORE IS LINEAR WITH Tin = 1071^{o}R, Tout = 1560^{o}R

-- AVERAGE TEMPERATURE IN EACH REGION WAS USED TO COMPUTE INPUT CROSS SECTIONS

-- 26 ENERGY GROUP INDIVIDUAL ISOTOPE INPUT CROSS SECTIONS WERE COLLAPSED INTO REGION-AVERAGED 4 ENERGY GROUP CROSS SECTIONS USING MACH-I COMPUTER CODE

-- 4 GROUP CROSS SECTIONS FROM MACH-I WAS INPUTED TO EXTERMINATOR-II TO CALCULATE

(1) CRITICAL DIMENSION

(2) CRITICAL MASS

(3) FISSION DENSITY AS FUNCTION OF POSITION

-- IN THE CALCULATION OF BREEDING RATIO, 26 GROUP CROSS SECTIONS OF Th^{232}, AND U^{233} WERE COLLAPSED INTO REGION-AVERAGED 4 ENERGY GROUP CROSS SECTION MANUALLY WITH FLUX WEIGHT.

$$B.R. = \frac{\sum_j \sum_i \Sigma_{ii}^{Th-232}{}_c \phi_{ij} V_j}{\sum_j \sum_i \Sigma_{ij}^{U-233}{}_a \phi_{ij} V_j}$$

i = ENERGY GROUP i

j = SPATIAL REGION j

Heat Generation in Molten Salt Blanket

Neutrons give rise to heat generation in non-fissile materials through four primary interactions: elastic scattering (n,n); charged particle ejections, particularly (n,α) and (n,p); inelastic scattering (n,n'γ); and radiative capture (n,γ). These four processes may be conveniently divided into two classes, direct and indirect, according to whether the heat is deposited at the site of the primary interaction or some distance away.

Elastic scattering and charged particle ejection reactions are direct heat generation processes in that the energy of the struck nucleus, or the alpha particle or proton, is converted to heat in the solid or liquid within distances of less than a millimeter from the site of the primary interaction.

Radiative capture is an indirect heat generation process since the gamma rays that are produced in the reaction are absorbed at various distances, often many centimeters, from the site of the primary interaction. The primary interaction, therefore, serves only as a source for the gamma rays. The kinetic energy given the nucleus as it recoils to conserve momentum when emitting the gammas is generally only of the order of 10 eV, and so may be neglected in heating calculations.

Inelastic scattering gives rise to both direct and indirect heat generation. The daughter nucleus, which recoils to conserve momentum upon emitting the inelastic neutron, deposits its kinetic energy at the site of the primary interaction. The gamma rays which are subsequently emitted by the excited nucleus deposit their energies at various distances from the site, just as do capture gammas.

The following energies per core fission were estimated deposited in the blanket:

TABLE IV-4

ENERGY DEPOSITION IN BLANKET PER FISSION

Reaction	Energy Deposition/Fission (MeV/Fission)
Neutrons from U-233 Fission	4
Prompt Gammas	3
Fission Product Gammas	0.5
(n,γ) in Thorium-232	9
Fissioning in Blanket	1.96
β^- from Th-233 Decay	0.5
β^- from $_{91}Pa^{233}$ Decay	0.1
Total	19.06

Because at the present time all calculations have been done for spherical geometries it was decided that a rough calculation of heat deposited in the blanket was sufficient. A more detailed analysis should wait until a two dimensional code can be used to calculate neutron fluxes and reaction rates.

In the fission process of U-233, 5 MeV goes into kinetic energy of the neutrons. Since almost all of the thermalization is done in the blanket, it was estimated that 4 MeV was deposited there. It was assumed that 3 MeV of the 7 MeV prompt gamma energy is deposited in the blanket. There will be some gamma energy deposited from fission product decay. This is normally 7 MeV; however, since the core is continuously being cleaned by reprocessing, most of these decays occur away from the core and it was assumed that only .5 MeV is deposited in the blanket.

When Th-232 absorbs a neutron, it undergoes an (n,γ) reaction to reach the ground state. The gamma energy is 7.5 MeV and since there are 1.2 reactions per fission with the breeding ration currently calculated, 9 MeV is deposited from this source. From the MACH code it was found that 1% of the total fissions occurs in the blanket. Thus 1.96 MeV is available per fission

in the system. The thorium decay scheme has two decays:

$$^{233}Th \xrightarrow{\beta^-} {}^{233}Pa \xrightarrow{\beta^-} {}^{233}U$$

These β^-'s have energy of 1.23 MeV and .25 MeV. Multiplying by 1.2 gives 1.5 MeV and .30 MeV per fission in the system.

Adding these energies gives a total of 20.25 MeV/fission. Since there is 196 MeV of recoverable energy per fission, the percent of heat generated in the blanket is about 9.72%

There is a $Li^6(n,\gamma)$ reaction, but the atom density of Li^6 is so low that this energy is negligible compared to that from other sources.

Results and Conclusions

Figure IV-3 presents a graph of the one dimensional results showing the effect of blanket thickness on the breeding ratio and critical mass. A blanket thickness of 90 centimeters corresponds to a breeding ratio of 1.18, and the breeding ratio does not increase as more blanket is added. On concludes that 90 centimeters is an optimum choice for the blanket thickness.

Figures IV-4 and IV-5 presents radial and axial power density distributions due to fissioning from the EXTERMINATOR results. Notice the fission density is relatively flat in the radial direction. The discontinuity in the axial fission density (Figure IV-5) is of course due to the regionwise representation in the EXTERMINATOR input, and is not a real phenomenon.

Figure IV-6 is a graph of the energy dependent fission density in the core. The median fission energy is 300 keV. Figures IV-7 and IV-8 are the group fluxes vs energy averaged over the core and reflector, respectively. The median flux in the core is 600 keV in the core and 34 keV in the blanket.

Figures IV-9 and IV-10 are graphs which show the effect on the spectrum of adding moderator (Be and graphite, respectively) to the molten salt blanket. As shown in Figure IV-9, the median neutron energy increases from 34 keV (zero % Be) to 73 keV (25% Be) and drops to 4.65 eV (75% Be). For carbon the median energy increases to 56 keV (25% C) and drops to 7 keV (75% C).

When changing the composition of blanket material from 100% molten salt (LiF, BeF_2 and ThF_4) to 75% molten salt and 25% carbon, we are reducing the atom density of lithium in blanket, which is a better moderator than carbon; therefore, the spectrum in the blanket region becomes harder. When the volume percent of carbon increases to 50%, there is a large increasing of atom density of carbon and a small decreasing of atom density of lithium. Since the effectiveness of moderator has to do with both atom density and cross sections,

the increasing of atom density of carbon may overcome the fact that some lithium is replaced by carbon (or beryllium). Table IV-5 and IV-6 show the effect on median energy, breeding ratio and critical radius when the composition of the blanket material is changed from 100% molten salt to 100% carbon and beryllium, respectively.

Table IV-7 summarizes and compares results of the one dimensional MACH calculations and the two dimensional EXTERMINATOR calculations. The four group spherical case was in reasonable agreement with the 26 group case, so one concludes that the change in going to four groups had a negligible effect on the calculated breeding ratio. The breeding ratio of 1.21 for the two dimensional reactor looks promising.

Further Work

Many areas, especially those itemized in Table IV-8, must be studied further in order to achieve a complete nuclear analysis.

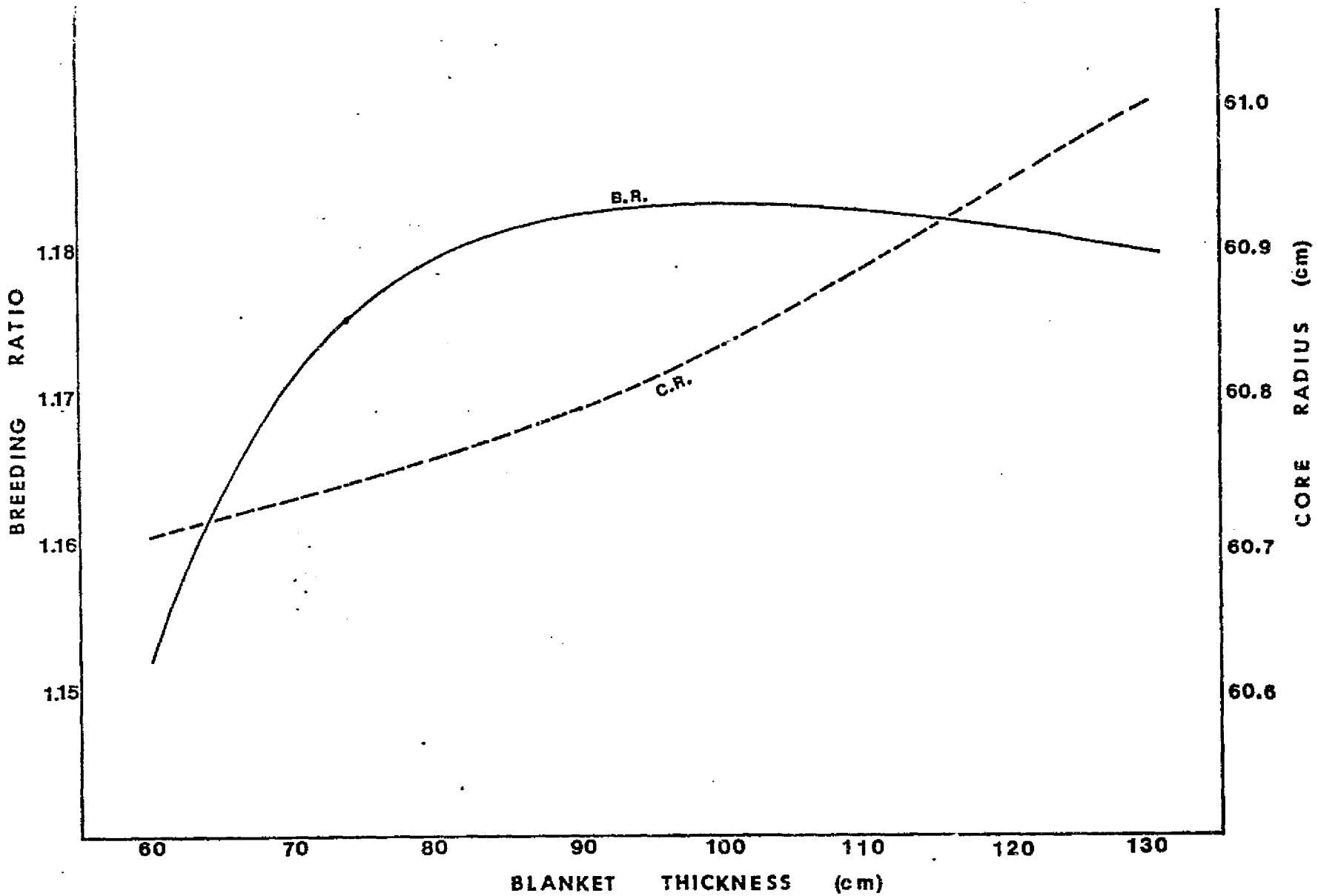

FIG. IV-3. MACH-I SURVEY OF BLANKET THICKNESS EFFECTS ON BREEDING RATIOS AND CORE RADIUS

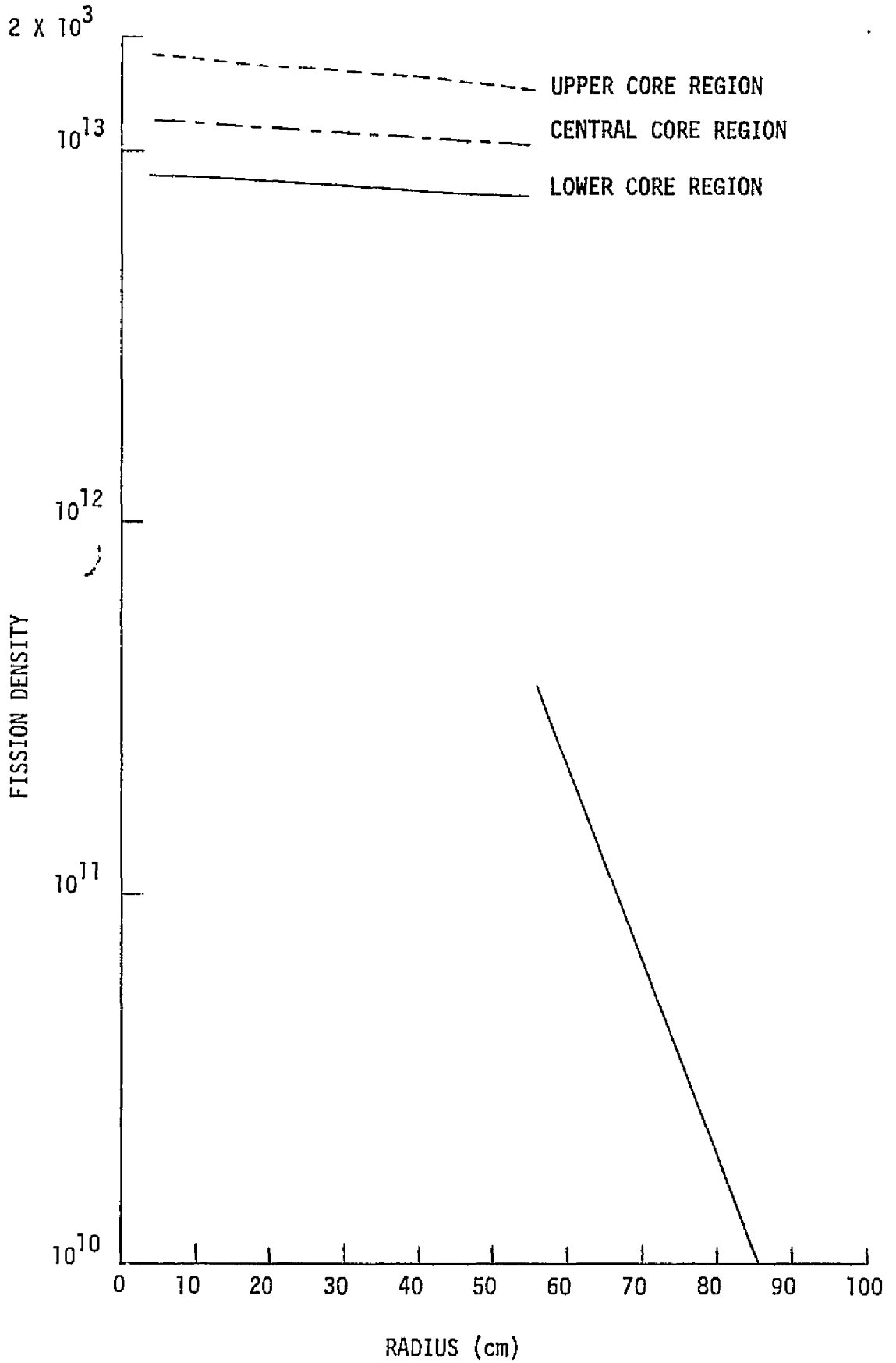

Fig. IV-4.
FISSION DENSITY DISTRIBUTION IN THE RADIAL DIRECTION OF THE CYLINDRICAL REACTOR

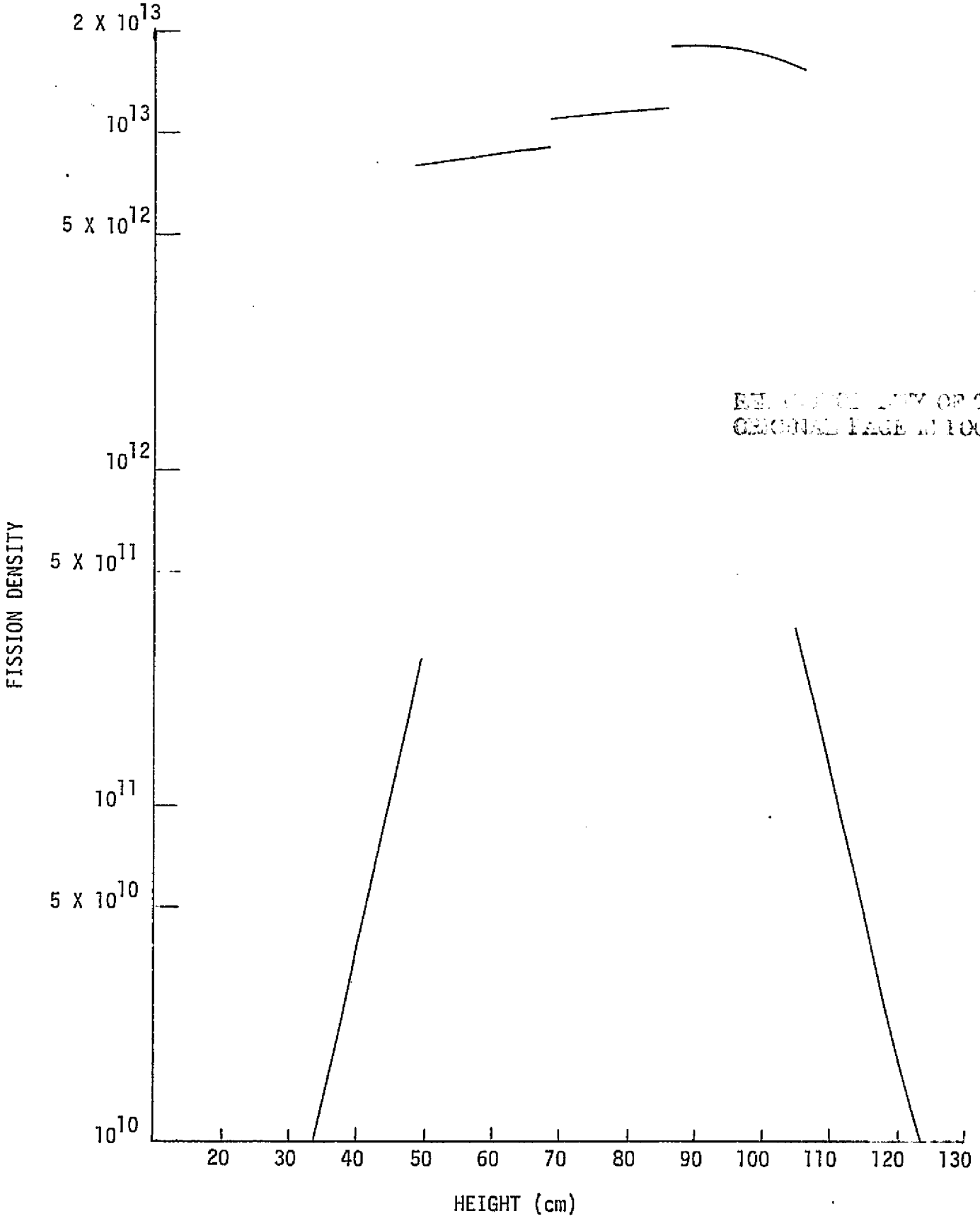

Fig. IV-5.
FISSION DENSITY DISTRIBUTION IN THE AXIAL DIRECTION OF THE CYLINDRICAL REACTOR

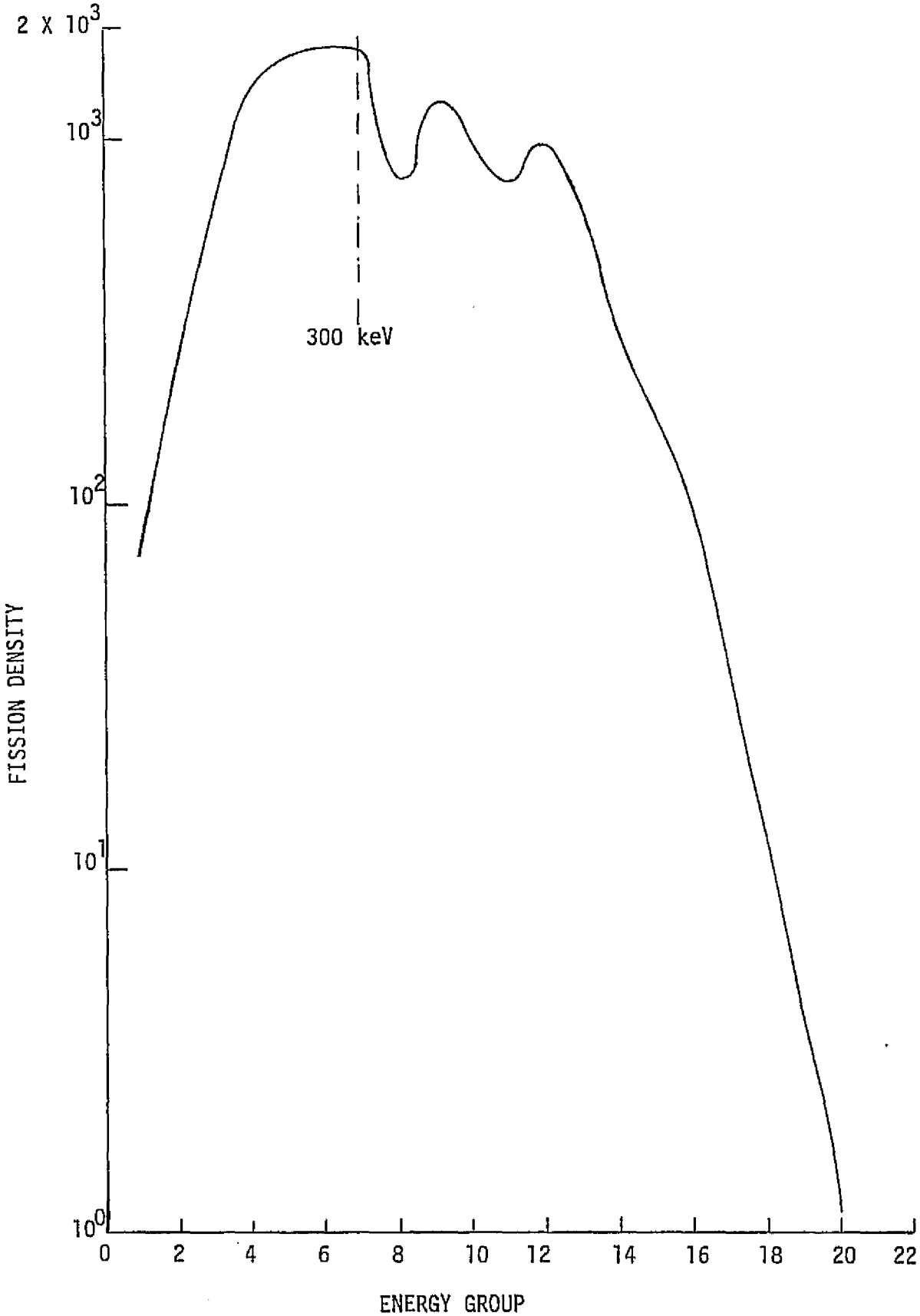

Fig. IV-6.
FISSION DENSITIES VS ENERGY GROUP IN 26 GROUP SPHERICAL CALCULATION

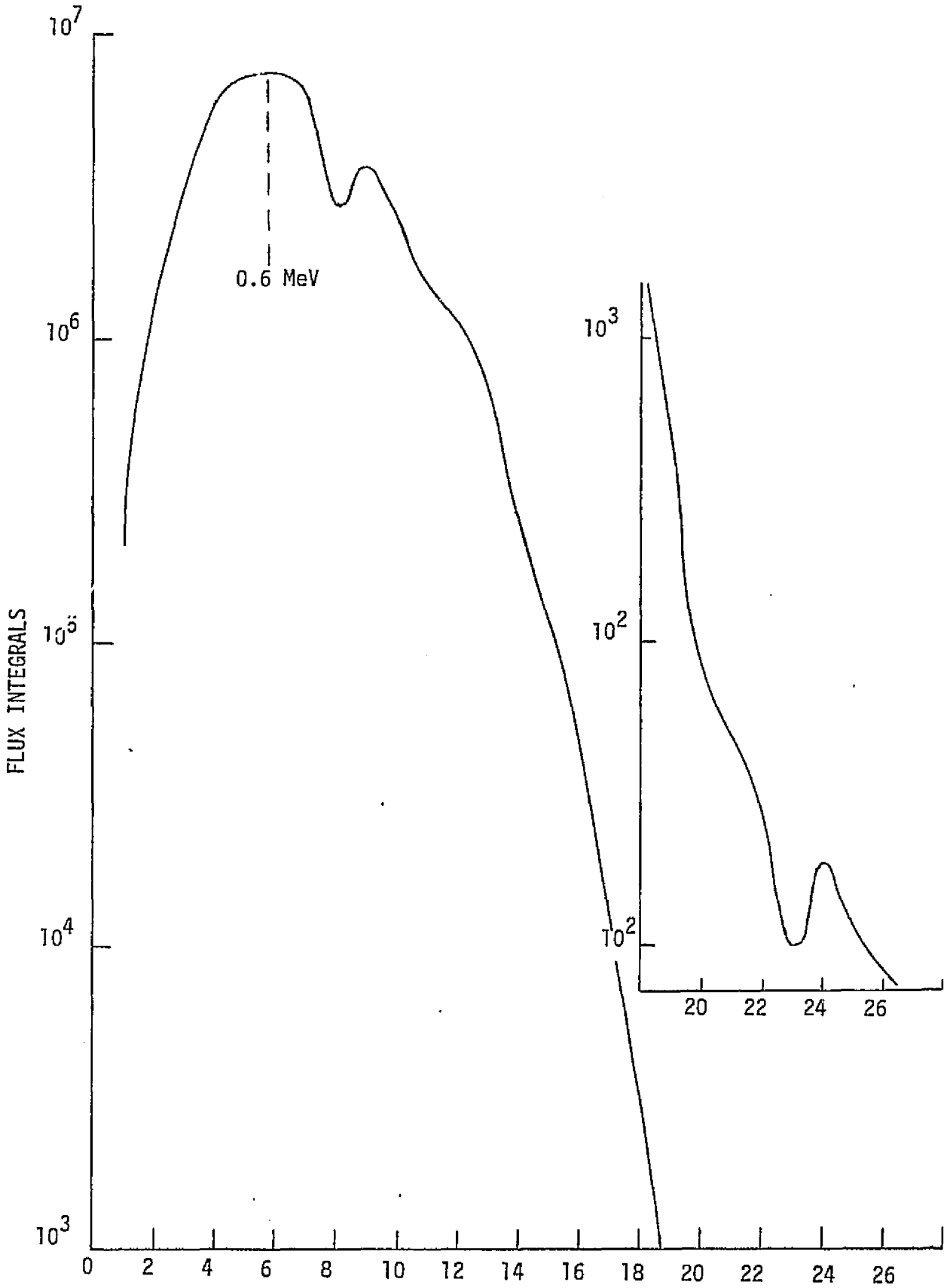

Fig. IV-7.
FLUX INTEGRALS VS ENERGY GROUP IN CORE REGION OF 26 GROUP SPHERICAL CALCULATION

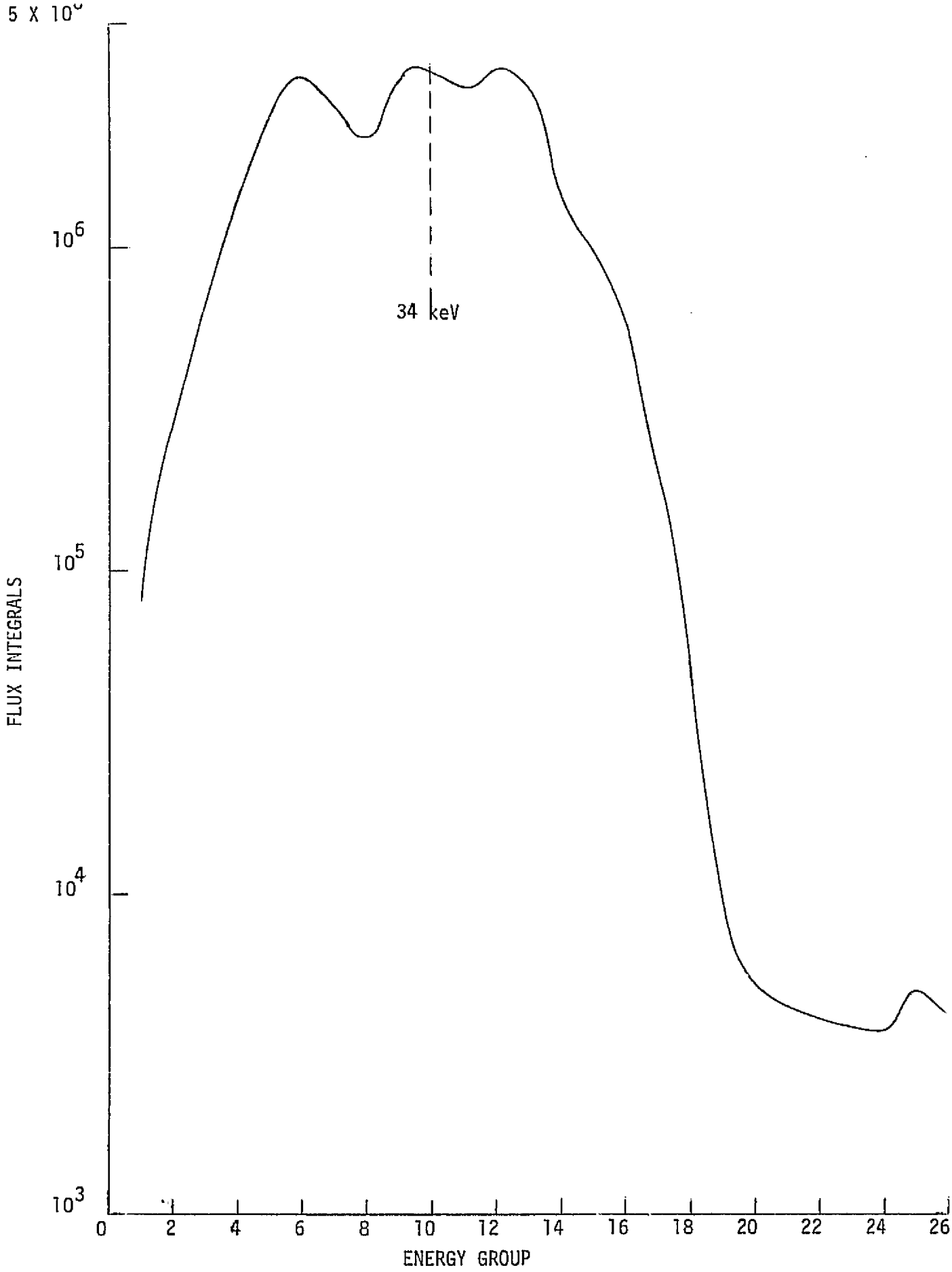

Fig. IV-8.
FLUX INTEGRALS VS ENERGY GROUP IN BLANKET REGION OF 26 GROUP SPHERICAL CALCULATION

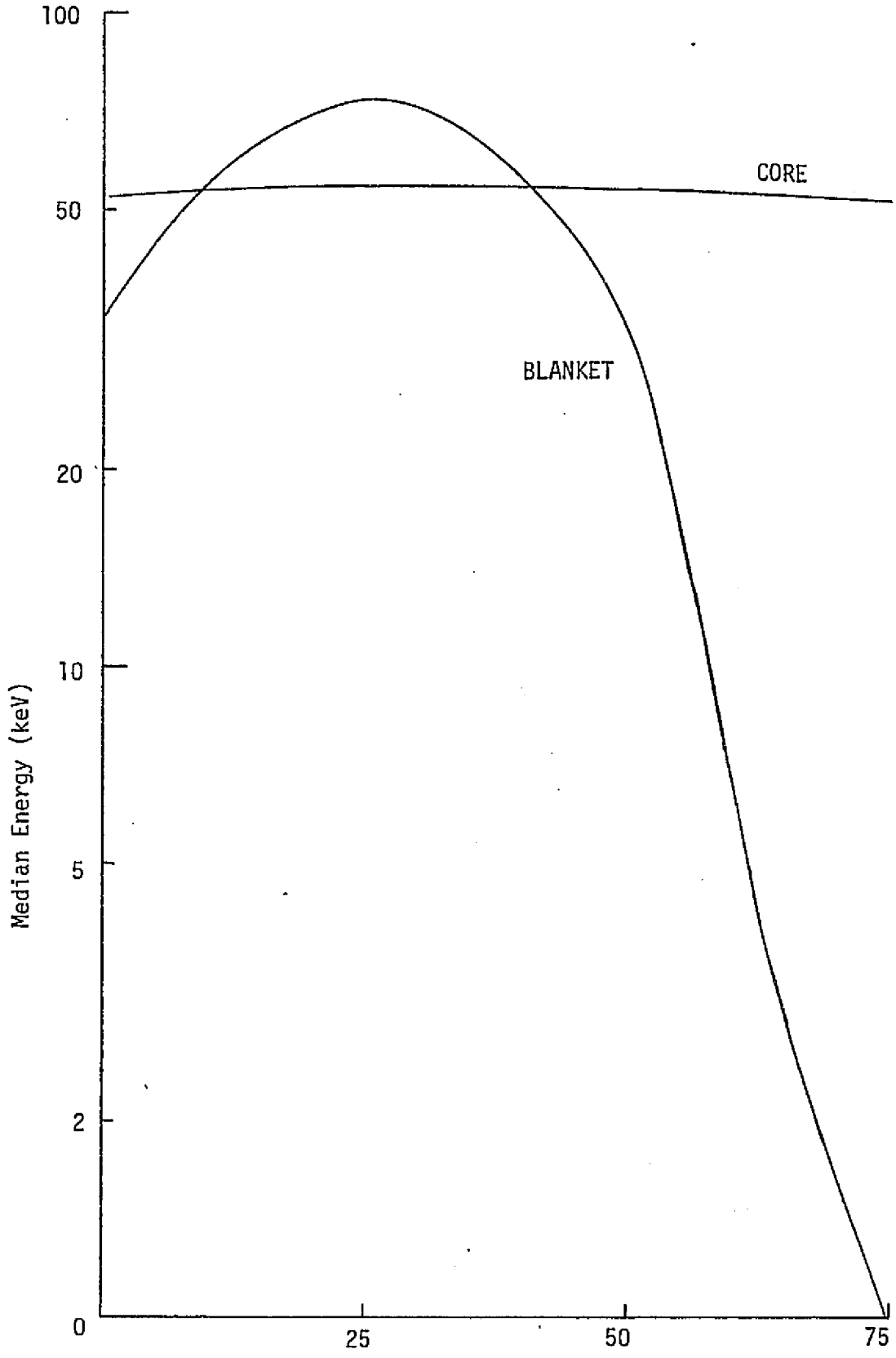

FIG. IV-9. GRAPH OF VOLUME % OF BERYLLIUM IN BLANKET VS MEDIAN NEUTRON ENERGY

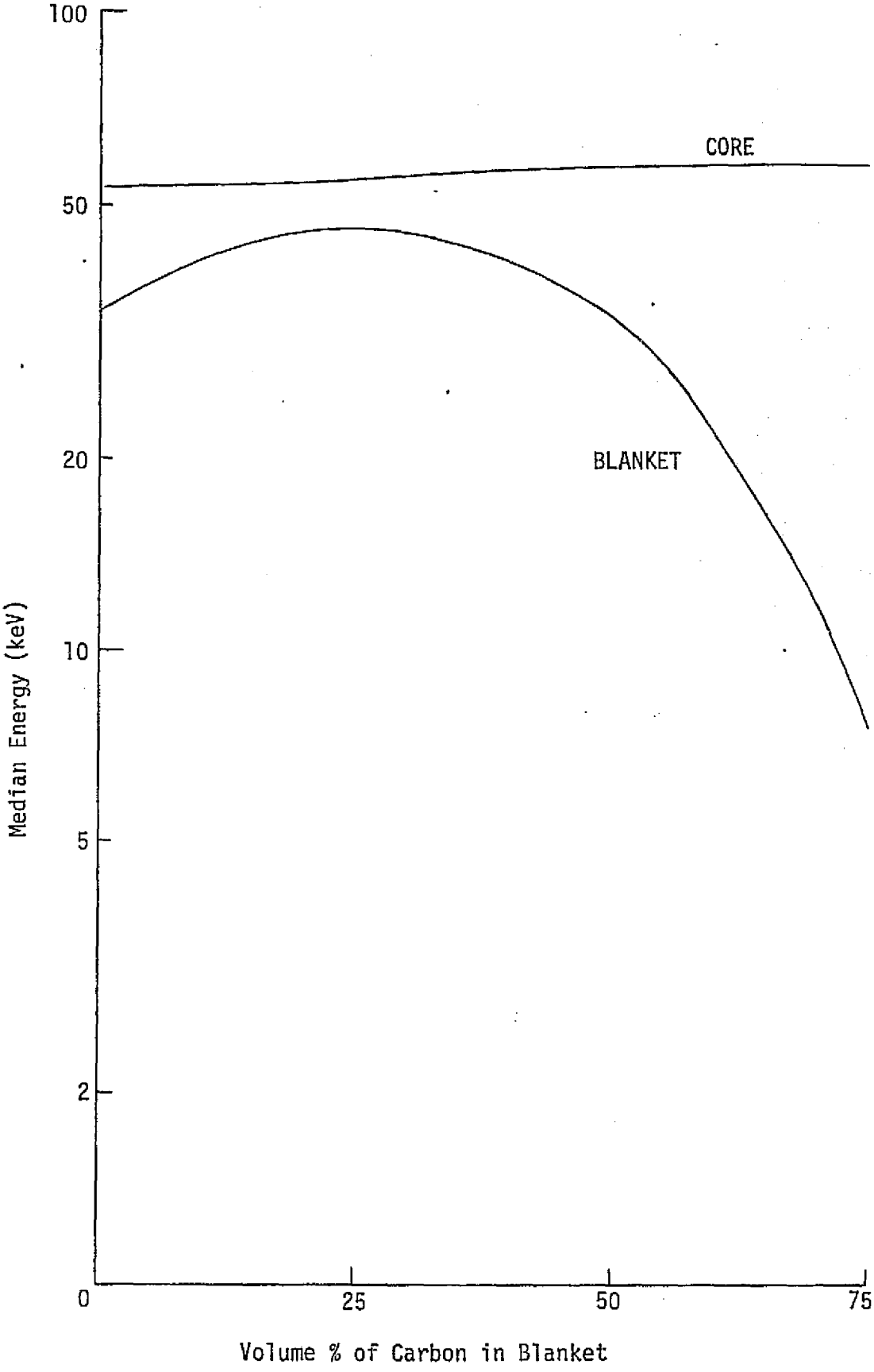

FIG. IV-10. GRAPH OF VOLUME % OF CARBON IN BLANKET VS MEDIAN NEUTRON ENERGY

TABLE IV-5

CRITICAL PARAMETERS VS VOLUME PERCENT OF CARBON IN BLANKET

PERCENT OF CARBON IN BLANKET	0%	25%	50%	75%	100%
MEDIAN ENERGY (MeV) IN CORE	.53147	.55617	.57032	.57663	.53016
MEDIAN ENERGY (keV) IN BLANKET	34	46.5	34	7.33	$.0252 \times 10^{-3}$
BREEDING RATIO	1.1827	1.196	1.190	1.1331	0
CRITICAL RADIUS (cm)	58.5916	60.9031	62.6357	61.3982	39.2433
CRITICAL MASS (kg U-233)	379.13	385.80	463.22	436.30	113.55

BLANKET THICKNESS = 114.38 cm

TABLE IV-6

CRITICAL PARAMETERS VS VOLUME PERCENT OF BERYLLIUM IN BLANKET

PERCENT OF Be IN BLANKET	0%	25%	50%	75%	100%
MEDIAN ENERGY (MeV) IN CORE	.53147	.55239	.55123	.52800	.44387
MEDIAN ENERGY (keV) IN BLANKET	34	73.3	34	4.65×10^{-3}	$.0252 \times 10^{-3}$
BREEDING RATIO	1.1827	1.2284	1.2032	1.0651	0
CRITICAL RADIUS	58.5916	61.8469	61.1468	53.4241	29.80
CRITICAL MASS (kg U-233)	379.13	445.94	430.96	287.43	49.88

BLANKET THICKNESS = 114.38 cm

TABLE IV-7

COMPARISION OF CRITICAL PARAMETERS

	SPHERICAL CORE (26 GROUP)	SPHERICAL CORE (4 GROUP)	CYLINDRICAL CORE (4 GROUP)
BREEDING RATIO	1.181	1.179	1.219
CRITICAL RADIUS	58.59 cm	60.91 cm	54.78 cm
CRITICAL CORE VOLUME	$8.425 \times 10^5 cm^3$	$9.466 \times 10^5 cm^3$	$1.033 \times 10^6 cm^3$
CRITICAL MASS (kg U-233)	379	426	496
BLANKET THICKNESS	114.38 cm	114.38 cm	100 cm

Table IV-8 Neutronic Areas for Further Study

1. Study more thermal reactor with additional moderation in blanket
   - Effect on spectrum
   - Effect on breeding ratio
   - Effect on control
2. Select control mechanism
   - Reactivity effectiveness of control mechanism
   - Effect on breeding ratio
   - Effect on power distribution
3. Calculate reactivity effects
   - Temperature and other reactivity coefficients
   - Effect of structure and impurities
   - Reactivity effects with lifetime
4. Iterations with thermal and fluid flow analysis
5. Heating rate in blanket
6. Dynamic and stability analysis
7. Analyze more check point experiments - improve model
8. Potential of co-axial flow gas core reactor - MHD
9. Investigate applications, especially use of gas core reactor for actinide burnup

References for Chapter IV

1. Whitmarsh, C. L., "Neutronics Analysis of an Open-Cycle High-Impulse Gas-Core Reactor Concept," NASA TM X-2534, April, 1972.

2. Kunze, J. F., et al., "Benchmark Gas-Core Critical Experiment," Nuclear Science and Engineering, 47, 59-65 (1972).

3. Hyland, R. E., "Evaluation of Critical Mass for Open-Cycle Gas-Core Rocket Reactors," Nuclear Technology, 12 (Oct., 1971).

4. Meneley, D. A., et al., "Mach-I, A One-Dimensional Diffusion Theory Package," ANL-7223 (1966).

5. Toppel, B. J. and Baksys, I., "The Argonne-Revised THERMOS Code," ANL-7023 (1965).

6. Bondarenko, I. I., Ed., Group Constants for Nuclear Reactor Calculations, Consultants Bureau, New York (1964).

7. Fowler, T. B., Tobias, M. L., and Vondy, D. R., "EXTERMINATOR-2; A Fortran IV Code for Solving Multigroup Neutron Diffusion Equations in Two Dimensions," ORNL-4078 (Apr. 1, 1967).

V. THERMODYNAMIC CYCLE ANALYSIS

In a previous report[1] the use of both Brayton and Rankine cycles employing UF_6 as a working fluid was evaluated. This report showed that Rankine cycles gave higher overall plant efficiencies. However, Brayton cycles should not be considered completely undesirable because their higher temperatures for heat rejection may make them more suitable for space applications. However, since this design is concerned with land-based power plants, the thermodynamic analysis was conducted using only Rankine cycles. The analysis of Ref. 1 is extended to include the evaluation of cycles with and without reheat capabilities. In addition, temperatures and pressures at certain selected locations were varied to optimize plant efficiency.

5.1 Cycle Evaluation

Calculations were performed for the Rankine cycle illustrated in Fig. V-1. Calculations were also done for a cycle with no reheater to determine how the cycle efficiency is affected by the reheater.

Because material limitations of the duct walls limited UF_6 temperature to less than 1660°R (921.89°K), the average temperature at the outlet of the reactor was chosen to be 1560°R (866.33°K). The reactor outlet pressure was set at 1450 psia (99.97 bars) which is approximately the pressure required from the core physics calculations to obtain a critical reactor.

The minimum temperature difference in the regenerative heat exchanger, ΔT_{6-7}, was specified as 50°R (28°K). The boiler feed pump and turbine efficiencies were taken to be 0.88 and the condenser pressure was maintained at 21.76 psia (1.5 bars). The pressure loss across the reactor was assumed to be 14.89 psi (1.03 bars) and the pressure loss across each side of the

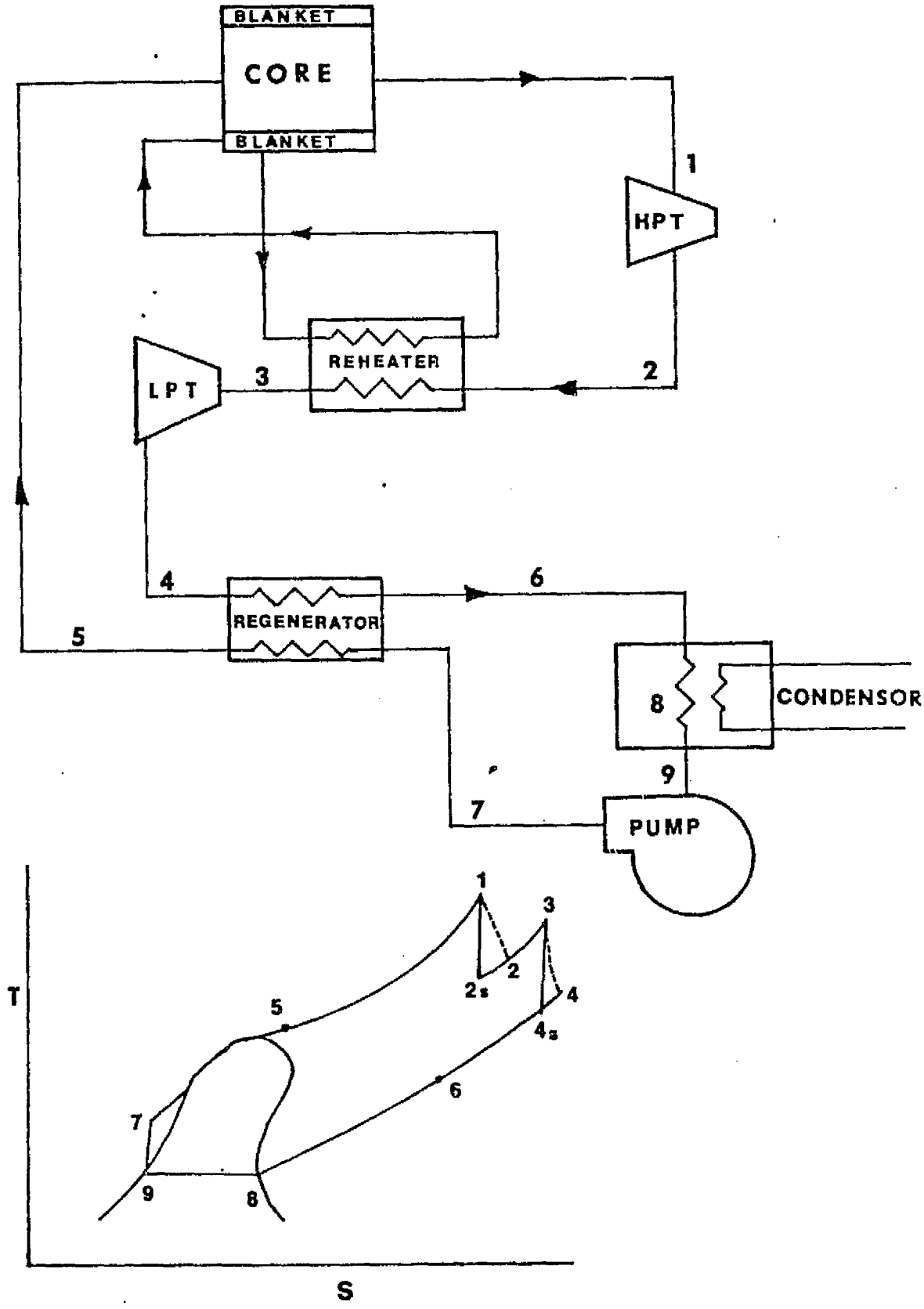

FIG. V-1 BREEDER POWER PLANT SYSTEM SCHEMATIC

regenerator and reheater was taken to be 7.445 psi (.51 bars). In these calculations, the pressure loss through the pipes was neglected because the plant design was not complete and therefore the length of the pipes between components was unknown.

5.2 Cycle Parameter Calculations

The thermodynamic cycle calculations were performed using the method outlined in Ref. 1. The thermodynamic properties of UF_6 are tabulated in Appendix A.

Initially, cycle parameters were calculated without reheating. This gave a plant efficiency of 39.03%. Then reheat was added between stages of the turbine using the heat generated in the blanket. It was apparent that an optimum pressure existed for removing the UF_6 from the high pressure turbine and, consequently, p_2 was varied. Figure V-2 illustrates overall plant efficiencies as a function of the high pressure turbine outlet pressure. The maximum efficiency was 41.44% at a pressure of 435.12 psia (30 bars).

From Fig. V-2 it appears that the efficiency begins to increase for pressures greater than 720 psia (50 bars). However, higher pressures cannot be used because the calculations indicated that for these higher pressures the reheat temperatures exceed 1560°R (866°K), which was not allowed because of material limitations.

Table V-1 summarizes the parameters for the optimized UF_6 gas-core reactor power plant.

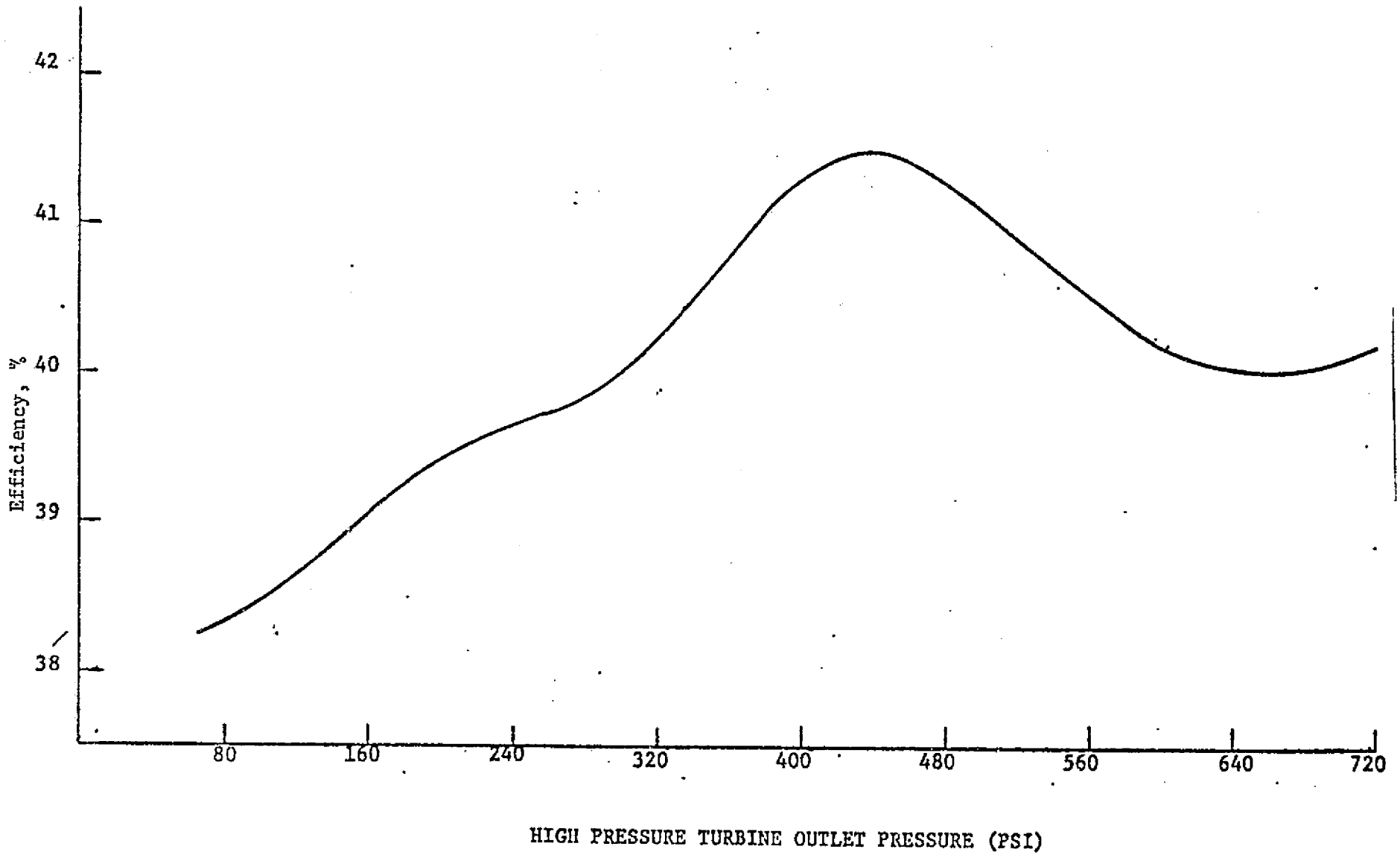

Fig. V-2 Power Plant Efficiency as a Function of High Pressure Turbine Exit Pressure

Table V-1

Summary of Optimum UF_6 Gas-Core Reactor Cycle

Overall Efficiency = 41.44%

$\eta_{turbine} = \eta_{pump} = 0.88$

Pressure Losses = 1 bar in reactor and 1/2 bar in each heat exchanger pass

State Points for Stream Locations Shown in Fig. V-1

#1

T = 1560.0°R (866.33°K)
P = 1450.00 psi (99.97 bars)
h = 123.88 Btu/lb_m (288.14 KJ/Kg)

#2

T = 1455.5°R (808.26°K)
P = 435.12 psi (30.00 bars)
h = 114.99 Btu/lb_m (267.46 KJ/Kg)

#3

T = 1516.3°R (842.06°K)
P = 427.67 psi (29.49 bars)
h = 121.63 Btu/lb_m (282.91 KJ/Kg)

#4

T = 1293.8°R (718.46°K)
P = 29.21 psi (2.01 bars)
h = 100.86 Btu/lb_m (234.60 KJ/Kg)

#5

T = 1036.8°R (575.65°K)
P = 1464.89 psi (100.99 bars)
h = 62.17 Btu/lb_m (144.61 KJ/Kg)

#6

T = 667.3°R (370.36°K)
P = 21.76 psi (1.50 bars)
h = 40.03 Btu/lb_m (93.09 KJ/Kg)

#7

T = 617.3°R (342.58°K)
P = 1472.34 psi (101.51 bars)
h = 35.26 Btu/lb_m (82.01 KJ/Kg)

#8

T = 606.9°R (336.83°K)
P = 21.76 psi (1.56 bars)
h = 35.26 Btu/lb_m (82.02 KJ/Kg)

#9

T = 606.9°R (336.83°K)
P = 21.76 psi (1.56 bars)
h = 0.00 Btu/lb_m (0 KJ/Kg)

REFERENCES FOR CHAPTER V

1. Williams, J. R. et al., "Analysis of UF_6 Breeder Reactor Power Plants," Progress Report No. 1, NASA Grant NSG-7067 (November 1974)

VI. HEAT TRANSFER AND FLUID FLOW

Because of the high power density in the gas core reactor, it is necessary to analyze the heat transfer and flow characteristics of the core in order to assure that unacceptably high temperatures are not achieved in the core. This requires solving the energy equation for the UF_6 flowing through the core. Because of radial symmetry in the core, the energy equation is given by

$$\rho c_p u_z(r,z) \frac{\partial T}{\partial z} = \frac{1}{r} \frac{\partial}{\partial r} \left(r K_E \frac{\partial T}{\partial r} \right) + q'''(r,z) \qquad (1)$$

where

$u_z(r,z)$ = axial velocity

ρ = density

c_p = specific heat at constant pressure

$K_E = k + \rho c_p \epsilon_H$

q''' = volumetric heat generation rate

ϵ_H = eddy diffusivity for heat transfer

Equation 1 is extremely complex because the UF_6 physical properties are highly temperature dependent and the volumetric heat generation term is spatially dependent due to the variable UF_6 density and neutron flux distributions. The thermal-physical properties of UF_6 are given in Appendix B.

6.1 Problem Formulation

Equation 1 was solved for two sets of boundary conditions: (i) an insulated liner wall in which no heat crosses the wall and (ii) an insulated liner wall until the wall temperature reaches 1660°R and then a constant

C-2

wall temperature set at 1660°R for the rest of the core length. Mathematically the boundary conditions are given by:

Case 1

$$T(r,0) = \text{constant} \tag{2a}$$

$$\left.\frac{\partial T}{\partial r}\right|_{r=r_o} = 0 \text{ for } 0 \leqq z \leqq L \tag{2b}$$

Case 2

$$T(r,0) = \text{constant} \tag{3a}$$

with

$$\left.\frac{\partial T}{\partial r}\right|_{r=r_o} = 0 \text{ if } T_w \leqq 1600°R \tag{3b}$$

and

$$T_w = 1660°R \text{ once } T_w = 1660°R \tag{3c}$$

where r_o is the core radius and L is the core length.

The axial velocity distribution was assumed to be given by a 1/7-power law, or

$$u_z(r,z) = u_{z,\,Max}\,(1-r/r_o)^{1/7} \tag{4}$$

$$= \frac{u_{z,\,Mean}}{0.8}\,(1-r/r_o)^{1/7}$$

where $u_{z,\,Max}$ is the maximum (centerline) fluid velocity and $u_{z,\,Mean}$ is the channel average velocity for a given axial location. Since the fluid is accelerating down the channel length because of the decreasing UF_6 density due to heating, the velocity distribution in the axial direction was modified by multiplying Eq. 4 by the ratio of the average inlet density to the average fluid density at a given axial location. Therefore the velocity distribution incorporated in Eq. 1 is

$$u_z(r,z) = \frac{u_{i,\,Mean}}{0.8} (\bar{\rho}_i/\bar{\rho}_z)(1-r/r_o)^{1/7} \qquad (5)$$

where $u_{i,\,Mean}$ is the mean velocity at the core inlet.

In order to calculate heat transfer within a fluid in a forced convection (turbulent) system, a property to explain the thermal mixing is needed. In turbulent flow the fluid has both radial and axial velocity components (the time-averaged radial component is zero) and the mixing of two regions (caused by turbulent convection) of different temperatures must be accounted for. The term to account for this mixing is the eddy diffusivity for heat transfer, ϵ_H. A basic assumption in dealing with ϵ_H is that it is approximately equal to the eddy diffusivity of momentum transfer, ϵ_M, (this holds for all fluids except liquid metals). Numerous expressions exist for ϵ_M. These expressions are normally obtained from differentiating empirical equations for velocity distributions. One of these expressions which is widely accepted is that of Dwyer which yields a value of zero at the channel centerline and wall. The expression for ϵ_H is in the following form[1]:

$$\epsilon_H = (\mu/\rho)\ .72(1/8\ f)^{\frac{1}{2}}\ N_{Re}\ R(1-R^{\frac{1}{3}}) \qquad (6)$$

where

μ = viscosity

ρ = density

f = Moody friction factor

N_{Re} = Reynolds number

$R = r/r_o$

r_o = radius to wall

The radial dependence of the volumetric heat generation rate was modeled from data obtained from a MACH-I core physics calculation of the power density in a spherical gas core reactor. In the axial direction the volumetric heat generation rate was assumed to decrease linearly to one-third that at the core entrance. In mathematical terms q''' is given by

$$q'''(r,z) = q'''_1\left[1 + 1.07\, e^{-0.19(r_o - r)}\right]\left[1 - \frac{2z}{3L}\right] \qquad (7)$$

Equation 1 was solved numerically by using finite difference representations for the partial derivatives and incorporating the terms given by Eqs. 4 to 7. A marching technique was employed which required iteration at each axial step in order to incorporate the temperature dependence of the UF_6 physical properties. The numerical methods used for solving Eq. 1 are given in Appendix D.

6.2 Results of Heat Transfer Calculations

It was estimated that 9.7% of the reactor power would be deposited in the blanket. Consequently, for a reactor power level of 1000 Mwth, 903 Mwth would be generated in the reactor core. From the thermodynamic analysis described in Chapter V it was found that the core inlet temperature would be 1036.8°R (575.7°K). For the specified outlet temperature of 1560°F (866.3°K), the UF_6 mass flow rate through the core must be 13,900 lb_m/sec.

The selected core geometry was a right cylinder with a 100 cm radius and a 200 cm length. Flow through the core entrance and exit is through numerous inlet and exit nozzles which permits assuming the velocity distribution given by Eq. 5. Since the core power is 903 Mw, integration of Eq. 7 over the core volume gives the constant q'''_1.

Figure VI-1 illustrates core linear wall temperatures and UF_6 fuel temperatures at the core axis as a function of core length for the insulated wall boundary condition given by Eq. 2. As shown by the calculations, after 50 cm down the channel length the liner wall temperature exceeds 1660°R which is considered unacceptably high. Figure VI-2 illustrates the radial dependence of UF_6 temperatures for various axial positions. The temperatures reach a peak at the wall because of the insulated wall, the volumetric heat generation rate has a maximum at the wall, and in particular because the fluid velocity at the wall is zero which means energy is transferred at that location only through conduction.

Figure VI-3 illustrates core liner wall temperatures and UF_6 fuel temperatures at the core axis as a function of core length for the boundary condition that the liner wall not exceed 1660°R (boundary condition given by Eq. 3). Figure VI-4 illustrates the radial dependence of UF_6 temperatures for various axial locations. The UF_6 temperature at a given axial location has a maximum near the channel wall because the fluid velocity is zero at the wall. The maximum UF_6 temperature occurs at the channel exit and is 2200°R which is far below temperatures required for substantial UF_6 ionization. Figure B-1 of Appendix B illustrates UF_6 composition as a function of temperature.

The boundary condition that the liner wall temperature not exceed 1660°R requires wall cooling after about 40 cm down the core length. Consequently, it is necessary to examine wall heat fluxes in order to determine the extent of the wall cooling. Figure VI-5 illustrates liner wall heat fluxes as a function of channel length. The maximum heat flux occurs at the channel exit and has a value of 650 Btu/hr-ft^2 (0.205 watts/cm^2). This is a small heat flux for which it would be easy to provide wall cooling.

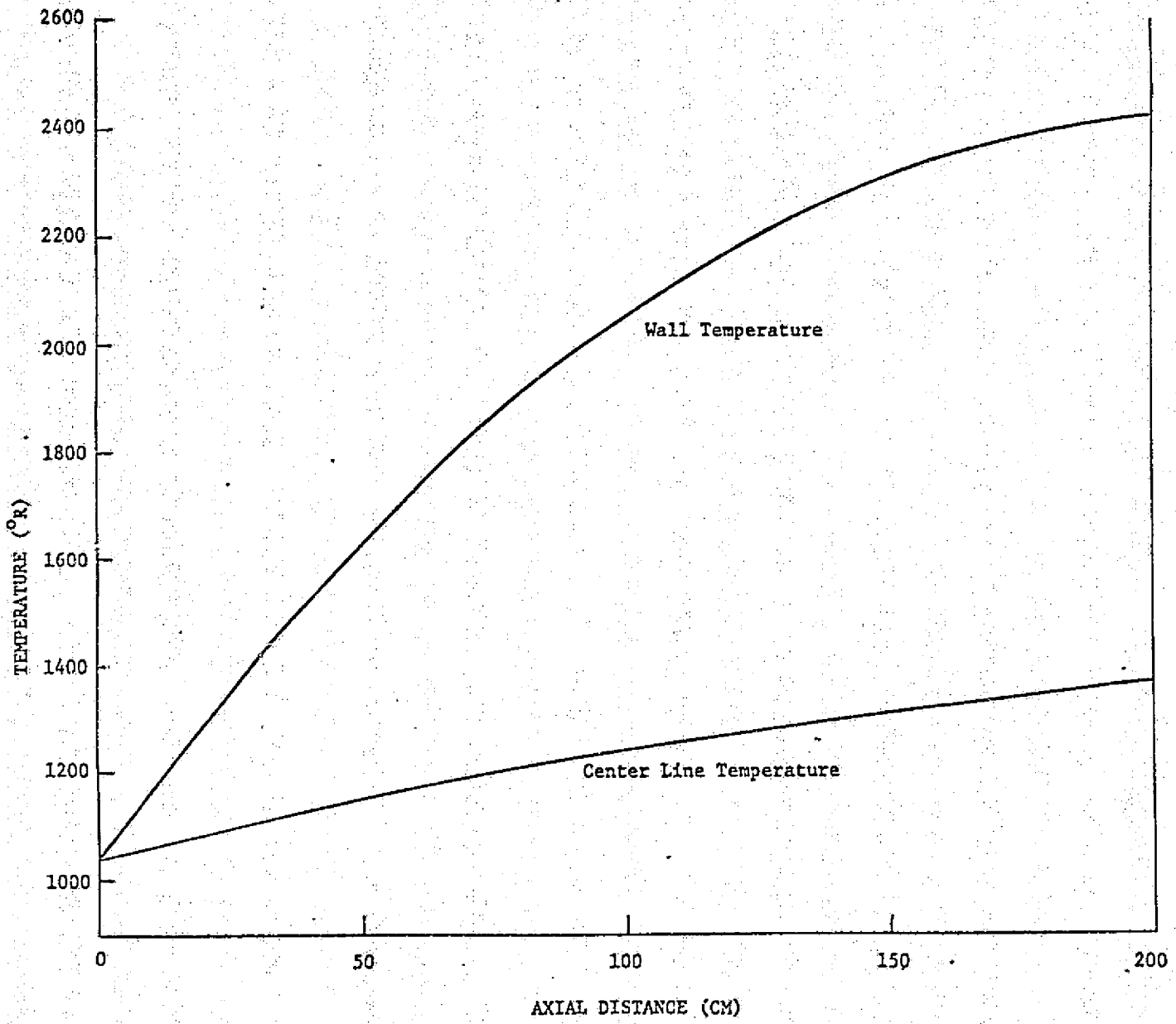

FIG. VI-1. WALL TEMPERATURE VS AXIAL DISTANCE (CASE 1)

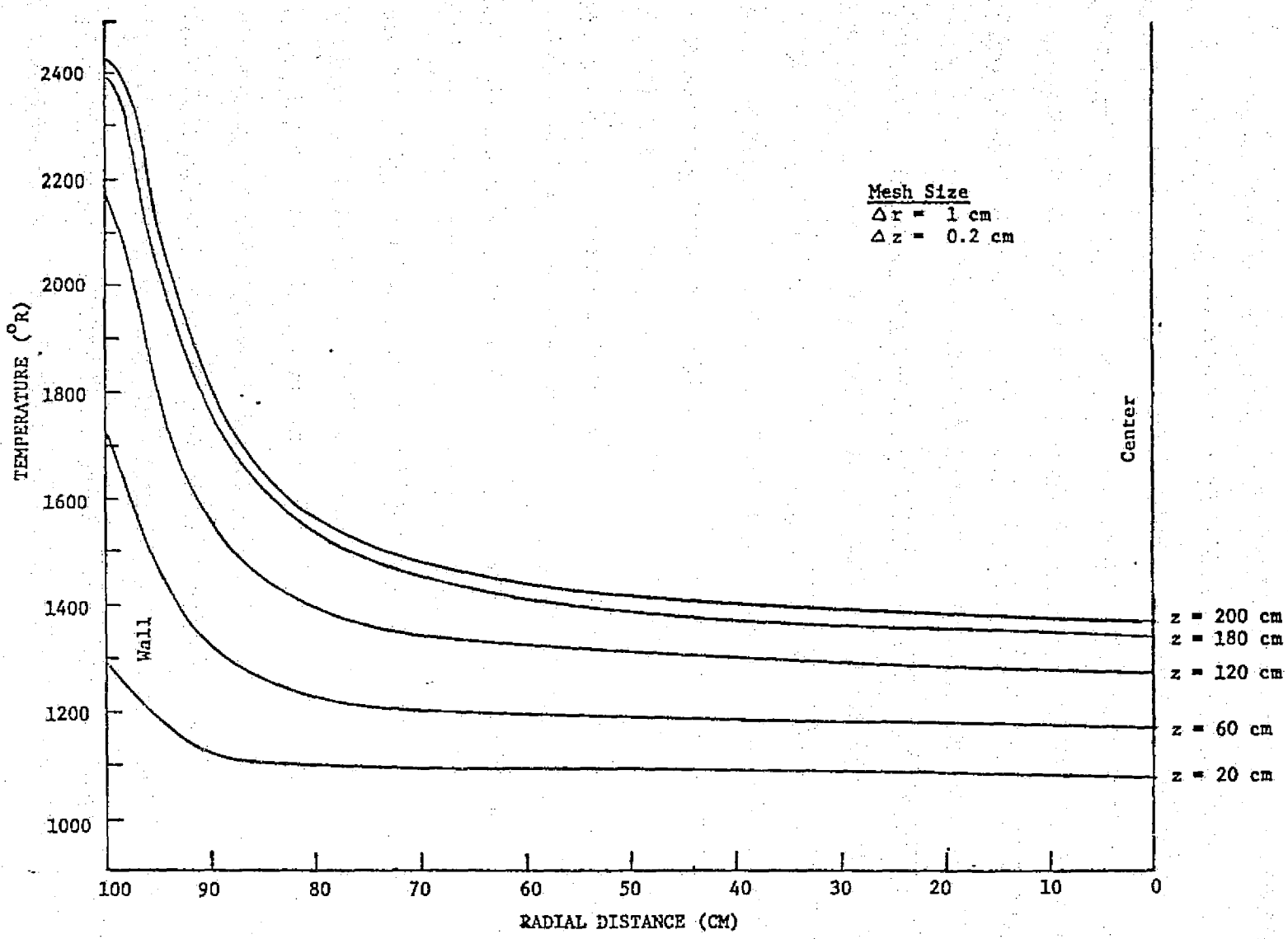

FIG. VI-2. TEMPERATURE VS RADIAL DISTANCE (CASE 1)

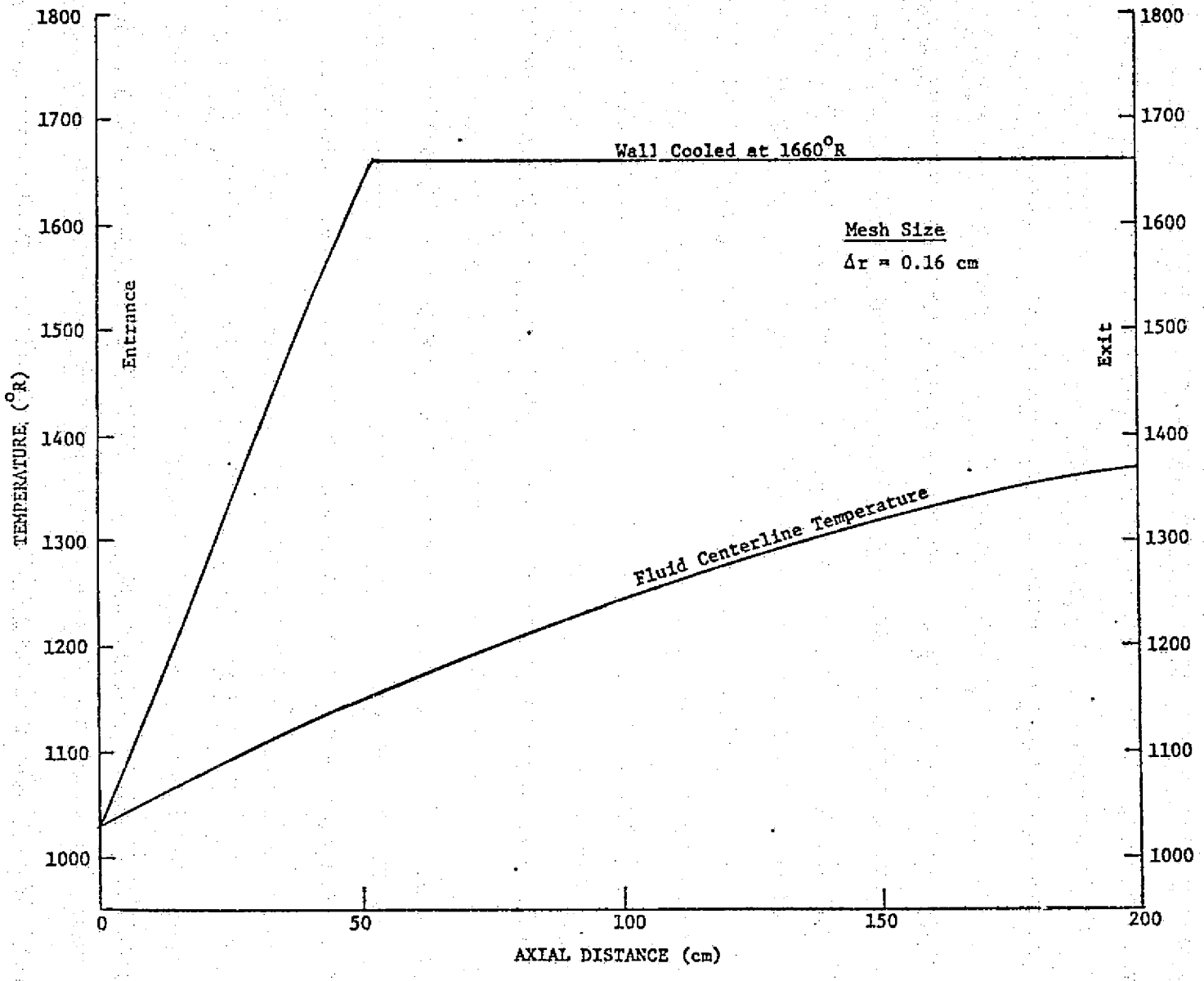

FIG. VI-3. WALL TEMPERATURE VS AXIAL DISTANCE (CASE 2)

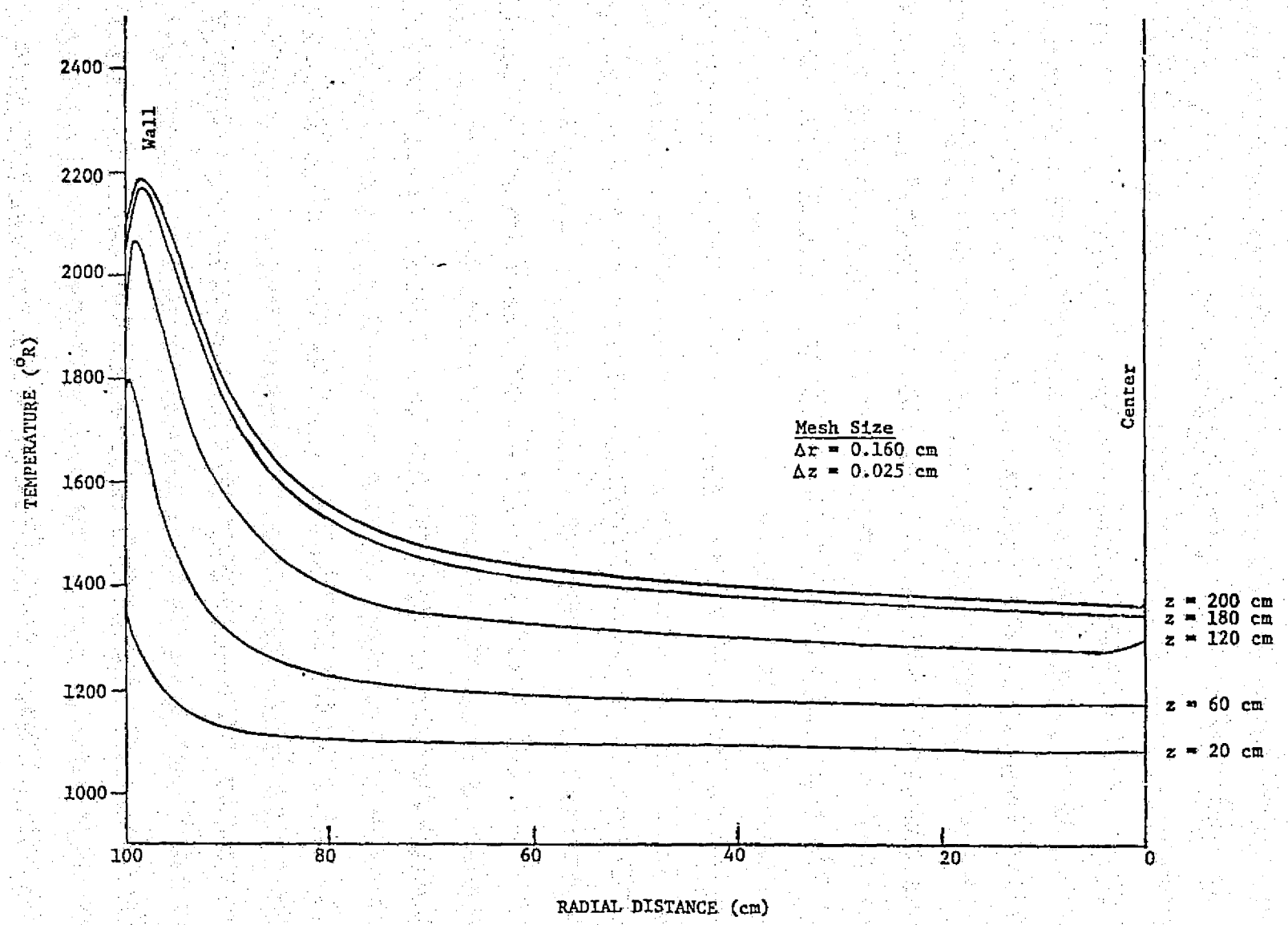

FIG. VI-4. TEMPERATURE VS RADIAL DISTANCE (CASE 2)

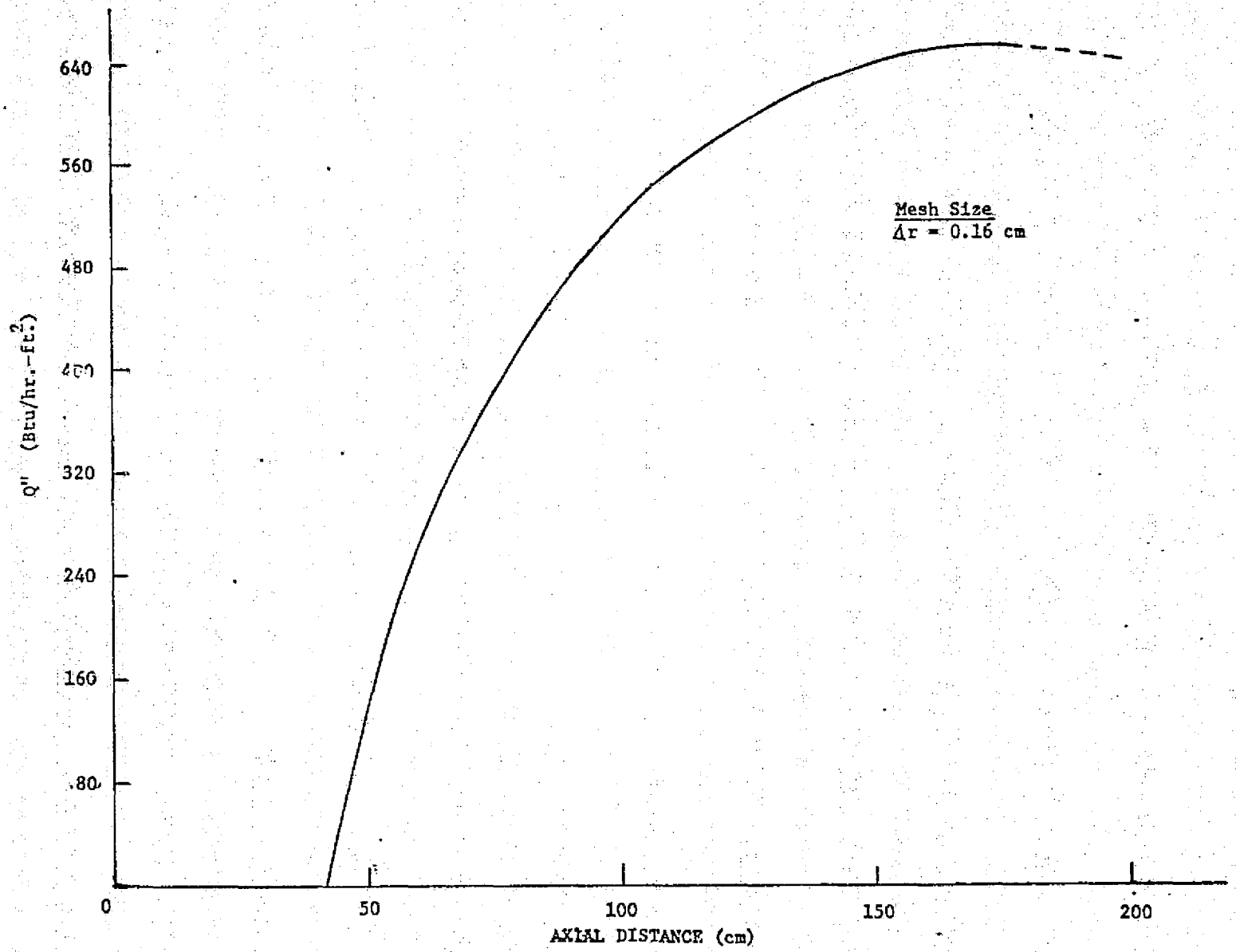

FIG. VI-5. WALL HEAT FLUX VS AXIAL DISTANCE (CASE 2)

The low thermal conductivity of UF_6 accounts for the low heat flux in the liner wall. The total wall cooling is less than 150 kw which represents a negligible amount of the core power.

References for Chapter VI

1. Dwyer, O. E., "Eddy Transport in Liquid-Metal Heat Transfer," A.I.Ch.E. Journal, 9(2), 261 (1963).

VII. MECHANICAL DESIGN

7.1 Design Criteria

The basis for this project was chosen to be a 1000 MW thermal, stationary power plant employing UF_6-fueled gas-core breeder reactor. The blanket for the reactor was initially chosen as a mixture of beryllium and thorium.

Based on this brief description the actual reactor could be designed and modified to take advantage of new ideas and information. The selected reactor configurations is shown in Fig. VII-1. This configuration demonstrates that a practical UF_6 gas-core breeder reactor can be constructed and this design will serve as a good starting point for future design work on this concept.

7.2 Preliminary Design Concepts

Based on the design criterion, a multitude of possible designs can be described. Numerous combinations were examined and the following concepts were considered the most promising or practical to be studied in greater depth:

1. A gaseous UF_6 core with a solid matrix blanket. (External blanket cooling loop required.)
2. A gas UF_6 core with a liquid blanket. (External loop used to cool blanket.)
3. A gaseous UF_6 core with a circulating liquid blanket.

After a brief preliminary study, the first two concepts were rejected and the last one chosen for a detailed design effort.

The first concept was abandoned since reprocessing the blanket material would require a system shutdown, at least a partial reactor disassembly, and the installation of new blanket material. The cost of fabricating new

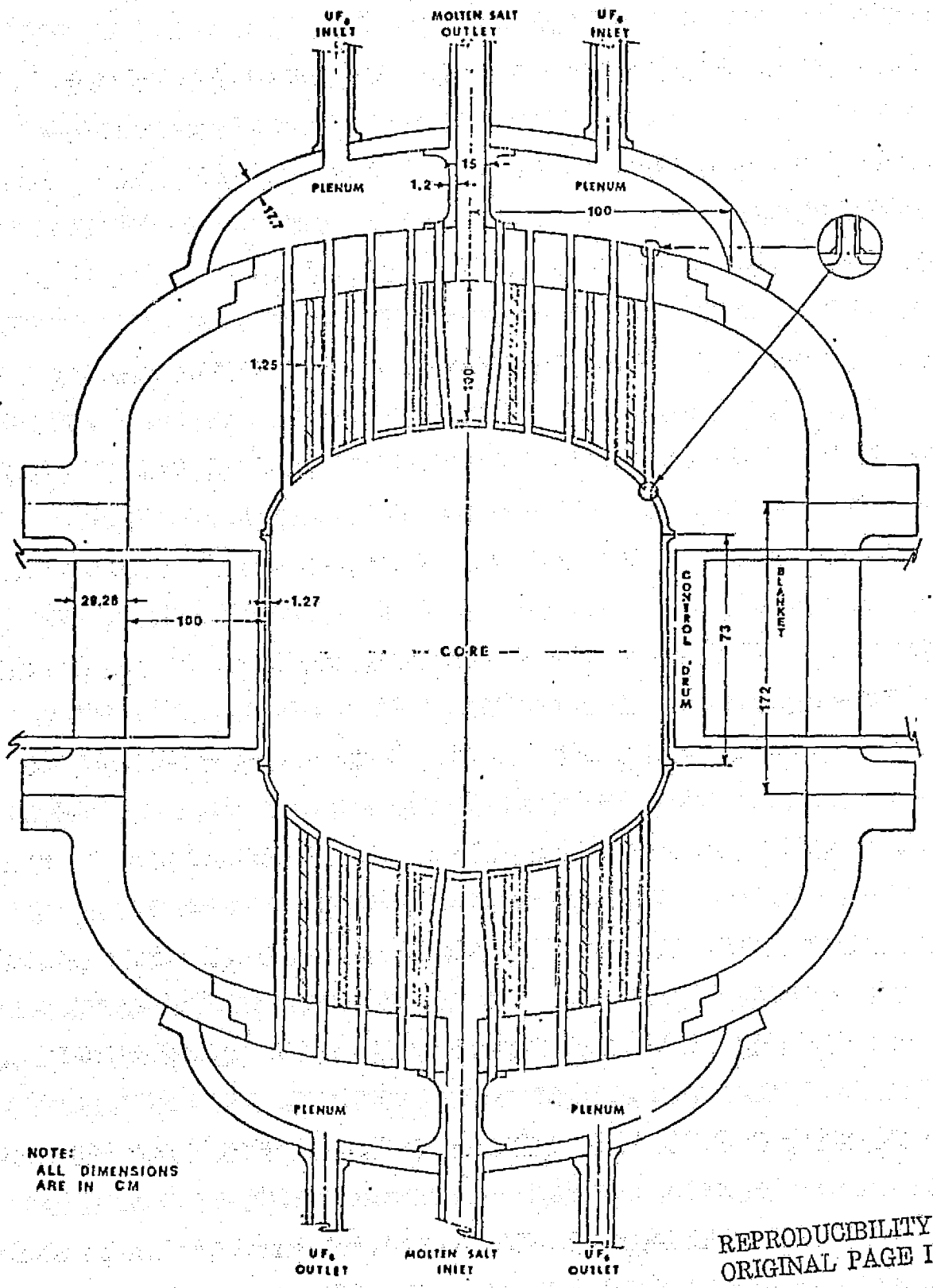

FIG. VII-1. UF_6 GAS-CORE REACTOR

blankets would add to the total power cost.

The second concept calls for an external coolant loop through the blanket which is undesirable from a neutron economy point of view. Some fraction of the blanket could be continuously bled off for reprocessing and fission product removal, a fact which makes this concept superior to concept 1.

The last concept was the one selected for the detailed design work. It employs a liquid blanket which will be continuously circulated for blanket cooling and reprocessing. No external coolant loop is required with this design. The problem of finding a suitable liquid blanket material containing correct amounts of thorium and beryllium, while being stable and having good thermal-physical properties, was quickly resolved and the circulating blanket concept accepted.

7.3 Reactors

7.3.1 Structure and Geometry

The initial calculations were based on a spherical core, which was necessary because the MACH-1 diffusion code can only do physics calculations in one-dimension. A spherical reactor, however, becomes impractical due to fabrication and flow distribution problems. A right cylinder with ellipsoid heads and radius approximately equal to the blanket thickness and height equal to the diameter is easily fabricated and good geometry to work with from both a practical and a calculational point of view.

A uniform velocity profile for the UF_6 flowing through the core is desirable to simplify calculations and maximum reactor performance. Several methods of flattening the velocity profile were considered, but the only practical solution was to use many small inlets and outlets to the reactor core. The tubes that carry the UF_6 into and out of the core are offset to

minimize neutron losses through the tubes.

The inlet and outlet flow passes through 100 tubes whose total cross sectional area comprises approximately one tenth of the area of the end of the cylinder. Figure VII-2 illustrates the inlet and outlet geometry for the core. The tubes will constitute approximately one tenth of the blanket volume at the ends of the core. The introduction of UF_6 and the tube structural materials into the blanket will have a degrading effect on the breeding ratio. There was no other apparent method which would distribute the flow and have less impact on the breeding ratio.

The blanket will be pressurized to the same pressure as the core (on the order of 100 atm.). The core liner will thus be designed to withstand a pressure difference of only 10 atmospheres. The outside pressure vessel will need to be capable of containing the 100 atmospheres of normal operating pressure plus a 20% safety margin, or 120 atmospheres total. These pressures are not extreme and can easily be accommodated. The reactor pressure vessel is designed according to specifications from the ASME Boiler and Pressure Vessel Code; Section III-Rules for Construction of Nuclear Power Plant Components.[1] The cylinder will have ellipsoid heads with a 2:1 major to minor axis ratio. The core liner thickness was selected as 1.27 cm. Since the core physics calculations indicated a height and diameter of 109.6 cm was necessary in order to achieve criticality, the core vessel had outside dimensions of 112.1 cm diameter and 130.4 cm maximum length.

Reactor physics studies indicated that the optimum blanket thickness for a gas-core breeder reactor is of the order of 100 cm. Consequently, the inside dimensions of the reactor pressure vessel were approximately 312 cm diameter and 330 cm maximum length. Because the modified Hastelloy-N pressure vessel was at the same temperature as the blanket material (1600°R),

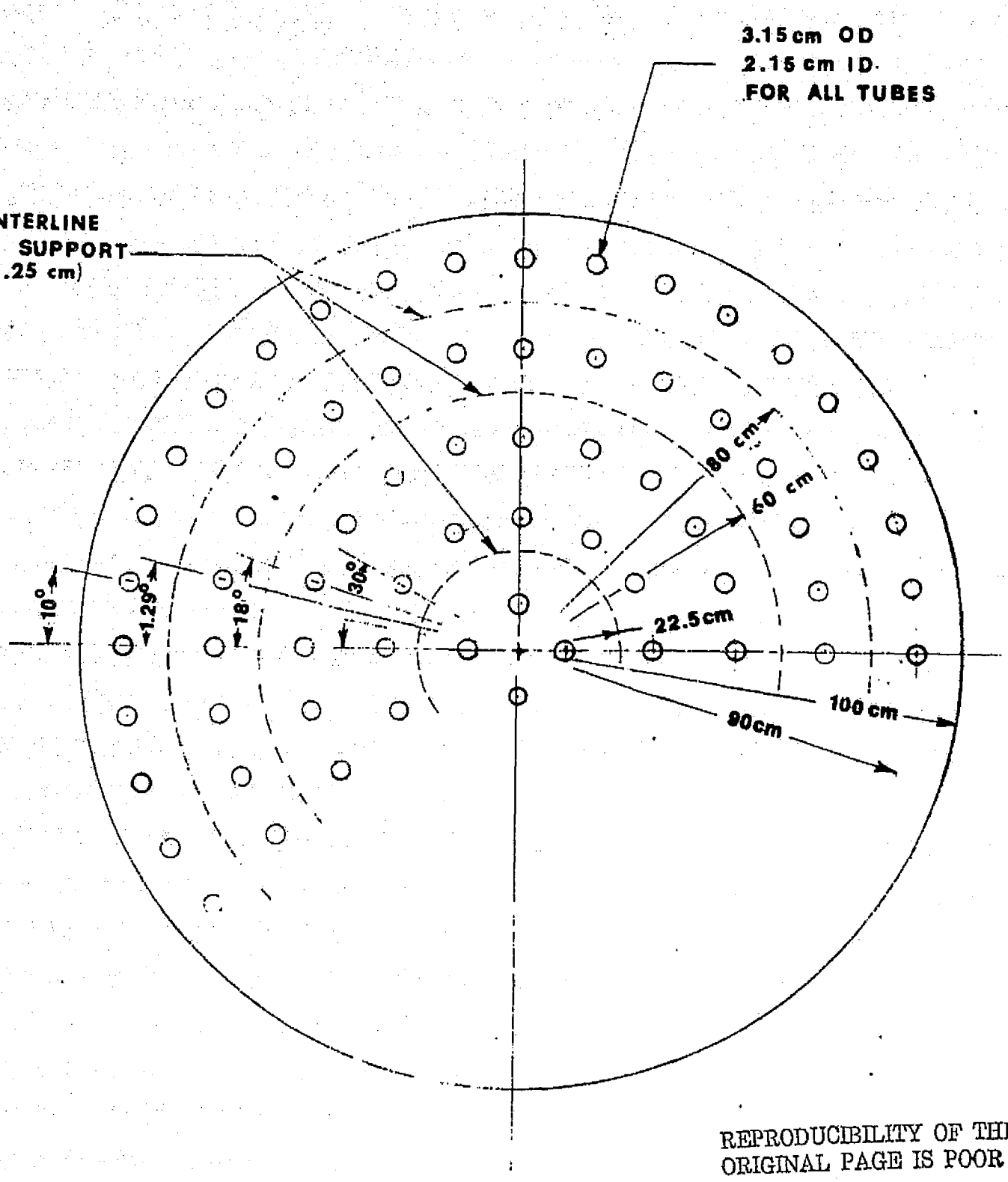

FIG. VII-2 CORE FLOW DISTRIBUTION PLATE

the maximum allowable stress in the pressure vessel is 10,000 psi in order to insure a long pressure vessel operating life (30 years). Using the techniques outlined in Reference 1, the required pressure vessel wall thickness is 29.3 cm. If the pressure vessel temperature is reduced by cooling, the wall thickness can be significantly reduced.

The 1.27 cm wall thickness for the core liner allowed 229 psi pressure difference between the UF_6 and blanket material to be sustained for long term reactor operation. In case of a rapid depressurization of the blanket, the core liner can withstand a pressure difference of 1,375 psi for a period of 6 minutes.

All stress calculations were based upon a 30 year operating life for the reactor. The difference in densities between the UF_6 and the molten salt blanket produced a buoyancy force on the core liner. This force was calculated to be 7,660 lb_f.

The reactor and primary coolant systems will be set in a pre-stressed concrete reactor vessel (PCRV). This PCRV will provide both safety and shielding. PCRV design was not included in this report since the details would depend on a precise system configuration and size.

Both the core liner and pressure vessel should be designed to prevent, or at least minimize, flow stagnation areas. The core vessel uses large numbers of entrances and exits to minimize stagnation and the blanket vessel uses symmetry and smooth, rounded surfaces to eliminate flow stagnation.

7.3.2 Control Systems

In a gas-core reactor, temperature, pressure, and flow rates can be expected to have significant effects on core reactivity. These effects will be even more pronounced in this reactor than in a water-moderated, fixed-fuel reactor. Some type of control system must be provided to account for

reactivity changes, as well as take care of start-ups and shut-downs.

The control system for this reactor is provided by six control drums evenly spaced around the core. The control drums are in the blanket, but as close to the core as possible to maximize their worth. This type of control systems has been used successfully on the SNAP and NERVA reactors in the United States and on the TOPAZ reactor in Russia.

Control rods of the type commonly in use on power reactors were considered but rejected. They would have to be inserted into the blanket instead of the core, and would thus have a smaller reactivity. In addition, stationary guide tubes through the blanket would reduce the breeding ratio. The ends of the reactor design are also rather complex and many extra control rod penetrations would complicate the design.

The control drums to be used on this reactor might consist of a fixed beryllium cylinder around which a sleeve of thermal neutron absorber (such as cadmium or boron carbide) rotates. By having the sleeve rotate instead of the entire drum, the response time can be decreased due to the much smaller inertia of the sleeve.

The control drums work by changing the size of the reflector area and thus the number of thermal neutrons reflected back into the core. When the poison sleeve is facing away from the reactor core, the beryllium cylinder thermalizes neutrons and reflects thermal neutrons back into the core. As the sleeve is moved around between the drum and the core, the neutrons striking the poison sleeve are absorbed, effectively reducing the number of neutrons reflected back into the core.

The control drums should be designed so that any four can shutdown the reactor. Under normal operating conditions, four drums will be used for reactor start-ups and shut-downs and reactivity control. The other two would

be used in an emergency situation, such as the failure of a regular drum or during a scram.

7.3.3 Seals

All of the major parts are joined together by either welding or by double "O" ring seals. The "O" ring seals used here are of the same type used in most current reactors, including PWR's, BWR's, and the molten salt reactor. The "O" rings should be made of a metal compatible with the substances they may come in contact with. The seal consists of two concentric "O" rings, each shaped like a hollow torus, with several holes drilled around the inside circumference of the ring. As pressure increases, the "O" rings inflate, forming the seal. (See Fig. VII-3)

7.4 System Layout

Figures VII-4 and VII-5 illustrate side and top views for the proposed 1000 Mwth power plant. The plant contains two turbines, each of which has a high pressure and low pressure component operating on the same shaft. Two regenerators are used at the exit of the low pressure turbine in order to keep the size of the components down to reasonable values. The entire power plant will be housed inside a prestressed concrete pressure vessel (PCRV) which will act as the containment structure for the power plant. PCRV's are presently employed as the containment for high temperature gas-cooled reactors which operate at higher temperatures (1870°R) than the UF_6 gas core reactor.

7.5 UF_6 Mass in Power Plant

An analysis was made of the power plant heat exchangers in order to estimate the mass of UF_6 required throughout the system. These heat exchangers comprise two reheaters, four regenerators, and two condensers. Table VII-1 summarizes the calculated UF_6 masses in these components.

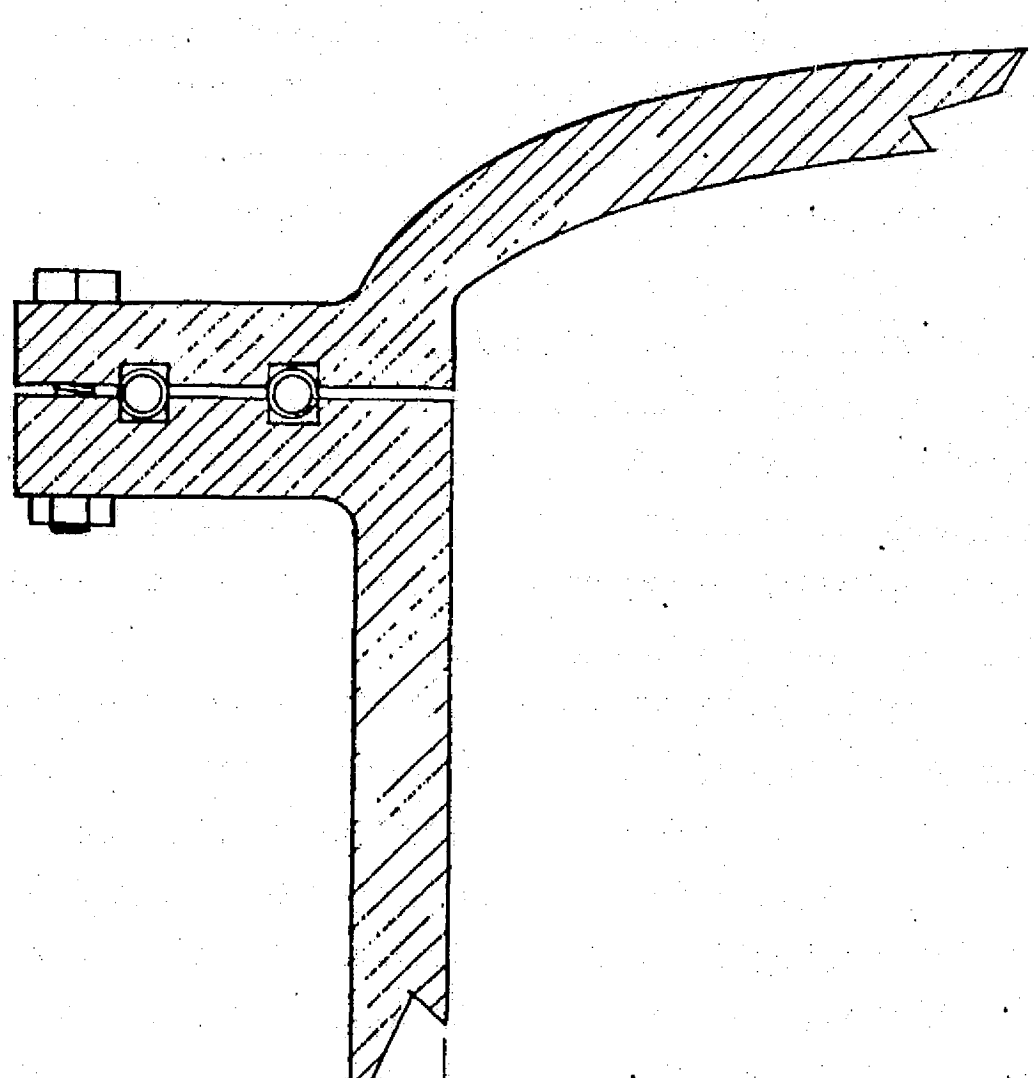

FIG. VII-3 PRESSURE VESSEL SEALS

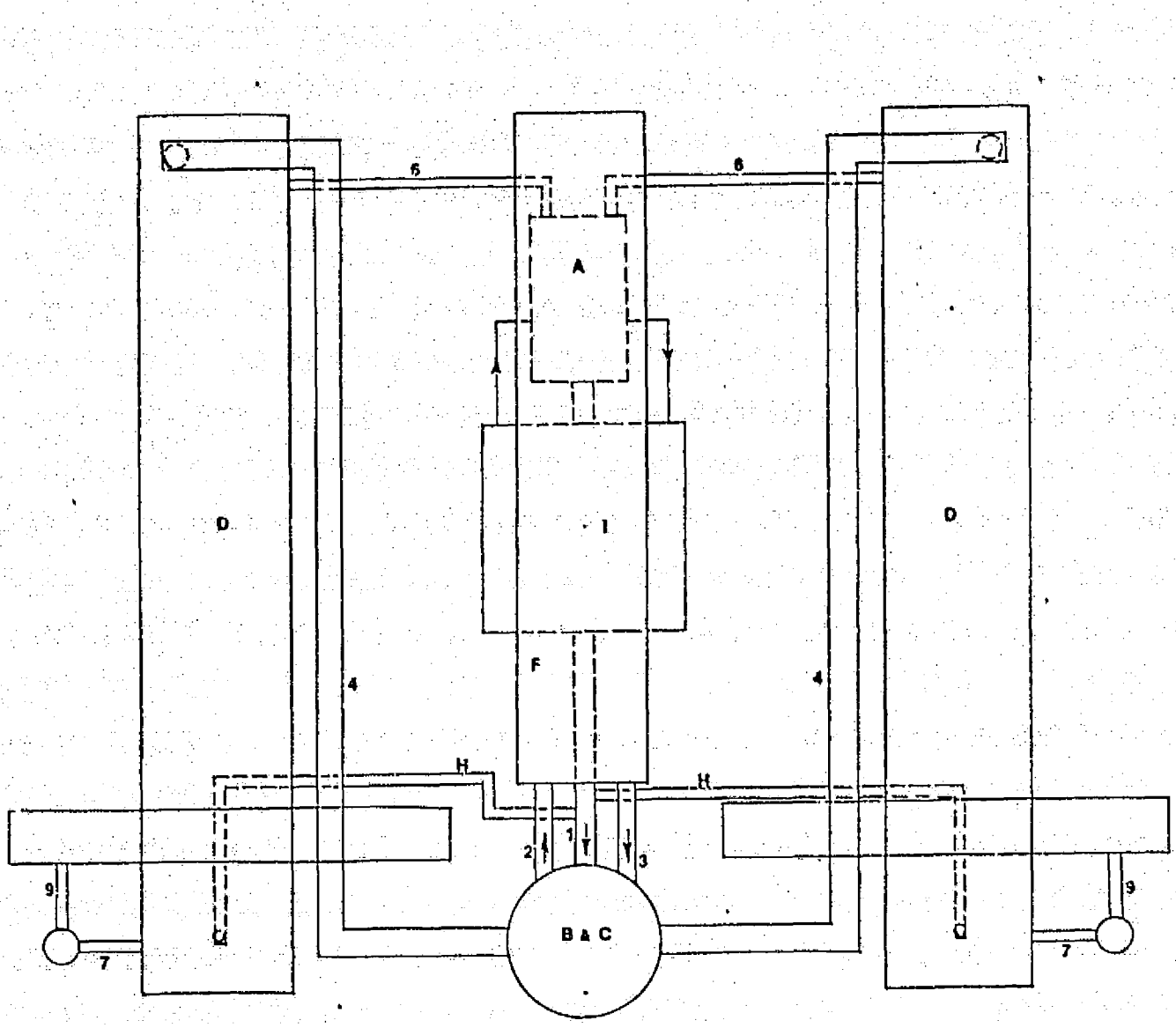

A - UF_6 Reactor
B - HP Turbine
C - LP Turbine
D - Regenerator
E - Condensor
F - Reheator
G - Pump
H - Emergency Turbine Bypass
I - Blanket Reprocessing Plant

FIG. VII-4 LAYOUT-SIDE VIEW

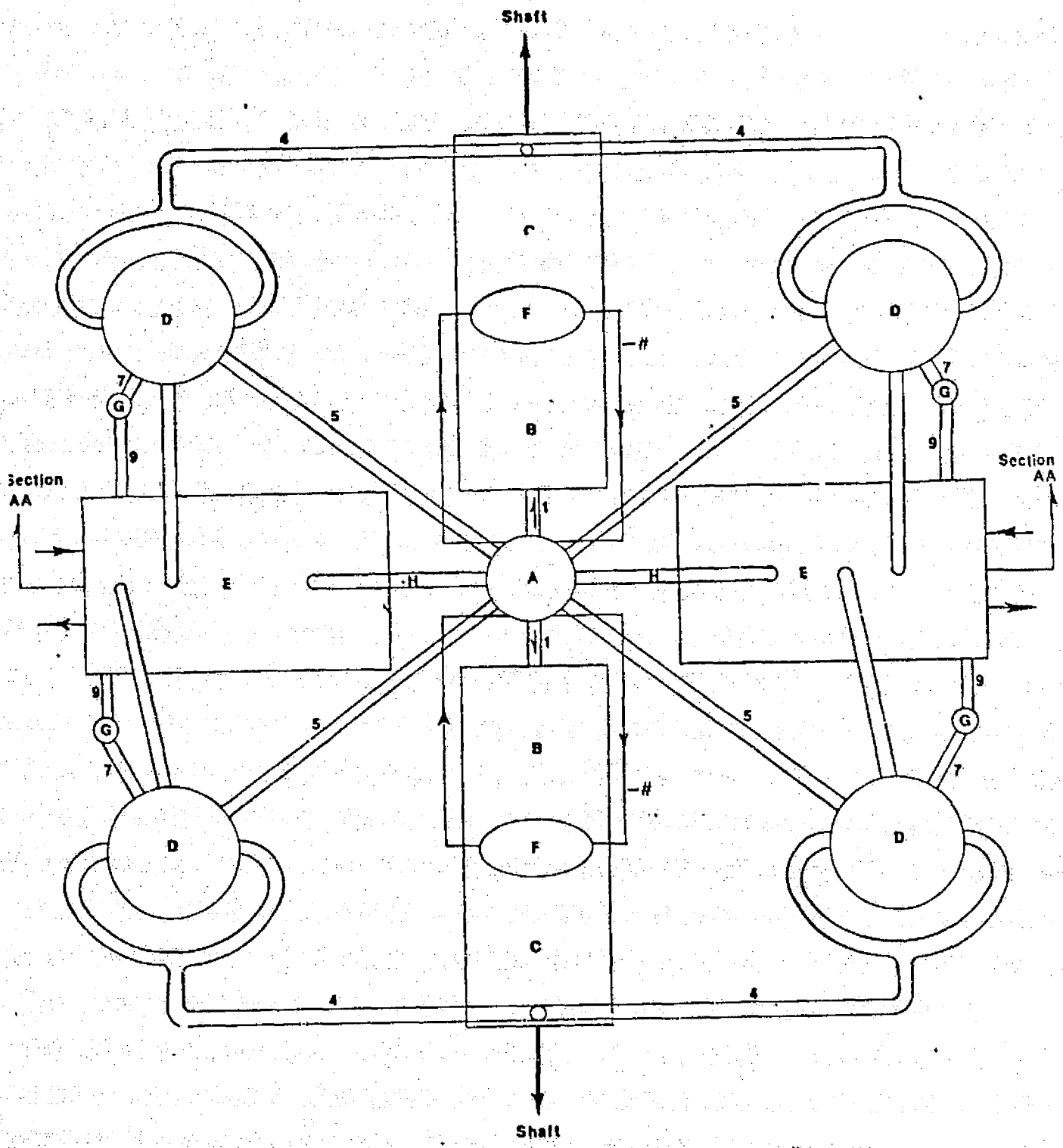

FIG. VII-5 LAYOUT-TOP VIEW

TABLE VII-1

MASS OF UF_6 IN POWER PLANT COMPONENTS

	MASS (lbm)
REACTOR	2,200
REHEATERS (TWO)	8,900
REGENERATORS (FOUR)	250,500
CONDENSERS (TWO)	19,700
TURBINES (TWO H-P, TWO L-P)*	---------
PIPING*	---------
TOTAL	280,700

* WERE NOT CALCULATED

The reheaters consisted of shell-and-tube heat exchangers with counterflow of the molten salt in the tubes and gaseous UF_6 in the shell side. The tubes were of 0.5 in. I.D. and 0.625 in. O.D. The UF_6 velocities were limited so the pressure loss across the shell side did not exceed the 0.5 bar pressure loss assumed in the thermodynamic calculations.

The regenerators also consisted of shell-and-tube heat exchangers with counterflow of the high pressure liquid and boiling UF_6 in the tube side and low pressure gaseous UF_6 in the shell side. Since most of the UF_6 mass was due to the liquid phase in the tubes, the tube diameters were kept small with 0.125 in. I.D. and 0.25 in. O.D. UF_6 velocities were also limited so that pressure losses did not exceed 0.5 bar in the shell side pass.

The condensors were of shell-and-tube construction with cross flow of the condensing UF_6 over the tubes. Tube diameters were 0.5 in. I.D. and 0.625 in. O.D.

The heat transfer calculations were performed using the standard techniques for analyzing heat exchangers discussed in Reference 2. In the regenerator, substantial temperature differences occurred in the UF_6 so the analysis was performed over these regions so that temperature variations in thermal-physical properties could be accounted for.

As shown in Table VII-1, the mass of UF_6 in the core and heat exchangers was 280,700 lb_m. This is an unacceptably high value. The reason for the large mass is that the low thermal conductivity of UF_6 caused small heat-transfer coefficients which in turn required large heat transfer surface areas in the heat exchangers in order to meet the required heat load. Significant reductions in UF_6 mass could be achieved by putting small amounts of a high conductivity gas such as helium in the UF_6. In addition, no effort was made to minimize the UF_6 mass in the power plant. By permitting

higher UF_6 pressure losses in the heat exchangers, the flow velocities can be increased with subsequent increase in heat-transfer coefficients. Another factor is that employing heat transfer enhancement techniques, such as using finned tubes, used in the design of compact heat exchangers can also produce significant reductions in heat exchanger volumes with consequent reduced UF_6 masses. By simultaneously using all of these techniques to minimize the UF_6 mass it is likely that an order of magnitude reduction in system mass can be achieved.

7.6 Areas of Further Study

Many aspects of this reactor power plant require further study. Many problem areas became apparent only as the design progressed. Much research and experimental work remains before these designs can be finalized.

The heat transfer calculations were performed using standard empirical correlations obtained from experiments with water and gases such as helium and air. Experiments need to be performed measuring heat-transfer coefficients of UF_6 for flow of single-phase liquid, boiling UF_6, and gaseous UF_6 in order to confirm the validity of using conventional heat-transfer coefficent correlations.

The control drums are an area that will require a great deal of further study. The required sizes and materials, as well as the corresponding reactivity worths, needs to be computed. The effects of the drums on the breeding ratio is also unknown. It is possible that these drums will not possess enough negative reactivity, considering their position out of the core, to control the reactor. They may also have too long a response time, moving from full out to full in. If for either of the above two reasons, control drums cannot be used, then a new system will need to be devised.

The control drums will need to be cooled. This can be accomplished by drilling vertical holes in the beryllium cylinder and pumping helium through the lower control drum drive assembly into the drum. It would then flow upward through the holes and the gap around the edge and out the control drum drive assembly at the top of the drum. The heat generation rates in the drums needs to be calculated, to see if helium can indeed do the cooling and at what rate it will need to be pumped.

Since the blanket is a molten salt with a high melting point, some type of electric heaters will need to be installed in the blanket to keep the salt fluid during prolonged shut-downs. The pipes in the blanket circulation system will also need to be electrically heated to prevent freezing. The feasibility needs to be analyzed.

A thermal shield will be necessary between the outer pressure vessel and the PCRV. It will probably need to be helium-cooled and heat generation rates in this shield need to be analyzed.

Thermal stresses in the pressure vessel and core liner need to be analyzed for this system. Piping and vessel thicknesses need to be calculated. The core vessel and control drums may need more support than currently specified.

REFERENCES FOR CHAPTER VII

1. "ASME Boiler and Pressure Vessel Code, Sections III - Rules for Construction of Nuclear Power Plant Components," American Society of Mechanical Engineers, New York (July 1971)

2. Krieth, F., "Principles of Heat Transfer," 2nd Ed., International Textbook Company, Scranton, Pennsylvania (1965)

APPENDIX A

THERMODYNAMIC PROPERTIES OF UF_6

Table A1. Thermodynamic Properties of UF_6 as an Overheated Vapor

specific volume, v, cu ft/lb_m
enthalpy, h, Btu/lb_m
entropy, S, Btu/lb_m-°R

T(°R)	v	h	S	v	h	S	v	h	S
	P = 14.504 psi			P = 72.52 psi			P = 145.04 psi		
720	--	44.075	0.3127	--	44.505	0.3042	--	--	--
900	1.828	60.845	0.3329	0.386	60.63	0.3236	0.172	60.2	0.3190
1080	2.235	78.690	0.3514	0.441	78.26	0.3418	0.215	71.83	0.3373
1260	2.634	97.610	0.3675	0.522	96.965	0.3583	0.257	96.325	0.3535
1440	2.882	115.67	0.3813	0.600	115.369	0.3724	0.298	114.595	0.3678
1620	3.390	135.235	0.3934	0.675	134.59	0.3845	0.337	134.165	0.3800
1800	3.760	153.51	0.4038	0.752	153.51	0.3951	0.375	153.08	0.3905
1980	4.151	172.43	0.414	0.830	172.43	0.4049	0.414	172.215	0.4005
2160	4.528	191.565	0.4238	0.905	191.479	0.4142	0.453	191.178	0.4099
2340	4.902	210.7	0.4328	0.982	210.485	0.4228	0.491	210.055	0.4184
2520	5.285	229.62	0.4408	1.058	229.491	0.4309	0.530	229.405	0.4266
2700	5.660	249.185	0.4486	1.134	249.185	0.4387	0.535	249.056	0.4343
	P = 290.08 psi			P = 435.12 psi			P = 580.16 psi		
720	--	--	--	--	--	--	--	--	--
900	.0758	58.695	0.3144	0.0418	56.545	0.3106	.0232	55.04	.3080
1080	.1030	76.97	0.3328	.0651	76.11	0.3303	.0461	74.82	.3279
1260	.1253	95.675	0.3494	.0810	95.245	0.3472	.0597	94.6	.3453
1440	.1469	113.95	0.3638	.0966	113.305	0.3610	.0715	112.875	.3590
1620	.1673	133.515	0.3762	.1108	132.87	0.3735	.0827	132.526	.3717
1800	.1871	152.65	0.3868	.1242	152.306	0.3845	.0929	152.005	.3827
1980	.2072	171.785	0.3968	.1380	171.441	0.3944	.1035	171.14	.3927
2160	.2267	190.92	0.4061	.1512	190.576	0.4037	.1135	190.318	.4022
2340	.2459	209.84	0.4144	.1644	209.41	0.4123	.1236	209.195	.4106
2520	.2657	229.19	0.4226	.1783	228.975	0.4204	.1336	228.803	.4189
2700	.2844	248.927	0.4302	.1900	248.755	0.4281	.1431	248.669	.4264
	P = 725.2 psi			P = 1160.32 psi			P = 1740.48 psi		
900	.0081	52.245	.3045	.0064	--	--	.0060	--	--
1080	.0393	73.1	.3255	.0177	69.23	.3201	.0102	64.93	.3152
1260	.0466	94.17	.3439	.0271	92.02	.3397	.0169	88.795	.3348
1440	.0565	112.445	.3576	.0342	111.37	.3543	.0222	109.865	.3512
1620	.0658	132.225	.3703	.0411	131.15	.3670	.0272	129.86	.3641
1800	.0742	151.575	.3814	.0447	150.801	.3782	.0308	150.07	.3754
1980	.0827	170.925	.3914	.0518	170.28	.3885	.0346	169.85	.3860
2160	.0910	190.146	.4007	.0570	189.544	.3977	.0385	188.985	.3952
2340	.0990	208.98	.4091	.0623	208.55	.4062	.0422	208.12	.4038
2520	.1070	228.674	.4174	.0674	228.33	.4145	.0457	228.115	.4121
2700	.1146	248.54	.4350	.0725	248.325	.4224	.0490	245.53	.4200

Table A1. Continued

T(°R)	v	h	S	v	h	S	v	h	S
	P = 2320.64 psi			P = 2900.8 psi			P = 4351.2 psi		
900	.0058	--	--	.0057	38.055	.2858	.0053	38.27	.2839
1080	.0102	61.705	.3113	.0074	60.845	.3094	.0065	60.2	.3070
1260	.0124	86.86	.3320	.0103	85.57	.3298	.0080	83.85	.3266
1440	.0165	108.79	.3571	.0134	107.5	.3464	.0098	105.35	.3427
1620	.0200	128.785	.3614	.0162	128.94	.3598	.0116	126.42	.3563
1800	.0233	149.425	.3734	.0189	148.651	.3714	.0133	147.705	.3686
1980	.0263	169.205	.3838	.0214	163.775	.3820	.0150	167.7	.3791
2160	.0292	188.426	.3932	.0238	187.91	.3915	.0167	187.265	.3887
2340	.0319	207.905	.4020	.0260	207.561	.4005	.0183	206.83	.3977
2520	.0348	227.9	.4103	.0283	227.556	.4087	.0199	227.04	.4061
2700	.0374	247.895	.4180	.0805	247.514	.4164	.0216	247.25	.4139

Table A2. Thermodynamic Properties of Saturated UF_6 [1]

specific volume of saturated liquid, v_f, cu ft/lb_m
specific volume of saturated vapor, v_g, cu ft/lb_m
enthalpy of saturated liquid, h_f, Btu/lb_m
enthalpy of saturated vapor, h_g, Btu/lb_m
entropy of saturated liquid, S_f, Btu/lb_m-°R
entropy of saturated vapor, S_g, Btu/lb_m-°R

T(°R)	P(psi)	h_f	S_f	v_f	h_g	S_g	v_g	h_{fg}
606.888	21.756	0	.2389	.004378	35.26	.2970	.5595	35.26
626.688	30.458	2.494	.2428	.004480	36.894	.2978	.4712	34.40
644.688	42.352	4.73	.2461	.004566	38.614	.2987	.4148	33.88
662.688	55.115	7.052	.2499	.004657	40.076	.2997	.3420	33.02
680.688	72.520	9.374	.2529	.004750	41.624	.3003	.2618	32.25
698.688	88.474	11.696	.2564	.004852	42.871	.3010	.2195	31.18
716.688	111.681	14.018	.2597	.004959	44.118	.3017	.1734	30.10
734.688	137.788	16.34	.2625	.005088	45.58	.3023	.1394	29.24
752.688	166.796	18.92	.2656	.005218	46.87	.3028	.1145	27.95
770.688	203.056	21.50	.2693	.005368	48.16	.3039	.0929	26.66
788.688	239.316	24.08	.2720	.005531	49.45	.3042	.0806	25.37
806.688	282.828	26.66	.2755	.005745	50.525	.3051	.0683	23.86
824.688	333.592	29.412	.2786	.006067	51.557	.3055	.0592	22.14
842.688	389.432	32.164	.2821	.006197	52.374	.3061	.0461	20.21
860.688	451.074	35.088	.2855	.006669	52.718	.3060	.0375	17.63
878.688	523.594	38.184	.2889	.007198	52.374	.3051	.0284	14.19
896.688	609.168	41.624	.2938	.008283	50.654	.3038	.0204	9.03
905.688	667.184	46.612	.2987	.011496	46.612	.2987	.0115	0

REFERENCES FOR APPENDIX A

1. Verkhivker, G. P., Tetel'baum, S. D. and Konyaeva, G. P., "Thermodynamic Properties of Uranium Hexafluoride (UF_6)," Atomnaya Energiya, 24(2), 158-162 (February 1968).

APPENDIX B

THERMAL-PHYSICAL PROPERTIES OF UF_6

Uranium hexafluoride is a clear, colorless, crystalline solid that sublimes at atmospheric pressure directly to the vapor state. Because of its extensive use in gaseous diffusion enrichment plants and fuel reprocessing plants, its physical and chemical properties at low and moderate temperatures have been extensively studied. Some UF_6 properties listed in the literature[1,2] are given in Table B1.

Table B1. Some Properties of Uranium Hexafluoride

Property	Value
triple point, at 1134 mm Hg, °C	64.052
sublimation point, °C	56.4
density	
solid, g/cm^3	5.09
liquid, g/ml	6.63
heat of formation, solid, at 25°C, kcal/mole	-516
heat of vaporization, at 64.01°C, kcal/mole	6.907
heat of fusion, at 64.01°C, kcal/mole	4.588
heat of sublimation, at 64.01°C, kcal/mole	11.495
critical temperature, °C	230.2
critical pressure, atm	45.5

Uranium hexafluoride is a highly reactive substance, acting as a moderately powerful fluorinating agent. It reacts vigorously with water to form uranyl fluoride (UO_2F_2) and hydrogen fluoride. It does not normally react with oxygen, nitrogen, or dry air. UF_6 is rapidly reduced by hydrogen gas.

UF_6 gas does not start disassociating until temperatures of about 1500°K (2700°F) are reached. Figures B1 and B2 illustrate the calculated composition

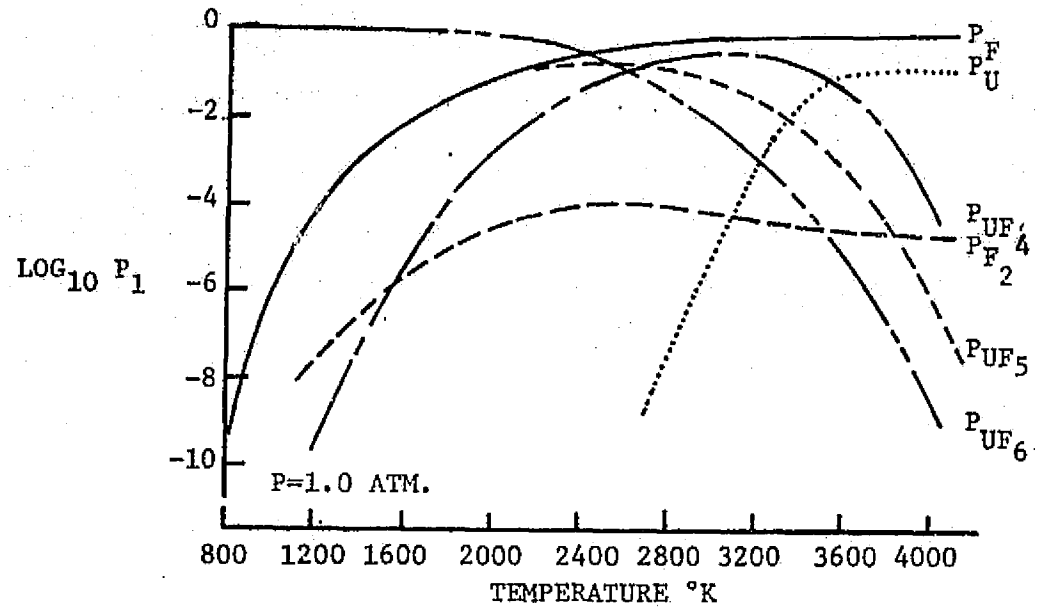

Fig. B-1. Composition of UF_6 Species at One Atmosphere Préssure[3]

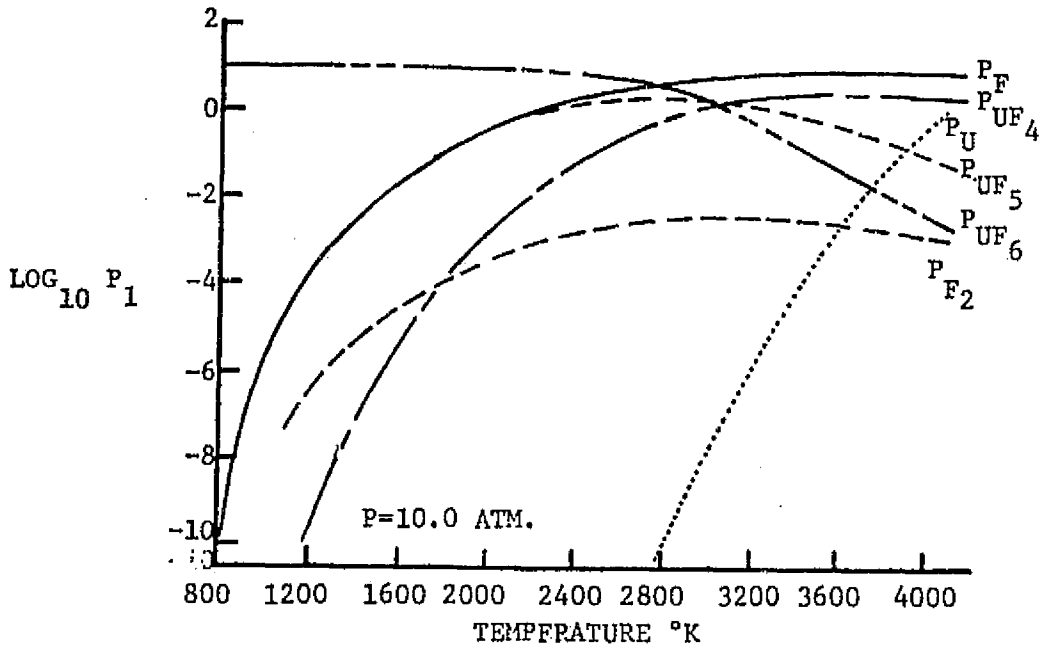

Fig. B-2. Composition of UF_6 Species at 10 Atmospheres Pressure[3]

of UF_6 species at temperatures to 4000°K for pressures of one and ten atmospheres, respectively. Figure B3 illustrates the ratio of specific heats out to 3000°K, and Figure B4 shows the results of Soviet calculations of the composition of UF_6 species out to 51,000°K. Gas turbine power plants will probably operate only at temperatures below 1500°K because of corrosion and other problems at higher temperatures.

Data on the ratio of specific heats is necessary for turbine and compressor performance calculations. These data were measured to 1500°K at the University of Florida,[5] and the results are presented in Figure B5.

Viscosity of liquid UF_6 between 70 and 210°C is given by the following equation[6]:

$$\eta = 1.67 \times 10^{-3} \, e^{(554-0.023P)/T} \qquad \text{(B1)}$$

where P is in pounds per square inch, T is in degrees Kelvin, and η is in poise.

The viscosity[7] of UF_6 vapor has been investigated by Llewellyn; and Fowler. Cohen summarized their data using the following empirical formulae:

For Fowler's data:

$$\eta = 2.46 \times 10^{-6} \, T^{0.772} \quad (85 \text{ to } 165°C) \qquad \text{(B2)}$$

$$\eta = 1.78 \times 10^{-6} \, T^{0.827} \quad (150 \text{ to } 260°C) \qquad \text{(B3)}$$

For Llewellyn's data:

$$\eta = 2.10 \times 10^{-6} \, T^{0.779} \quad (0 \text{ to } 200°C) \qquad \text{(B4)}$$

where T is in degrees Kelvin; η is in poise.

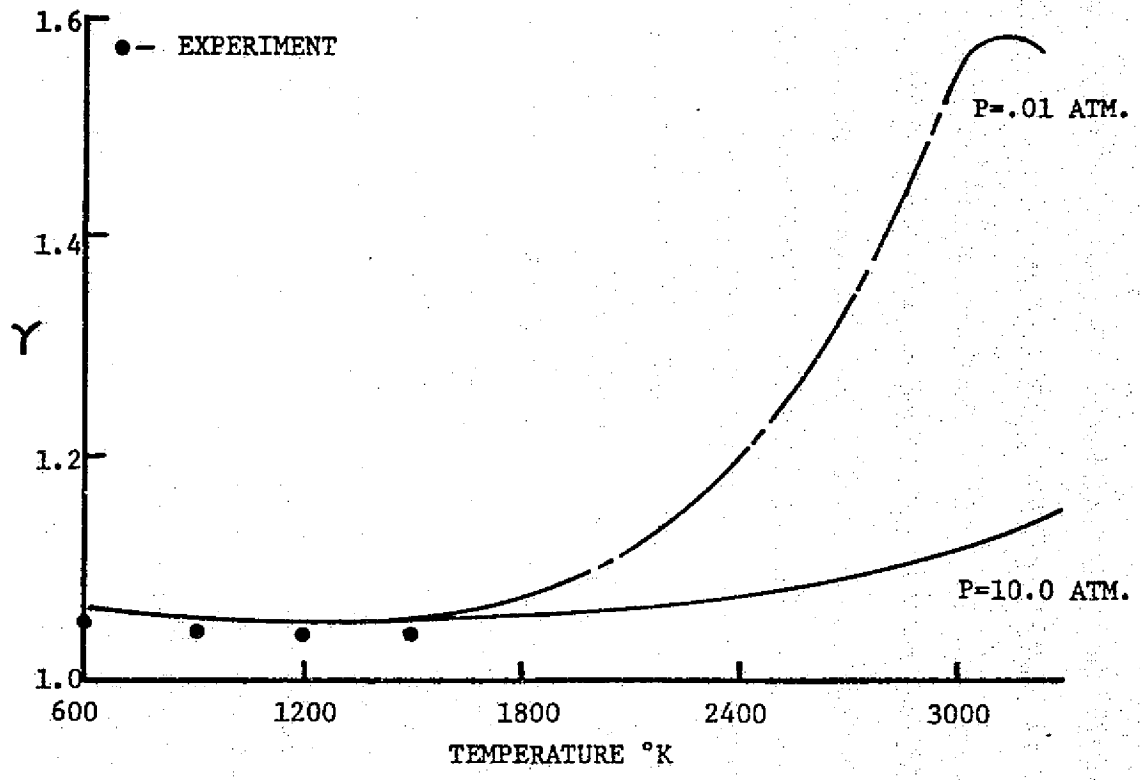

Fig. B-3. Ratio of Specific Heats for UF_6

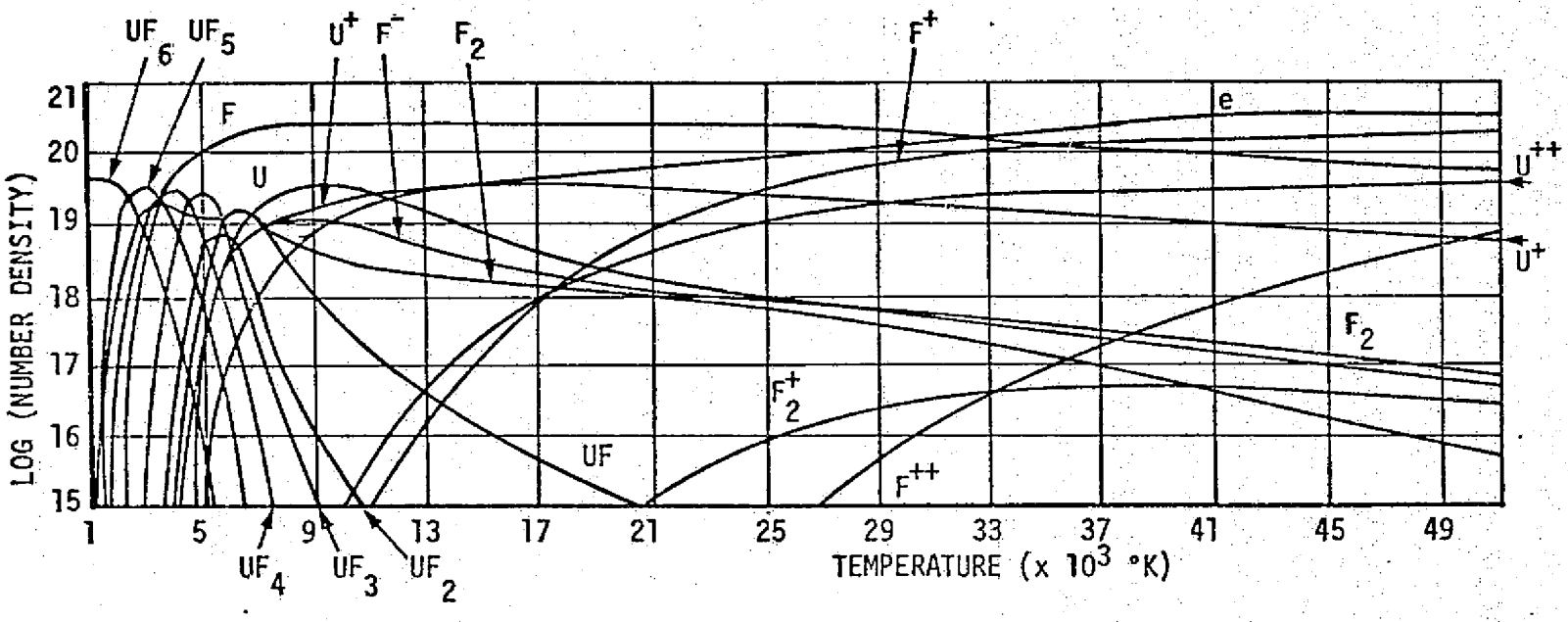

Fig. B-4. Composition of UF_6 Species to 51,000 °K[4]

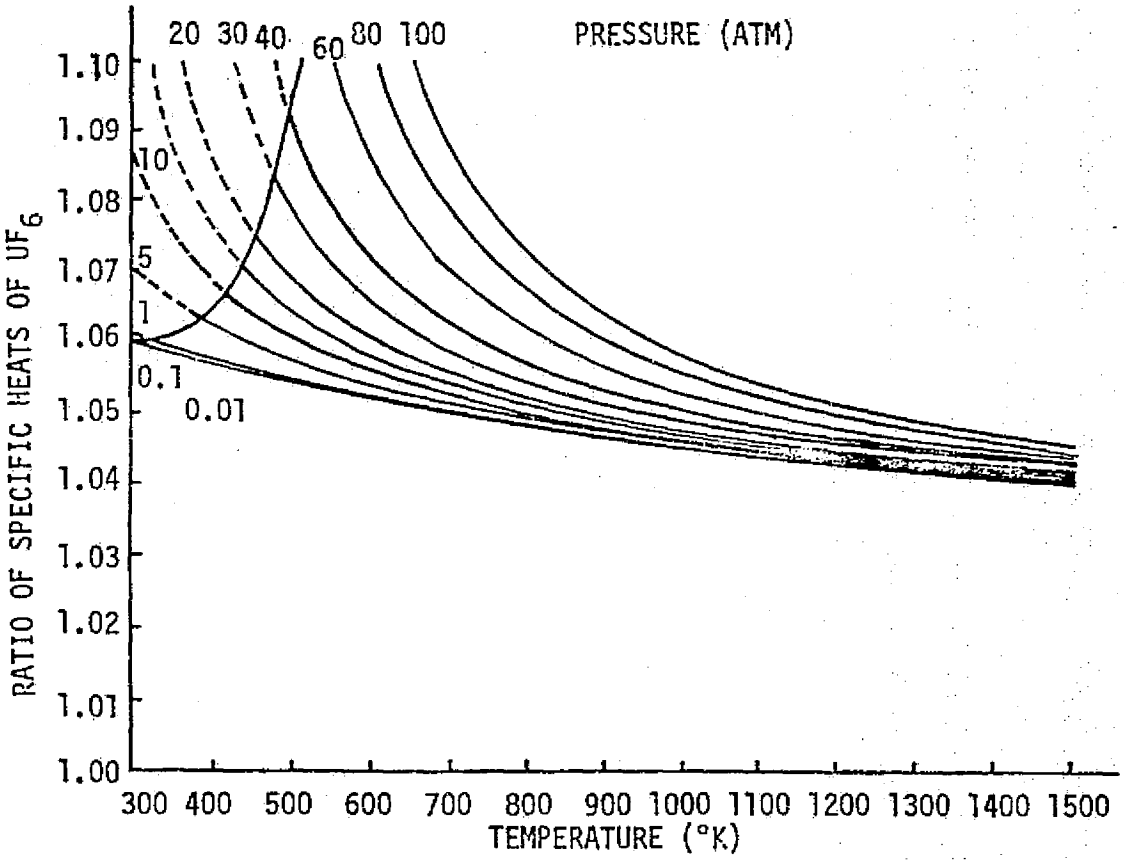

Fig. B-5. Ratio of Specific Heats for Uranium Hexafluoride[5]

The most reliable thermal conductivity[8] values of UF_6 vapor for temperatures between 0 and 100°C are represented by the following equation:

$$K_{av} = 1.46\ (1 + 0.0042t°C) \times 10^{-5}\ \text{cal/cm-sec-°C} \qquad \text{(B5)}$$

where K_{av} is the average of the experimental and calculated conductivity value.

REFERENCES FOR APPENDIX B

1. Harrington, C. D. and Ruehle, A. E., "Uranium Production Technology," D. Van Nostrand Co., Inc., New York, 1959.

2. Oliver, G. D., Milton, H. T. and Grisand, J. W., "The Vapor Pressure and Critical Constants of Uranium Hexafluoride," J. Am. Chem. Soc., 75, 2827-9 (1952).

3. Hassan, H. A. and Deese, J. E., "Thermodynamic Properties of UF_6 at High Temperatures," NASA CR-2373 (1974).

4. Dmitrievskii, V. A. and Zaklyaz'minskii, L. A., "Induction Magnetohydrodynamic Generator with a Hollow Nuclear Reactor," Teplofizika Vysokikh Temperatur, 9, No. 2, 405-412 (March-April, 1971).

5. Sterritt, D. E., Lalos, G. T. and Schneider, R. T., "Thermodynamic Properties of UF_6 Measured with a Ballistic Piston Compressor," Dept. of Nuclear Engineering Sciences, University of Florida (March, 1973).

6. DeWitt, R., "Uranium Hexafluoride: A Survey of the Physico-Chemical Properties," GAT-280, Goodyear Atomic Corporation, p. 44 (Aug., 1960).

7. Ibid., pp. 38-39.

8. Ibid., p. 44.

APPENDIX C

THERMO-PHYSICAL PROPERTIES OF MOLTEN SALT REACTOR FUEL

Molten salt reactor fuel is composed of LiF (71.7 mole%), BeF_2 (16 mole%), ThF_4 (12 mole%) and UF_4 (0.3 mole%). Some of its properties are[1]:

molecular weight = 64

melting point = 930°F

vapor pressure at 1150°F < 0.1 mm Hg

Cp = 0.324 Btu/lb.

The fuel density and viscosity can be represented as functions of temperature by the following relations:

$$\rho(\text{lb/ft}^3) = 235.0 - 0.02317t \ (°F) \qquad (C1)$$

$$\mu(\text{lb/ft-hr}) = 0.2637 \exp\ (7362/T°(R)) \qquad (C2)$$

Thermal conductivities at three different temperatures are listed below:

at 1300°F	K = 0.69	Btu/hr-ft-°F
at 1175°F	K = 0.71	
at 1050°F	K = 0.69	

REFERENCES FOR APPENDIX C

1. Robertson, R. C., "Conceptual Design Study of a Single-Fluid Molten Salt Breeder Reactor," ORNL-4541 (June, 1971).

APPENDIX D

SOLUTION OF ENERGY EQUATION

D.1 Mathematical Model

The energy equation in cylindrical coordinates is given by[1]:

$$\frac{\partial}{\partial t}\rho C_p T = -(\nabla\cdot\rho C_p T\vec{u}) - (\nabla\cdot\vec{q}) - (\tau:\nabla\vec{u}) + \left(\frac{\partial \ln v}{\partial \ln T}\right)\frac{Dp}{Dt} + \rho T\frac{DC_p}{Dt} + q''' \qquad (D.1)$$

Certain assumptions can be made to simplify this expression:

(1) assume steady state conditions;

(2) neglect viscous forces;

(3) assume velocity in r and θ directions negligible;

(4) assume constant pressure in the core;

(5) assume axial conduction negligible.

Noting $\nabla\vec{q} = -\nabla\cdot(K_E\nabla T)$, Eq. (D.1) reduces to

$$\nabla\cdot\rho C_p T\vec{u} = \nabla\cdot K_E\nabla T + q''' \qquad (D.2)$$

Expanding Eq. (D.2) and using the assumptions above

$$\frac{\partial}{\partial z}(\rho C_p T u_z(r,z)) = \frac{1}{r}\frac{\partial}{\partial r}\left(r\,K_E\frac{\partial T}{\partial r}\right) + q'''(r,z) \qquad (D.4)$$

and rearranging

$$u_z(r,z)\frac{\partial T}{\partial z} = \frac{1}{r}\frac{\partial}{\partial r}\left(r\frac{K_E}{\rho C_p}\frac{\partial T}{\partial r}\right) + \frac{q'''}{\rho C_p} \qquad (D.5)$$

The expression for the eddy diffusivity for heat transfer is assumed

$$\varepsilon_H \approx \varepsilon_M = \left(\frac{\mu}{\rho}\right)(.72)\left(\frac{1}{8}\ f\right)^{\frac{1}{2}} N_{Re}\ \frac{r}{r_o}\left(1 - \left(\frac{r}{r_o}\right)^{\frac{1}{2}}\right) = A\ \frac{r}{r_o}\left(1 - \left(\frac{r}{r_o}\right)^{\frac{1}{2}}\right) \quad (D.6)$$

Then the right side of Eq. (D.5) can be expanded

$$\frac{1}{r}\frac{\partial}{\partial r}\left(r(\alpha+\varepsilon_H)\frac{\partial T}{\partial r}\right) = (\alpha+\varepsilon_H)\frac{\partial^2 T}{\partial r^2} + \left\{\frac{\alpha}{r} + \frac{A}{r_o}\left(2 - \frac{5}{2}\left(\frac{r}{r_o}\right)^{\frac{1}{2}}\right)\right\}\frac{\partial T}{\partial r} \quad (D.7)$$

Thus Eq. (D.5) becomes

$$u_z\frac{\partial T}{\partial z} = (\alpha+\varepsilon_H)\frac{\partial^2 T}{\partial r^2} + \left\{\frac{A}{r_o}\left[2 - \frac{5}{2}\left(\frac{r}{r_o}\right)^{\frac{1}{2}}\right] + \frac{\alpha}{r}\right\}\frac{\partial T}{\partial r} + \frac{q'''}{\rho C_p} \quad (D.8)$$

Equation (D.8) is the mathematical model whose solution gives the temperature profile of the design reactor. The partial derivatives may be estimated using finite differences

$$\frac{\partial T}{\partial z} = \frac{T_{i,2} - T_{j,1}}{S}\ ;\ \frac{\partial T}{\partial r} = \frac{T_{i+1,1} - T_{i-1,1}}{2h}\ ;\ \frac{\partial^2 T}{\partial r^2} = \frac{T_{i+1,1} - 2T_{i,1} + T_{i-1,1}}{h^2} \quad (D.9)$$

In finite difference form and rearranging Eq. (D.8) becomes

$$T_{i,2} = T_{i,1} + \frac{S(\alpha+\varepsilon_H)}{u_z}\left[\frac{T_{i+1,1} - 2T_{i,1} + T_{i-1,1}}{h^2}\right] + \frac{S}{u_z}\left\{\frac{A}{r_o}\left[2 - \frac{5}{2}\left(\frac{r}{r_o}\right)^{\frac{1}{2}}\right] + \frac{\alpha}{r}\right\}\left[\frac{T_{i+1,1} - T_{i-1,1}}{2h}\right] + \frac{S\ q'''}{\rho C_p u_z} \quad (D.10)$$

where

S = mesh size in the axial direction

h = mesh size in the radial direction

$\alpha = k/\rho C_p$

$A = (\mu/\rho)(.72)(\frac{1}{8} f)^{\frac{1}{2}} (N_{Re})$

$\epsilon_H = A \frac{r}{r_o}\left(1 - \left(\frac{r}{r_o}\right)^{\frac{1}{2}}\right)$

Rewriting Eq. (D.10) using the heat generation term developed

$$T_{i,2} = T_{i,1} + \frac{S(\alpha+\epsilon_H)}{u_z}\left[\frac{T_{i+1,1}-2T_{i,1}+T_{i-1,1}}{h^2}\right]$$

$$+ \frac{S}{u_z}\left\{\frac{A}{r_o}\left[2 - \frac{5}{2}\left(\frac{r}{r_o}\right)^{\frac{1}{2}}\right] + \frac{\alpha}{r}\right\}\left[\frac{T_{i+1,1}-T_{i-1,1}}{2h}\right]$$

$$+ \frac{SQ_1'''}{\rho C_p u_z}\left[1 + 1.07\, e^{-.19(r_o-r)}\right]\left[1 - \frac{2}{3}\frac{z}{L}\right] \qquad \text{(D.11)}$$

where

$$u_z = \frac{u_{im}}{.8}\left[\frac{\bar{\rho}_i}{\bar{\rho}_z}\right]\left[1 - \frac{r}{r_o}\right]^{1/7}$$

Therefore, given the core geometry, inlet temperature, power level, and flow rate the temperature profile of the core can be determined.

D.2 Computer Model

Equation (D.11) was solved using a marching technique down the channel on the Georgia Tech CDC CYBER 74 computer. The program steps the temperature radially and down the channel. Two cases of boundary conditions governing the solution were considered:

Case I: (a) Uniform inlet temperature distribution ($T_1^i = 1036.77°R$)

(b) Insulated boundary $\left.\frac{\partial T}{\partial r}\right|_{r=r_o} = 0$ along the entire length of the core

(c) Symmetrical distribution radially $\left.\frac{\partial T}{\partial r}\right|_{r=0} = 0$ along the entire length of the core

Case II: (a) Uniform inlet temperature distribution ($T_i = 1036.77°R$)

(b) Insulated boundary up to the axial position where $T_{wall} = 1660°R$; constant wall temperature thereafter ($T_{wall} = 1660°R$)

(c) Symmetrical distribution radially.

Equation (D.11) poses problems when $u_z = 0$ (when $r=r_o$) or when $r = 0$. Therefore, wall and centerline temperatures must be computed using another method. The method used is finding an equation for an appropriate curve which will satisfy the boundary conditions and extrapolate to the desired temperature.

At the wall the temperature is assumed of the form

$$T = a_0 + a_1 r^2 + a_2 r^3 \tag{D.12}$$

Using the boundary condition $\left.\frac{\partial T}{\partial r}\right|_{r=r_o} = 0$ and knowing the temperature at two points near the wall

$$\frac{\partial T}{\partial r} = 0 = 2a_1 r_0 + 3a_2 r_0^2, \quad r = r_0$$

$$T_1 = a_0 + a_1 r_1^2 + a_2 r_1^3, \quad r = r_1$$

$$T_2 = a_0 + a_1 r_2^2 + a_2 r_2^3, \quad r = r_2 \tag{D.13}$$

where

r_0 = radius at the wall

r_1, r_2 = two points near the wall

T_1, T_2 = temperatures at r_1 and r_2

The unknown coefficients are found using determinants. Knowing them, $T(r=r_0)$ can be readily determined using Eq. (D.12).

At the channel centerline the temperature is assumed of the form

$$T = a_0 + a_1 r^2 \tag{D.14}$$

which satisfies the boundary condition $\left.\frac{\partial T}{\partial r}\right|_{r=0} = 0$.

Using known temperatures at two other points near the centerline

$$T_1 = a_0 + a_1 r_1 \ , \ r = r_1$$
$$T_2 = a_0 + a_1 r_2 \ , \ r = r_2 \tag{D.15}$$

The unknown coefficients are found using determinants. Then the centerline temperature at r = 0 follows from Eq. (D.14), i.e., $T = a_0$.

D.3 Iteration, Convergence, and Stability

An iterative approach was taken so that properties were computed near the (j+1) temperature as opposed to the properties being evaluated at the (j) temperatures. Only one iteration was needed because temperatures did not change significantly for any given row.

Convergence was the most time consuming portion of the numerical analysis. Due to the complexity of Eq. (D.11), the effect of various parameters was somewhat masked, and trial-and-error was almost the rule in determining mesh size for convergence. Next to the stability criteria (to be discussed next), the size of the step in the r direction is the most significant factor in converging to a solution. Ideally the minimum Δr should be determined below which the temperature profile is no longer dependent on the size of

Δr (within an acceptance criterion). The step in the r direction was reduced to .16 cm. It is not known if this is the minimum step size since smaller steps result in either exceeding the time limit on the CDC CYBER 74 authorized for this group or, if too small, results in an instability the cause of which is unknown.

The stability criterion was determined to be $\frac{\Delta z}{\Delta r} < 1$; there $\frac{\Delta z}{\Delta r} = \frac{1}{5}$ was chosen for all calculations.

REFERENCES FOR APPENDIX D

1. Bird, R. B., Stewart, W. E. and E. N. Lightfoot, Transport Phenomena; John Wiley and Sons, Ltd., New York, 1960.